Decoherence of Phonons in Weakly and Strongly-Interacting Bose-Einstein Condensates

Richard Howl

School of Physics and Astronomy

University Of Nottingham

A thesis submitted for the degree of

MSc by Research (Physics)

First Supervisor: Dr. Lucia Hackermüller [†]

Second Supervisor: Prof. Ivette Fuentes [‡]

[†]School of Physics and Astronomy
[‡]School of Mathematical Sciences

Abstract

This work investigates the theoretical and experimental decoherence of phonons in weakly and strongly-interacting Bose-Einstein Condensates (BECs). The theoretical analysis treats phonons as open quantum systems where the environment comprises all other quasi-particle modes of the BEC. The phonons are assumed to be Gaussian states and the time in which they decohere is estimated from the evolution of their purity and nonclassical depth in the dissipative channel. The calculations are performed for various BEC systems and it is found that the excited phonon states will always decohere much more rapidly than the rate at which they relax back to equilibrium with the environment.

Part II of this work considers how the decoherence of the phonons can be measured experimentally. The experiment that is currently being investigated uses a strongly-interacting ^{6}Li BEC where the scattering length can be varied with an external magnetic field. In a strongly-interacting Bose gas the mutual interaction between the condensed and noncondensed components plays a greater role than in weakly-interacting gases and results in distinct absorption images. Understanding the effects from this mutual interaction is vital to model the in-situ absorption images of a strongly-interacting BEC in order to extract accurate information such as that which will facilitate the experimental measurement of decoherence. Three theoretical models that could be used to fit in-situ absorption images of a strongly-interacting gas are analysed. These are the bi-modal, semi-ideal and Hartree-Fock models, which will be fit against the absorption images of the ^{6}Li BEC for various scattering lengths. The validity of these models is also investigated to determine when beyond mean-field effects may be observed in the Bose gas.

Controlling decoherence is essential to the operation and physical realisation of many quantum information tasks and quantum technologies. Recently, new technologies have emerged from relativistic quantum information science that, in principle, are more precise than their non-relativistic counterparts. The practical setup of these devices utilizes phonons of BECs but the decoherence of the phonons has not been considered. In this work, one of the BEC systems used to estimate the decoherence time of the phonons has been chosen to be based on these devices. This calculation is expected to inform the practical realization of these devices and inspire future related studies. Analogue gravity investigations based on BECs also utilize phonons, for example, in the analogue of Hawking radiation. The quantum properties of these states is of particular interest in these studies and understanding how they decohere, and at what rate, could potentially inform the theory of black hole physics as well as dictate what is possible to measure experimentally.

Acknowledgements

I would like to thank all the people who have contributed in some way to the work described in this thesis. My deepest gratitude is to my supervisors Ivette Fuentes and Lucia Hackermüller. Thank you both for providing me with this opportunity and for all your ideas that, without which, would never have resulted in this thesis being written. I have been astonished at the amount of support and guidance you have provided and I am very grateful for your friendship and the confidence that you have had in me. Your knowledge of your subjects is exceptional and I knew that I could always count on you for any help. I could not have imagined better supervisors.

I would also like to thank all the members of the Relativistic Quantum Information Theory and Ultracold Mixtures teams. You have all been incredibly welcoming and always willing to answer my questions. A special thanks goes out, in particular, to Carlos Sabín and Nathan Welch who have both contributed invaluably to this work.

My parents continue to provide me with incredible support no matter what crazy routes I embark upon, for which I am eternally grateful. Thank you for your continuing belief in me.

Last but in no way least, I would like to thank my wife Lizzie. Thank you for your bewildering patience, understanding and always being there for me.

Contents

Introduction

The superposition principle is one of, if not the, most significant fundamental postulates of quantum mechanics. The fact that we do not observe this principle in our macroscopic world leads to our lack of intuition of quantum theory and to astonishing results. This is a well-known and long-outstanding issue for quantum mechanics and many theories have been proposed to facilitate a resolution. The theory of quantum decoherence, in particular, offers promising insight into a potential resolution [1]. This theory comprises the notion that realistic quantum systems can never be isolated and are instead continuously interacting with their surrounding environment. This is in contrast to classical physics where the objective reality of a system can always be separated from the environment. There the environment just creates experimental noise which prevents the observation of the true objective reality of the system of interest. In quantum theory, however, the entangling of states perfectly demonstrates the inherent non-isolation of quantum systems. The continuous interaction of a quantum system with its environment often leads to the appearance of a non-unitary evolution of the system and, in some cases, to the local suppression of interference between particular states. This loss of quantum coherence is the basis of the theory of decoherence and essentially results in the quantumness of the system "leaking" into the environment. Viewed in isolation and a particular basis, the system has then gone from a coherent quantum superposition of states to behaving like a classical statistical ensemble of states, although a total superposition of the global system-environment wave function still exists. This process often occurs in extremely short time scales [2], providing insight into a potential resolution of the non-observation of quantum superpositions in the macroscopic world (for further discussion see e.g. [3]).

The theory of decoherence was introduced in 1970 by Zeh [1] and quantitatively measured for the first time by in 1996 by Haroche et al. [4] using rubidium atoms where each was in a superposition of two states. As well as playing a prominent role in fundamental notions of quantum physics, decoherence also has applications in quantum thermodynamics [5], biology [6], and, in particular, in the rapidly developing fields of quantum information science and quantum technology. In quantum information science decoherence is re-interpreted as the loss of information from a system to the environment. The information contained in a quantum state is vital in quantum information science and the loss of information is to the detriment of a particular task. Therefore, understanding how a particular quantum system decoheres is crucial to the performance and realisation of quantum information tasks. Understanding the process of decoherence is also of critical importance to the related field of quantum technology. This is a relatively new field of physics and engineering that harness the fundamental principles of quantum physics to gain a functionality or performance which cannot be attained from classical concepts. For example, a modern classical computer relies on classical information theory and stores information in binary bits. Therefore, even though an understanding of quantum physics is required to manipulate the transistors which are used to carry out the classical information tasks, the computer is fundamentally based on classical concepts. Quantum computers on the other hand store information in quantum states and rely on the superposition principle. They are, therefore, fundamentally quantum devices. These devices offer a performance that cannot be achieved by classical computers such as factoring integers in polynomial time [7] and a quadratic speedup for function inversion [8]. Given this, and the fact classical computers are beginning to reach the physical limitations of Moore's law [9], quantum computers are widely considered to be the future of computing. However, this promise is reliant on understanding and limiting decoherence in these devices since this results in the degradation of quantum superpositions which are vital to the performance and realisation of the device. Furthermore, limiting decoherence is similarly also of critical importance to other applications of quantum

technology such as quantum communication, which, in principle, offers absolutely secure messaging, and quantum metrology and sensing, which offer super-resolution measurements.

Bose-Einstein condensates (BECs), where bosonic atoms or molecules form a collective state at low temperatures, are considered to be promising candidates for the implementation of various quantum technologies since they can usually be relatively well isolated from their surroundings and, therefore, offer relatively long coherence times. In particular, two-component Bose-Einstein condensates, either as bosons condensed in two different sites [10] or as condensed bosons in different hyperfine levels coupled by a laser [11], have been widely considered for the implementation of certain quantum technologies. The primary application for such two-component BECs is considered to be quantum metrology [12], such as atomic clocks and accelerometers, but quantum simulation and computation have also been investigated in this context [13]. A major advancement in this area has been the development of BECs on atom chips, which facilitates the control of many BECs [14].

Bose-Einstein condensates have also recently been applied to the field of Relativistic Quantum Information Theory (RQIT) [15]. This field is concerned with formulating a theory of quantum information that is fully compatible with the relativistic structure of spacetime. It has so far uncovered unexpected obstacles to quantum information tasks, such as relativistic degradation of entanglement, as well as completely new possibilities such as generation of entanglement and improved precision of measurement devices [16–18]. Many implementations and applications of quantum information, such as space based applications, employ relativistic systems and, as the precision of quantum devices improves, it is becoming increasingly important to determine how relativistic effects can affect quantum information tasks [17, 19, 20]. The field also has important applications in fundamental questions of cosmology, black hole physics and quantum gravity.

In a relativistic setting, the phononic excitations of a BEC satisfy a Klein-Gordon equation on a curved background metric that has two terms, one corresponding to the real spacetime metric, and a second that is an

acoustic analogue to a spacetime metric [21]. The second term is manipulated in analogue gravity experiments [22] and has culminated in the recent observation of an acoustic analogue of the elusive Hawking radiation of a black hole [24]. The first term, on the other hand, allows for the observation of real relativistic effects on BECs due to motion-induced transformations and changes in the real gravitational field. This has been utilized with concepts from RQIT to formulate a quantum accelerometer and gravitational wave (GW) detector [17, 18] where the strength of the acceleration and GW are estimated from the change of state of the phonons. Due to the much slower propagation of the phonic excitations compared to that of light in vacua, these relativistic quantum technologies are anticipated to be highly precise and offer an accuracy that is orders of magnitude above that of the current state-of the art [17, 18].

The utilisation of BECs to carry out information tasks in these relativistic quantum devices is fundamentally distinct to their use in traditional quantum technologies. As discussed above, the latter are generically based on two-component BECs and thus utilize the condensed atoms and molecules of the Bose gas. On the other hand, the relativistic quantum devices utilize the phononic excitations of the Bose gas (the quantized long-wavelength oscillations of the condensate). The mechanism of decoherence of these relativistic devices will, therefore, be completely different to that of the traditional quantum devices that use BECs. In fact decoherence has yet to be considered in these relativistic quantum devices and the phononic excitations of the BEC have been assumed to exist for as long as the BEC. However, the decoherence time of the phononic excitations is expected to be important for the practical realisation of the GW detector and accelerometer since they rely on long enough times to extract the quantum information induced in the phononic excitations.

Motivated by the above relativistic quantum devices, the work presented here is primarily concerned with estimating the decoherence time of the phononic excitations of BECs [25]. This can then be used to appraise the potential realisation of the devices. Thus far, only the time scale for the energy relaxation of phononic excitations of BECs has been investigated

[26–29]. This is the time scale required for the approximate vanishing of the populations of quantum states [30–32] and constitutes a strict upper bound on the decoherence time. However, in this work it is shown that phonons can decohere in time scales which are orders of magnitude shorter than their corresponding relaxation time scales, placing constraints on the practical realisation of the relativistic quantum devices.

Decoherence and, in particular, the degradation of entanglement [33] of phononic states, is also likely to be important in analogue gravity or related setups based on BECs [34–36].[1] For example, the observation of entanglement and nonclassical correlations in Hawking radiation relies on these properties existing for a non-negligible time in the BEC. Furthermore, the observation of nonclassical correlations in phonon states created by an acoustic version of the dynamical Casimir effect [37, 38] will also be reliant on a non-vanishing decoherence time. BECs have in fact emerged as one of the most promising platforms to simulating the physics of a quantum field on a generic curved space-time. Here the equation describing the propagation of phonons in the moving fluid can be recast in terms of a massless scalar field propagating in a curved space time with a suitably chosen acoustic metric. This can, for example, lead to an acoustic simulation of a black holes where it is phonons rather than photons that cannot escape. An advantage of this acoustic black hole (BH) is that, unlike for gravitational BHs, Hawking radiation can be observed [24] and the quantum description is well-understood at the microscopic level, potentially facilitating an improved understanding of the intrinsic issues in the standard derivation of Hawking radiation. At the time of writing, quantum properties such as entanglement have yet to be observed but such a signature would be of major significance to the analogue gravity field and potentially to BH physics.[2]

[1] The robustness of entanglement generation in quasi-particles against temperature has also been theoretically studied for these systems [36].

[2] Shortly after the submission of this thesis a measurement of the entanglement of acoustic Hawking radiation was reported in [39]. Entanglement was not observed at low frequencies but, given the results of this thesis and [33], this is unlikely to be due to decoherence effects since it is expected that this would only increase with frequency (although it is possible that, due to differences in experimental setup, this situation could change). This measurement opens the door to investigations into measuring the decoherence of phonons of BECs.

Understanding how this entanglement degrades via decoherence processes could thus potentially inform the theory of BH physics as well as dictate what is possible to measure in experiments.

In this work the decoherence of phonon states of BECs is investigated by treating them as open quantum systems in the Born-Markov approximation. The phonon states are then further assumed to be Gaussian states, which are states whose Wigner function is of Gaussian form. Such states are commonly employed in continuous variable quantum information and quantum optics, and have been recently applied to the extension of quantum metrology to relativistic settings [17, 40]. The principle advantage of these states is that the infinite number of degrees of freedom required to describe a general quantum field state is reduced to just the entries of a two dimensional vector and square matrix. The latter is commonly referred to as the covariance matrix and all informationally relevant properties can be derived from it [41–43]. Under the Gaussian and Born-Markov approximations, the rate of decoherence of the phonons is then shown to be quantifiable by analysing the evolution of certain global entropic measures and nonclassical indicators of Gaussian states following [44].

The decoherence of the phonons is investigated for several BEC setups where different values of thermodynamic quantities such as temperature are used as well as different microscopic quantities such as the mass and interaction strength of the atoms or molecules. In particular, the decoherence time is estimated for a BEC setup inspired by that used in [18] for the theoretical analysis of the relativistic GW detector, as well as a BEC setup that is currently being investigated in order to determine the decoherence time of phonons experimentally. The latter investigation is also the subject of this work and uses a strongly-interacting Lithium Bose gas where molecules of ^{6}Li condense [45]. The decoherence time is then expected to be extracted from in-situ absorption images of this Bose gas at various temperatures.

In a strongly-interacting Bose gas the mutual interaction between the condensed and noncondensed components plays a greater role than in weakly-interacting gases and is expected to result in absorption images that are quite distinct from those of weakly-interacting Bose gases even at relatively

low temperatures. Understanding the effects from the mutual interaction is thus vital to the extraction of the decoherence time. Numerous theories have been developed to successfully model this mutual interaction. Popular methods are those that utilize the Popov or Hartree–Fock approximations, which are mean-field theories for finite temperature systems [46–48]. To determine the density profiles seen in absorption images, the resulting equations from these models have to be solved either self-consistently or numerically. This in contrast to the most generically used model for modelling absorption images, the so-called bi-modal model. This model is an analytical model that treats the condensed and noncondensed components as independent systems. It further treats the noncondensed component as an ideal gas and ignores the kinetic energy of the condensate in the Thomas-Fermi limit [49, 50].

To facilitate the experimental measurement of the decoherence time of the phonons, three models for extracting the density profiles of in-situ absorption images of the molecular ^{6}Li Bose gas are currently being compared [51]. The three models are the analytical bi-modal model, a model based on the Hartree-Fock approximation, and the semi-ideal model [52]. A similar analysis has been carried out previously for a Rubidium Bose gas [53] but the Lithium Bose gas used here is much more strongly interacting and Feshbach resonances allow for the effective interaction strength to be varied. Furthermore, the study discussed in this work uses in-situ absorption images rather than time-of-flight images as in [53].

The analysis of the above three models forms Part II of this work and, as well as facilitating the experimental measurement of the decoherence time, is also expected to inform the BEC community on the validity of the generically used bi-modal model for modelling strongly-interacting Bose gases as well as the effects of the mutual interaction between the condensed and noncondensed components. The experiment is also expected to provide insight into the legitimacy of mean-field theories for modelling strongly interacting Bose gases and thus whether beyond-mean field theories need to be used.

Thesis Outline

The proceeding chapter reviews the theory of phononic excitations of BECs and introduces their principle interaction channels, the Beliaev and Landau interactions. Chapter 2 then treats a single phonon mode as an open quantum system with the environment comprising all the other excitation modes, and the mutual interaction being provided by the Beliaev and Landau interactions. The evolution in time of the density operator of the single phonon mode is then derived in the Born-Markov and secular approximations. Chapter 3 simplifies the description for the evolution of the phonon mode by assuming a Gaussian state. The evolution of the state is then fully defined by the evolution of the entries of a two-dimensional vector called the displacement vector and the covariance matrix. This derived evolution is used in Chapter 4 to estimate the time scales for which phonon states decohere and relax to equilibrium. This is performed for various BEC setups at various temperatures, including setups based on the relativistic GW detector [18] and the ^{6}Li Bose gas that will be used to measure the decoherence time experimentally. Chapters 5-6 then form Part II of this work and consider the experimental investigation into the decoherence time of the strongly-interacting Lithium Bose gas. In particular, Chapter 6 compares the three different models discussed above that can be used to analyse the absorption images of a strongly-interacting Bose gas. Finally, Chapter 7 summarizes the findings and outlines future prospects.

Part I

Theoretical Analysis of the Decoherence of Phonons in BECs

CHAPTER 1

Phonons of Bose-Einstein Condensates

This chapter investigates the dominant interaction channels of the phononic excitations of interacting BECs, which are shown to be the Beliaev and Landau interaction channels. Subsequent chapters will then show that these interactions cause the phonons to decohere. The chapter starts with an introduction to the theory of Bose-Einstein condensation with an analysis of non-interacting Bose gases as in Einstein's original work [54]. Section 1.2 then investigates interacting Bose gases and derives the elementary excitation spectrum for such gases using the Bogoliubov approximation [55]. The dominant interaction channels for these excitations, the Landau and Beliaev processes, are then finally derived in Section 1.3.

1.1 Bose-Einstein Condensation

A BEC is a state of matter in which essentially all the atoms or molecules occupy the same quantum state. Following the work of Bose on the statistics of photons [56], this state of matter was first discovered by Einstein when he considered a gas of non-interacting atoms obeying Bose-Einstein statistics and concluded that a phase transition associated with the condensation of the boson in the lowest-energy state would occur below a certain temperature.

For a system of non-interacting (independent) identical particles the

grand partition function is given by:[1]

$$Z = \prod_i \sum_{\{n_i\}} e^{n_i(\mu-\epsilon_i)/k_BT} \tag{1.1}$$

where ϵ_i are the single-particle eigenstates; T is the temperature; n_i is the number of particles in energy state ϵ_i; $\{n_i\}$ denotes the set of occupation numbers allowed by the symmetry of the particles; and μ is the chemical potential, which can be defined as the amount by which the internal energy of a system will change if you add a particle without changing the system's volume or entropy.

For fermions the Pauli exclusion principle only allows $\{n_i\} = \{0, 1\}$, whereas, for bosons $\{n_i\}$ is any integer number of particles $\{n_i\} \in \mathbb{N}$. The grand partition function for these types of particles is then given by:

$$Z = \prod_i (1 \pm e^{(\mu-\epsilon_i)/k_BT})^{\pm 1} \tag{1.2}$$

and thus the average number of particles in each energy level is:

$$\langle n_i \rangle = \frac{1}{e^{(\epsilon_i-\mu)/k_BT} \pm 1} \tag{1.3}$$

where $+$ is for fermions and $-$ is for bosons. In the limit $(\epsilon - \mu) \gg k_BT$ we just recover the Boltzmann distribution $e^{-(\epsilon-\mu)/k_BT}$. In this case identical particle statistics becomes irrelevant since the density is low (μ is small) and so there are many more states thermally accessible to the particles than there are particles [57].

The distribution function for bosons from (1.3) is called the Bose-Einstein distribution function. This requires that $\mu < \epsilon_0$ for bosons otherwise the states with energy smaller than μ would have negative occupation numbers. As $\mu \to \epsilon_0$ the occupation number for the ground state increases and this is the mechanism behind Bose-Einstein condensation. If the volume and

[1]The term 'particle' is used here to refer to the fundamental constituent of the gas, which could be an atom or molecule depending on the particular gas.

the particle number are fixed, then the chemical potential μ increases towards ϵ_0 as the temperature decreases. At a certain temperature T_c, bosons will begin to fill up the ground state, and this temperature is known as the critical temperature for Bose-Einstein condensation. However, at the low temperature required for Bose-Einstein condensation, the majority of systems will form condensed phases (liquid or solid) because of attractive inter-atomic interactions. Therefore, to achieve Bose-Einstein condensation, conditions are required that facilitate this condensation to occur more rapidly relative to the longer time scales needed for the competing phase changes. Experimental setups that were used to achieve this are discussed in Chapter 5.

Taking the energy of the atoms to be given by $\epsilon_{\boldsymbol{p}} = p^2/2m$, for example, and treating $\boldsymbol{p}$ as continuous, the density of the particles that are not in the condensate is given by:[2]

$$\begin{aligned} n_T &= \int \frac{d\boldsymbol{p}}{(2\pi\hbar)^3} \frac{1}{e^{(\epsilon_p - \mu)/k_B T} - 1} \\ &= \frac{1}{\lambda_T^3} g_{3/2}(z) \end{aligned} \tag{1.4}$$

where $z = e^{\mu/k_B T}$ is the fugacity and $g_a(z)$ is the defined by:

$$g_a(z) = \sum_{l=1}^{\infty} \frac{z(\boldsymbol{r})^l}{l^a}. \tag{1.5}$$

In (1.4) λ_T is the thermal de Broglie wavelength, which is can be considered to be the average de Broglie wavelength of the gas particles in an ideal gas:

$$\lambda_T = h/p = \frac{h}{\sqrt{2m\epsilon_p}} = \sqrt{\frac{2\pi\hbar^2}{mk_B T}} \tag{1.6}$$

using the fact that the effective kinetic energy of free particles is $\pi k_B T$.

Defining $n_c := n_T(\mu = 0)$, Bose-Einstein condensation will occur when $n_c < n$ where $n = N/V$ is the density of the gas with N the total num-

[2]For a walk-through of this derivation see e.g. [48, 58].

ber of particles. Thus, Bose-Einstein condensation will take place when the thermal de Broglie wavelength λ_T becomes comparable to the average separation between particles such that the quantum mechanical wave nature of the particles leads to all atoms becoming increasingly correlated, eventually forming a coherent quantum superposition.

1.2 Bose-Einstein Condensation in Interacting Gases

The previous Section considered Bose-Einstein condensation in an ideal gas. However, although interactions were not explicitly included in the formulations, it was assumed that the gas is in thermal equilibrium, which cannot be achieved in a completely non-interacting system. This section reviews Bose-Einstein condensation in interacting Bose gases paying particular attention to the derivation of phonon-like excitations in the so-called Bogoliubov approximation.

Investigations into the theory of Bose-Einstein condensation in weakly interacting BECs was sparked by the discovery of superfluity in liquid helium, which was shortly considered to be associated with Bose-Einstein condensation by London [59]. An alternative explanation for superfluidity was then subsequently offered by Landau who used elementary excitations without reference to condensation [60]. These two seemingly contrasting theories were later unified by Bogoliubov when he derived the elementary excitation spectrum for an interacting Bose gas undergoing Bose-Einstein condensation [55], which approximated to a phonon-like spectrum for the low-energy excitations. This theory was subsequently extended to liquid Helium by Feynman in 1955 [61] and lead to a period of intensive study of interacting Bose-condensed systems. Following the result of several decades of research and the advent of laser cooling, atomic traps, and evaporative cooling [62], Bose-Einstein condensation in interacting Bose gases was finally demonstrated experimentally for the first time in 1995 using the alkali atoms Rubidium [63], Sodium [64] and Lithium [65], which has lead to an explosion of interest in these systems both theoretically and experimentally.

Here the theory of interacting Bose-condensed fluids is formulated in

terms of quantum field operators, which is the approach that was first initiated by Bogoliubov in 1947 [55]. In position space, the quantum field operators are $\hat{\psi}^\dagger(\boldsymbol{r})$ and $\hat{\psi}(\boldsymbol{r})$ where the former creates a particle at position $\boldsymbol{r}$ and the latter annihilates a particle at position $\boldsymbol{r}$. For a Bose gas these quantum field operators satisfy the usual Bose-commutation relation:

$$[\hat{\psi}(\boldsymbol{r}), \hat{\psi}^\dagger(\boldsymbol{r})] = \delta(\boldsymbol{r} - \boldsymbol{r}') \tag{1.7}$$

where $\delta(\boldsymbol{r})$ is the Dirac delta function.

Under the assumption that the gas is rarefied, only two-body interactions need to be considered since interactions involving three or more particles are very rare and so can be safely neglected. This is possible because, by definition, the range of inter-atomic forces is much smaller than the average distance between the particles in these gases. For example, the alkali systems that were used in the first Bose-Einstein condensation experiments were around 10^4 less dense than air even at there densest points. The quantum field Hamiltonian for a rarefied Bose gas can then be written as:

$$\begin{aligned}\hat{H} = \int d\boldsymbol{r}\hat{\psi}^\dagger(\boldsymbol{r})\Big[-\frac{\hbar^2}{2m}\nabla^2 + \mathcal{V}(\boldsymbol{r})\Big]\hat{\psi}(\boldsymbol{r}) \\ + \frac{1}{2}\int d\boldsymbol{r}d\boldsymbol{r}'\hat{\psi}^\dagger(\boldsymbol{r})\hat{\psi}^\dagger(\boldsymbol{r}')\mathcal{U}(\boldsymbol{r}' - \boldsymbol{r})\hat{\psi}(\boldsymbol{r})\hat{\psi}(\boldsymbol{r}')\end{aligned} \tag{1.8}$$

where $\mathcal{U}(\boldsymbol{r})$ is the two-body potential and $\mathcal{V}(\boldsymbol{r})$ is the external potential. For a uniform gas occupying a box of volume $V = L^3$, with cyclic boundary conditions, the solutions are plane-waves:

$$\hat{\psi}(\boldsymbol{r}) = \frac{1}{\sqrt{V}}\sum_{\boldsymbol{p}} \hat{a}_{\boldsymbol{p}} e^{i\boldsymbol{p}.\boldsymbol{r}/\hbar} \tag{1.9}$$

where $\hat{a}_{\boldsymbol{p}}$ is the operator that annihilates a particle in the single-particle state with momentum $\boldsymbol{p}$, which is given in discrete units such that $\boldsymbol{p} = 2\pi\hbar\boldsymbol{n}/L$ where $\boldsymbol{n}$ is a vector with components n_x, n_y, $n_z \in \mathbb{N}$. Substituting (1.9) into (1.8), the Hamiltonian of a uniform Bose gas in a volume V is

then found to be:

$$\hat{H} = \sum_{\boldsymbol{p}} \frac{p^2}{2m} \hat{a}^\dagger_{\boldsymbol{p}} \hat{a}_{\boldsymbol{p}} + \frac{1}{2V} \sum_{\boldsymbol{p},\boldsymbol{p}',\boldsymbol{q}} \mathcal{U}_{\boldsymbol{q}} \hat{a}^\dagger_{\boldsymbol{p}+\boldsymbol{q}} \hat{a}^\dagger_{\boldsymbol{p}'-\boldsymbol{q}} \hat{a}_{\boldsymbol{p}'} \hat{a}_{\boldsymbol{p}} \tag{1.10}$$

where $\mathcal{U}_{\boldsymbol{q}}$ is the Fourier transform of $\mathcal{U}(\boldsymbol{r})$.

1.2.1 Bogliubov Quasi-Particles

Assuming that the condensate is macroscopically occupied, $\hat{a}_0$ and $\hat{a}^\dagger_0$ can be replaced with their approximate classical expectation value $\sqrt{N_0}$ where N_0 is the average occupation of the ground state $N_0 = \langle \hat{a}^\dagger_0 \hat{a}_0 \rangle$.[3] This was first used by Bogoliubov [55] and is equivalent to ignoring the non-commutativity of the operators and treating them classically. Separating out the condensate component a_0 from the non-condensate components $\hat{a}_{\boldsymbol{p}\neq 0}$ so that:

$$\sum_{\boldsymbol{p}} \hat{a}_{\boldsymbol{p}} = \hat{a}_0 + \sum_{\boldsymbol{p}\neq 0} \hat{a}_{\boldsymbol{p}}, \tag{1.11}$$

the Hamiltonian (1.10) can then be written as:

$$\hat{H} = \hat{H}_0 + \hat{H}^I_2 + \hat{H}^I_3 + \hat{H}^I_4 \tag{1.12}$$

where [66]:

$$\hat{H}_0 := \sum_{\boldsymbol{p}} \frac{p^2}{2m} \hat{a}^\dagger_{\boldsymbol{p}} \hat{a}_{\boldsymbol{p}} + \frac{\mathcal{U}_0}{2V} \hat{a}^\dagger_0 \hat{a}^\dagger_0 \hat{a}_0 \hat{a}_0, \tag{1.13}$$

$$\hat{H}^I_2 := \frac{1}{2V} \sum_{\boldsymbol{p}\neq 0} \Big(\mathcal{U}_{\boldsymbol{p}} a^\dagger_0 a^\dagger_0 \hat{a}_{\boldsymbol{p}} \hat{a}_{-\boldsymbol{p}} + \mathcal{U}_{\boldsymbol{p}} \hat{a}^\dagger_{\boldsymbol{p}} \hat{a}^\dagger_{-\boldsymbol{p}} a_0 a_0 + 2(\mathcal{U}_{\boldsymbol{p}} + \mathcal{U}_0) \hat{a}^\dagger_{\boldsymbol{p}} a^\dagger_0 \hat{a}_{\boldsymbol{p}} a_0 \Big), \tag{1.14}$$

$$\hat{H}^I_3 := \frac{1}{V} \sum_{\boldsymbol{p},\boldsymbol{p}'\neq 0} \mathcal{U}_{\boldsymbol{p}} \Big(a^\dagger_0 \hat{a}^\dagger_{\boldsymbol{p}+\boldsymbol{p}'} \hat{a}_{\boldsymbol{p}'} \hat{a}_{\boldsymbol{p}} + \hat{a}^\dagger_{\boldsymbol{p}'} \hat{a}^\dagger_{\boldsymbol{p}} a_0 \hat{a}_{\boldsymbol{p}+\boldsymbol{p}'} \Big), \tag{1.15}$$

$$\hat{H}^I_4 := \frac{1}{2V} \sum_{\boldsymbol{p},\boldsymbol{p}',\boldsymbol{q}\neq 0} \mathcal{U}_{\boldsymbol{q}} \hat{a}^\dagger_{\boldsymbol{p}+\boldsymbol{q}} \hat{a}^\dagger_{\boldsymbol{p}'-\boldsymbol{q}} \hat{a}_{\boldsymbol{p}'} \hat{a}_{\boldsymbol{p}}. \tag{1.16}$$

[3] That is, $\hat{a}^\dagger_0 |N_0\rangle = \sqrt{N_0 - 1} |N_0 - 1\rangle \approx \sqrt{N_0} |N_0\rangle$, for example, since $N_0 \gg 1$.

Note that there is no $\hat{H}_1$ term since that would violate conservation of momentum. The interaction terms involving the condensate and non-condensate modes in $\hat{H}_2^I$, $\hat{H}_3^I$ and $\hat{H}_4^I$ are illustrated in Figure 1.1, and $\hat{H}_3^I$ will be considered in detail in Section 1.3. Since $a_0 \approx a_0^\dagger \approx \sqrt{N_0} \gg 0$, then $\hat{H}_2^I \gg \hat{H}_3^I \gg \hat{H}_4^I$, and in this Section we will ignore the more suppressed terms $\hat{H}_3^I$ and $\hat{H}_4^I$, which is the basic assumption that leads to the so-called Bogoliubov model.

For Bose-Einstein condensation to occur, the temperature must be smaller than the critical temperature as discussed Section 1.1. Therefore, only low-momentum calculations need to be considered and the short-wavelength degrees of freedom of the two-body interaction, which reflect the correlations between the two particles, can be integrated out. The exact shape of the inter-particle potential can then be ignored and we are left with an effective interaction to which perturbation theory can be safely applied. Furthermore, since only small momenta are involved, only the $\boldsymbol{p} = 0$ value of the Fourier transform is allowed to be considered [48]. Therefore, under the above assumptions, (1.12) simplifies to:

$$\hat{H} = \sum_{\boldsymbol{p}} \frac{p^2}{2m} \hat{a}_{\boldsymbol{p}}^\dagger \hat{a}_{\boldsymbol{p}} + \frac{\mathcal{U}_0}{2V} \hat{a}_0^\dagger \hat{a}_0^\dagger \hat{a}_0 \hat{a}_0 + \frac{\mathcal{U}_0}{2V} \sum_{\boldsymbol{p} \neq 0} \left(4 \hat{a}_{\boldsymbol{p}}^\dagger \hat{a}_0^\dagger \hat{a}_{\boldsymbol{p}} \hat{a}_0 + \hat{a}_0^\dagger \hat{a}_0^\dagger \hat{a}_{\boldsymbol{p}} \hat{a}_{-\boldsymbol{p}} + \hat{a}_{\boldsymbol{p}}^\dagger \hat{a}_{-\boldsymbol{p}}^\dagger \hat{a}_0 \hat{a}_0 \right) \tag{1.17}$$

where:

$$\mathcal{U}_0 = \int \mathcal{U}_{\text{eff}}(r) d\boldsymbol{r}. \tag{1.18}$$

For the third term, $\hat{a}_0$ and $\hat{a}_0^\dagger$ can be replaced with $\sqrt{N}$ using the approximation that $N_0 \sim N$. However, for the other term involving $\hat{a}_0$ and $\hat{a}_0^\dagger$, higher accuracy is required using the normalization relation $\hat{a}^\dagger \hat{a}_0 + \sum_{\boldsymbol{p} \neq 0} \hat{a}_{\boldsymbol{p}}^\dagger \hat{a}_{\boldsymbol{p}} = N$ so that, neglecting higher order effects, the term can be replaced with [48]:

$$\hat{a}_0^\dagger \hat{a}_0^\dagger \hat{a}_0 \hat{a}_0 = N^2 - 2N \sum_{\boldsymbol{p} \neq 0} \hat{a}_{\boldsymbol{p}}^\dagger \hat{a}_{\boldsymbol{p}}. \tag{1.19}$$

To lowest order in perturbation theory, $\mathcal{U}_0$ is given by the Born approximation $\mathcal{U}_0 = g$ where g is the interaction coupling constant, which is defined in terms of the s-wave scattering length a that characterizes the interactions:

$$g = \frac{4\pi\hbar^2 a}{m}. \tag{1.20}$$

However, to ensure a convergent result for the ground state energy, one must go to the next order in perturbation theory where [48, 67]:

$$\mathcal{U}_0 = g + \frac{g^2}{V}\sum_{\boldsymbol{p}\neq 0}\frac{m}{p^2}. \tag{1.21}$$

Substituting (1.19) and (1.21) into (1.17), and neglecting terms that are suppressed by fewer powers of N, the Hamiltonian for the Bose gas is then given by:

$$\hat{H} = \frac{N^2 g}{2V} + \sum_{\boldsymbol{p}\neq 0}\frac{p^2}{2m}\hat{a}^\dagger_{\boldsymbol{p}}\hat{a}_{\boldsymbol{p}} + \frac{ng}{2}\sum_{\boldsymbol{p}\neq 0}\Big(2\hat{a}^\dagger_{\boldsymbol{p}}\hat{a}_{\boldsymbol{p}} + \hat{a}^\dagger_{\boldsymbol{p}}\hat{a}^\dagger_{-\boldsymbol{p}} + \hat{a}_{\boldsymbol{p}}\hat{a}_{-\boldsymbol{p}} + \frac{mgn}{p^2}\Big). \tag{1.22}$$

This Hamiltonian can be diagonalized by applying the following Bogoliubov transformation:

$$\hat{a}_{\boldsymbol{p}} := u_p\hat{b}_{\boldsymbol{p}} + v_p\hat{b}^\dagger_{-\boldsymbol{p}}, \tag{1.23}$$

$$\hat{a}^\dagger_{-\boldsymbol{p}} := u_p\hat{b}^\dagger_{-\boldsymbol{p}} + v_p\hat{b}_{\boldsymbol{p}}. \tag{1.24}$$

where:

$$u_p, v_p := \pm\Big(\frac{p^2/2m + gn}{2\epsilon(p)} \pm \frac{1}{2}\Big)^{\frac{1}{2}} \tag{1.25}$$

and the operators $\hat{b}^\dagger_{\boldsymbol{p}}$, $\hat{b}_{\boldsymbol{p}}$ obey the Bose commutation relations $[\hat{b}_{\boldsymbol{p}}, \hat{b}^\dagger_{\boldsymbol{p}'}] = \delta_{\boldsymbol{p},\boldsymbol{p}'}$ where $\delta_{\boldsymbol{p},\boldsymbol{p}'}$ is the Kronecker delta.

In this new basis, (1.22) becomes:

$$\hat{H} = \epsilon_0 + \sum_{\boldsymbol{p}\neq 0} \epsilon_p \hat{b}^\dagger_{\boldsymbol{p}} \hat{b}_{\boldsymbol{p}} \tag{1.26}$$

where:[4]

$$\epsilon_0 := \frac{gN^2}{2V} + \frac{1}{2}\sum_{\boldsymbol{p}\neq 0}\Big(\epsilon_p - gn - \frac{p^2}{2m} + \frac{m(gn)^2}{p^2}\Big), \tag{1.28}$$

$$\epsilon_p := \sqrt{c_s^2 p^2 + \Big(\frac{p^2}{2m}\Big)^2}, \tag{1.29}$$

$$c_s := \sqrt{\frac{gn}{m}}. \tag{1.30}$$

The Hamiltonian (1.26) describes a system of independent quasi-particles whose creation and annihilation operators are $\hat{b}^\dagger_{\boldsymbol{p}}$ and $\hat{b}_{\boldsymbol{p}}$, and whose energy-momentum relation is given by (1.29) where c_s is the speed of sound, and the ground-state energy of the system is ϵ_0.[5] Therefore, by a simple change of basis, we have gone from an interacting system of particles described by (1.22) to a non-interacting system of quasi-particles described by (1.26).

For small momenta $p \ll mc_s$, the dispersion law of the quasi-particles from (1.29) is that of phonons $\omega_p = c_s k$ where $\epsilon_p = \hbar\omega_p$ and $p = \hbar k$. The long-wavelength quasi-particles are, therefore, phonons. In this regime $u_p \sim v_p \sim \sqrt{mc_s/2p}$ and so, from calculating $\langle \hat{b}^\dagger_{\boldsymbol{p}} \hat{b}_{\boldsymbol{p}} \rangle$, the phonons can be thought of as composed of approximately the same number of particles moving in the quasi-particle direction as those moving in the opposite direction [69]. On the other hand, for high momenta $p \gg mc_s$ the dispersion law approximates to $p^2/2m + gn$ and the quasi-particles behave like free particles. Therefore, in summary, for a Bose gas in thermal equilibrium, at high temperatures

[4]The quasi-particle ground-state energy ϵ_0 can be calculated by replacing the sum with an integral in momentum space giving [68]:

$$\epsilon_0 = g\frac{N^2}{2V}\Big(1 + \frac{128}{15\sqrt{\pi}}\sqrt{na^3}\Big). \tag{1.27}$$

[5]These quasi-particles can be thought of as squeezed momentum eigenstates since, from (1.23), they are squeezed combinations of opposite momenta states.

(but lower than the critical temperature) the excitations behave like free particles, whereas, for low temperatures, phononic excitations dominate.

Since the quasi-particles are non-interacting we have an ideal gas of quasi-particles, and so their average occupation $N_{\boldsymbol{p}}$ is simply:

$$N_{\boldsymbol{p}} := \langle \hat{b}^\dagger_{\boldsymbol{p}} \hat{b}_{\boldsymbol{p}} \rangle = \frac{1}{e^{\beta_p} - 1} \tag{1.31}$$

where $\beta_p := \hbar\omega_p / k_B T$. Note that the addition of a quasi-particle does not change the total particle number and so $\mu = 0$. Consequently, there is no occupation of quasi-particle modes at zero temperature since there is no $p = 0$ mode by definition. However, this does not mean that the condensate is fully occupied at absolute zero since, using (1.23)-(1.24), $\langle \hat{a}^\dagger_{\boldsymbol{p}} \hat{a}_{\boldsymbol{p}} \rangle$ is given by:

$$\langle \hat{a}^\dagger_{\boldsymbol{p}} \hat{a}_{\boldsymbol{p}} \rangle = |u_p|^2 \langle \hat{b}^\dagger_{\boldsymbol{p}} \hat{b}_{\boldsymbol{p}} \rangle + |v_p|^2 [1 + \langle \hat{b}^\dagger_{-\boldsymbol{p}} \hat{b}_{-\boldsymbol{p}} \rangle] \tag{1.32}$$

and so, at absolute zero, $\langle \hat{a}^\dagger_{\boldsymbol{p}} \hat{a}_{\boldsymbol{p}} \rangle = |v_p|^2$. The condensate is therefore depleted at zero temperature due to the interactions in the gas.

1.3 Quasi-Particle Interactions

The previous section considered an interacting Bose gas in the Bogoliubov approximation where the elementary excitations can be described by non-interacting quasi-particles which, therefore, have infinite lifetimes. However, in this approximation only terms that are at most quadratic in $\hat{a}_{\boldsymbol{p}}$ and $\hat{a}^\dagger_{\boldsymbol{p}}$ were represented in the Hamiltonian since $\hat{H}^I_3$ and $\hat{H}^I_4$ in (1.12) were neglected. If the terms that are cubic and quartic in $\hat{a}_{\boldsymbol{p}}$ and $\hat{a}^\dagger_{\boldsymbol{p}}$ are re-introduced then, after the Bogoliubov transformation (1.23), these terms will provide interactions between the quasi-particles, resulting in finite lifetimes. Since the terms from $\hat{H}^I_4$ are suppressed relative to the terms from $\hat{H}^I_3$, only the latter terms will be examined here. For a single quasi-particle momentum mode $\boldsymbol{q}$, these terms result in the following interaction Hamil-

tonian [26, 27, 70]:

$$\hat{H}_I = \hat{b}_{\boldsymbol{q}}\hat{Q}^\dagger + \hat{b}^\dagger_{\boldsymbol{q}}\hat{Q} \tag{1.33}$$

where:

$$\hat{Q} := \hat{A} + \hat{B} + \hat{L}, \tag{1.34}$$

$$\hat{A}^\dagger := g\sqrt{\frac{n}{V}} \sum_{\boldsymbol{p},\boldsymbol{p}'\neq\{\boldsymbol{0},\boldsymbol{q}\}} \mathcal{A}_{p,p'}\hat{b}_{\boldsymbol{p}}\hat{b}_{\boldsymbol{p}'}\delta_{-\boldsymbol{q},\boldsymbol{p}+\boldsymbol{p}'}, \tag{1.35}$$

$$\hat{B}^\dagger := g\sqrt{\frac{n}{V}} \sum_{\boldsymbol{p},\boldsymbol{p}'\neq\{\boldsymbol{0},\boldsymbol{q}\}} \mathcal{B}_{p,p'}\hat{b}^\dagger_{\boldsymbol{p}}\hat{b}^\dagger_{\boldsymbol{p}'}\delta_{\boldsymbol{q},\boldsymbol{p}+\boldsymbol{p}'}, \tag{1.36}$$

$$\hat{L}^\dagger := g\sqrt{\frac{n}{V}} \sum_{\boldsymbol{p},\boldsymbol{p}'\neq\{\boldsymbol{0},\boldsymbol{q}\}} \mathcal{L}_{p,p'}\hat{b}_{\boldsymbol{p}}\hat{b}^\dagger_{\boldsymbol{p}'}\delta_{\boldsymbol{q},\boldsymbol{p}'-\boldsymbol{p}}, \tag{1.37}$$

$$\begin{aligned}\mathcal{A}_{p,p'} :=\ & u_q(v_pv_{p'} + u_pv_{p'} + v_pu_{p'}) \\ & + v_q(u_pv_{p'} + v_pu_{p'} + u_pu_{p'}),\end{aligned} \tag{1.38}$$

$$\begin{aligned}\mathcal{B}_{p,p'} :=\ & u_q(u_pu_{p'} + v_pu_{p'} + u_pv_{p'}) \\ & + v_q(v_pv_{p'} + v_pu_{p'} + u_pv_{p'}),\end{aligned} \tag{1.39}$$

$$\begin{aligned}\frac{1}{2}\mathcal{L}_{p,p'} :=\ & u_q(v_pu_{p'} + u_pu_{p'} + v_pv_{p'}) \\ & + v_q(u_pv_{p'} + u_pu_{p'} + v_pv_{p'}).\end{aligned} \tag{1.40}$$

Note that $\hat{Q}^\dagger$ and $\hat{Q}$ are operators acting on the Hilbert space of the rest of the quasi-particles but they are not, in general, creation and annihilation operators since $[\hat{Q}, \hat{Q}^\dagger] \neq 1$ unless further approximations are made (see [71] for an idea of the approximations that need to be assumed).

The resonant interactions $\hat{b}_{\boldsymbol{q}}\hat{L}^\dagger$ and $\hat{b}_{\boldsymbol{q}}\hat{B}^\dagger$ are the well-known Landau and Beliaev interactions [26]. In the Landau process $\hat{b}_{\boldsymbol{q}}\hat{L}^\dagger$, a quasi-particle from the mode $\boldsymbol{q}$ collides with a quasi-particle from another mode to create a higher-energy quasi-particle. Since this requires the thermal occupation of

a quasi-particle mode, the process vanishes at zero temperature. On the other hand, in the Beliaev process $\hat{b}_{\boldsymbol{q}}\hat{B}^{\dagger}$, a quasi-particle of mode $\boldsymbol{q}$ spontaneously annihilates into two new quasi-particles with lower energies, which is analogous to parametric down-conversion in quantum optics [72] and can occur at absolute zero.[6] Both these processes are illustrated in Figure 1.2. Since the processes originate from $\hat{H}_3^I$, they can also be considered from the point-of-view of four-body interactions between the condensate and the thermal cloud, which are illustrated in Figure 1.1.

If a phonon mode is excited out of equilibrium then these interaction processes will damp the excitation back to equilibrium with the rest of the Bose gas. This has been demonstrated in various experiments [73] and the damping rate has been measured. For example, in [74, 75], the observed damping is consistent with the theory of Landau damping [26], which will be derived in the next chapter. The time it takes for the excited phonon mode to be damped (relax back to equilibrium) sets an upper limit for the decoherence time of the mode [32]. However, the actual decoherence time could be much smaller, as will be demonstrated in the subsequent chapters.

1.4 Summary

This chapter has derived the dominant interaction channels for phonic excitations of a BEC, which are the Beliaev and Landau interaction processes. The next chapter will investigate a framework for describing how excited phonon states will evolve in time due to these Landau and Beliaev interactions with the other quasi-particle modes. This will then be simplified in Chapter 3 and used in Chapter 4 to estimate the decoherence and relaxation times of the phonons.

[6] However, it should be noted that, due to the discretization of energy levels in trapping potentials, the Beliaev process is not active for the lowest energy modes, unlike in the uniform systems considered here.

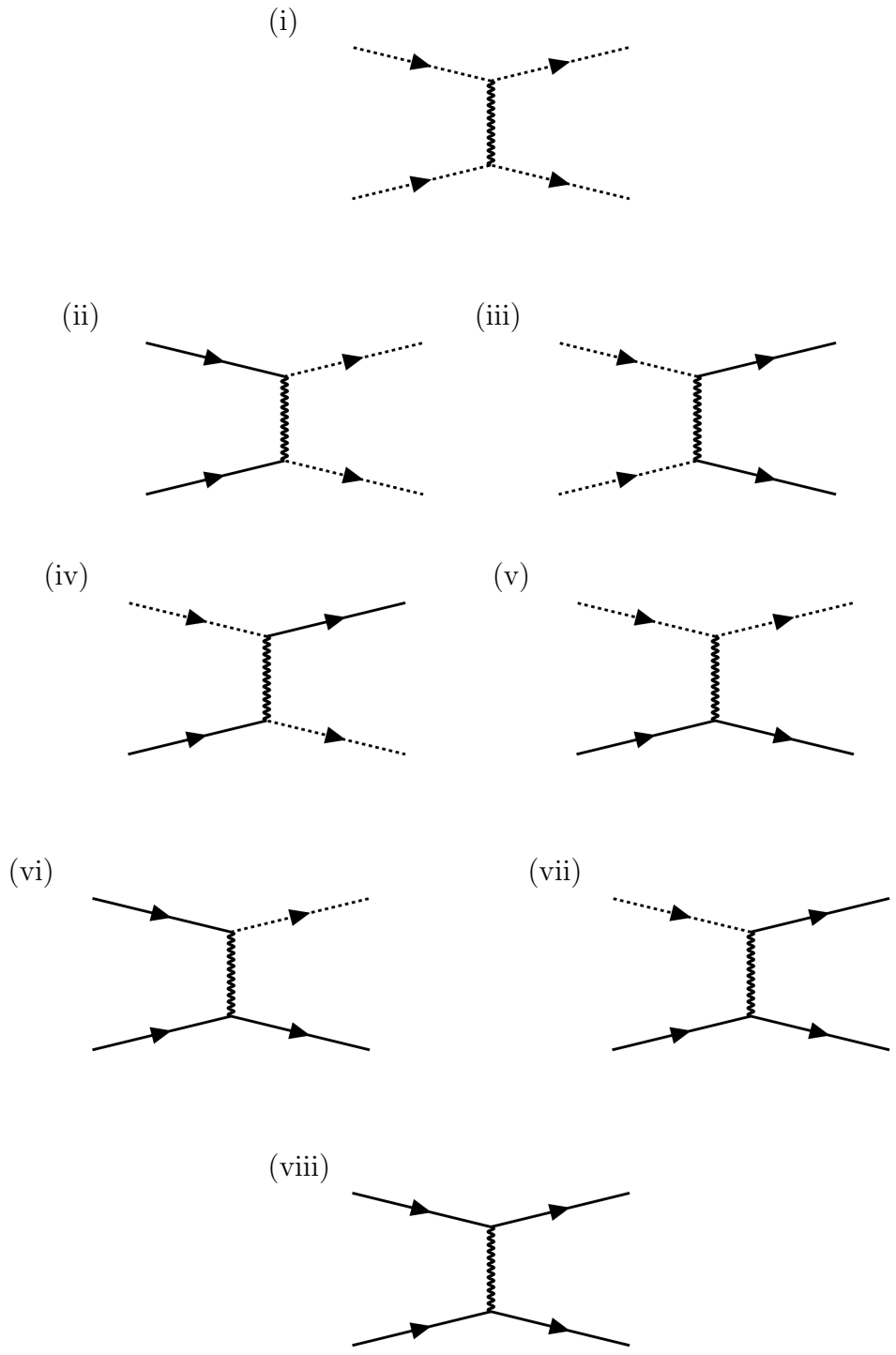

Figure 1.1: These vertex diagrams represent the interaction terms in the Hamiltonian (1.12) [66]. The dashed lines correspond to a condensate particle, the solid line refers to a noncondensate particle, and the wavy line denotes the interaction. Diagram (i) describes the interaction term in (1.13), (ii)-(v) correspond to the interaction terms in (1.14), (vi)-(vii) refer to the interaction terms in (1.15), and (viii) denotes the interaction term (1.16). Note that in a normal, noncondensed, system only (viii) is present.

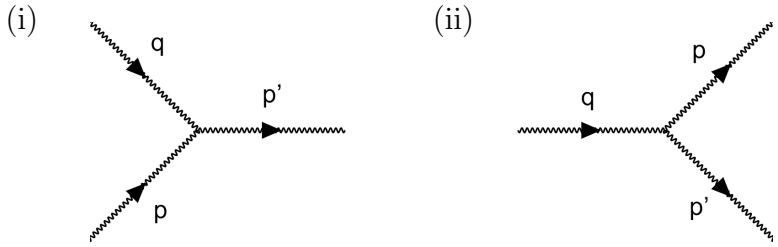

Figure 1.2: These vertex diagrams represent the on-resonance quasi-particle interaction terms in (1.33). Diagram (i) describes the Landau interaction whereas (ii) corresponds to the Beliaev interaction.

CHAPTER 2

Phonons as Open Quantum Systems

The previous chapter investigated a theoretical description of phonons of BECs from a microscopic point-of-view and derived the expected dominant interaction processes for a single phonon mode, which are the Landau and Beliaev interaction processes. How these interaction processes affect the time evolution of a phonon mode that has been taken out of equilibrium with the rest of the quasi-particle modes is the subject of this chapter, and subsequent chapters will use this to determine how quickly the phonon mode decoheres.

The framework used to calculate the time evolution of the state is that of open quantum systems. Absolute isolation of a quantum system from its surroundings, which is called its environment, is not possible and a complete description of the environment is impractical since it is typically composed of an extremely large number of degrees of freedom. All quantum systems are, therefore, essentially open systems. This is of greater fundamental importance than in classical mechanics given the entirely nonclassical phenomenon of entanglement, where widely spatially separated systems can still be highly correlated, and the measurement process. Furthermore, due to the much greater size of space that quantum calculations are performed in compared to classical mechanics, even if it were possible to completely describe the environment, this would present an intractable amount of information. The theory of open quantum systems is therefore essential to many applications of quantum physics, as well as fundamental questions.

In this theory the lack of knowledge about the environment is expressed

by averaging (mathematically tracing) over the possible states of its degrees of freedom. In contrast to the case of an idealized closed quantum system, this generically results in a non-unitary evolution of the open quantum system, with only the combined system obeying the unitary evolution of a closed system. This theory and how it is applied to the phononic excitations of a BEC will be discussed in greater detail in the following sections.

To begin with, Section 2.1 reviews the mathematics of closed quantum systems, which obey unitary dynamics. Section 2.2 then moves to the theory of open quantum systems and considers the time evolution of a general open quantum system in the Born-Markov approximation, which represents the simplest case of the dynamics of open quantum systems and provides a first-order linear differential equation for the open system known as the quantum Markovian master equation in Lindblad form. Section 2.3 then applies this general theory to the specific case that is of interest to this work, a phonon mode of a BEC, where the environment of this open quantum system is taken to be all the other quasi-particle modes (which could be empty). This results in a description of the time evolution of a phonon mode due to the Landau and Beliaev interactions with the rest of the quasi-particle modes, which is then further simplified in Chapter 3.

2.1 Evolution of a Closed Quantum System

In non-relativistic quantum mechanics the state vector $|\psi(t)\rangle$ of a closed quantum state evolves in time according to the Schrödinger equation:

$$i\hbar\frac{d}{dt}|\psi(t)\rangle = \hat{H}(t)|\psi(t)\rangle \tag{2.1}$$

where $\hat{H}(t)$ is the Hamiltonian of the closed system. The solution of this equation can be expressed as:

$$|\psi(t)\rangle = \hat{U}(t)|\psi(0)\rangle \tag{2.2}$$

where $\hat{U}(t)$ is a unitary time-evolution operator which, for a general time-dependent Hamiltonian is given by:[1]

$$\hat{U}(t) = \underset{\leftarrow}{T} e^{-\frac{1}{\hbar}\int_0^t \hat{H}(t')dt'} \tag{2.3}$$

where $\underset{\leftarrow}{T}$ is the time-ordering operator. If the Hamiltonian is time-independent then the unitary time-evolution operator is simply $\hat{U}(t) = e^{-i\hat{H}t/\hbar}$.

If the closed quantum system is a statistical ensemble of several quantum states, a mixed state, then the density operator $\hat{\rho}$ provides a useful means of characterizing the system and has an analogy with the phase-space probability measure in classical statistical mechanics. In this case there is not enough information to specify the state vector and only the probabilities p_i that the system is in a normalized state $|\psi_i\rangle$ are known. The density operator $\hat{\rho}$ is then defined as:

$$\hat{\rho} := \sum_i p_i |\psi_i\rangle\langle\psi_i| \tag{2.4}$$

where $\sum_i p_i = 1$. Note that, with this definition, the expectation value of a quantum operator $\hat{O}$ acting on the system can be expressed as:

$$\langle\hat{O}\rangle = \sum_i p_i \langle\psi_i|\hat{O}|\psi_i\rangle = \mathrm{Tr}(\hat{\rho}\hat{O}). \tag{2.5}$$

From the evolution of the state vectors (2.2), the density operator for a closed quantum system evolves in time as:

$$\hat{\rho}(t) = \hat{U}(t)\hat{\rho}(0)\hat{U}^\dagger(t), \tag{2.6}$$

$$\implies \frac{d}{dt}\hat{\rho}(t) = -\frac{i}{\hbar}[\hat{H}(t), \hat{\rho}(t)]. \tag{2.7}$$

The latter equation (2.7) is the von Neumann equation and can be writ-

[1]For example, the Hamiltonian could be time-dependent if the system is driven by a time-dependent external potential $V(t)$. In this case the system is still said to be 'closed' but not 'isolated'.

ten in a form that is analogous to the classical Liouville equation, which is the equation of motion for the probability density in classical statistical mechanics (see e.g. [32]).

2.2 Evolution of an Open Quantum System

An open quantum system can be considered as a subsystem of a larger closed quantum system that consists of the open quantum system and another quantum system called the environment which it couples to. The Hamiltonian of the full system $\hat{H}$ can then be represented as:

$$\hat{H} = \hat{H}_S \otimes \hat{I}_E + \hat{I}_S \otimes \hat{H}_E + \hat{H}_I \tag{2.8}$$

where $\hat{H}_S$ is the open system's free Hamiltonian and acts in the Hilbert space $\mathcal{H}_S$; $\hat{H}_E$ is the free Hamiltonian of the environment and acts in the Hilbert space $\mathcal{H}_E$; $\hat{I}_S$ and $\hat{I}_E$ are identity operators for the spaces $\mathcal{H}_S$ and $\mathcal{H}_E$ respectively; and $\hat{H}_I$ is the Hamiltonian that describes the interaction between the system and the environment and acts in the full space $\mathcal{H}_S \otimes \mathcal{H}_E$. From now on the identity operators will be suppressed, in which case the full system's Hamiltonian is simply written as:

$$\hat{H} = \hat{H}_S + \hat{H}_E + \hat{H}_I. \tag{2.9}$$

Since it is a closed system, the density operator of the full system $\hat{\rho}$ evolves via the von Neumann equation (2.7), which is greatly simplified by transforming to the interaction picture. In this picture the density operator of the full system $\tilde{\rho}$ transforms as:

$$\frac{d}{dt}\tilde{\rho}(t) = -\frac{i}{\hbar}[\tilde{H}_I(t), \tilde{\rho}(t)] \tag{2.10}$$

where the interaction picture operators, which are denoted by tildes rather than hats, are defined as:

$$\tilde{\rho}(t) := e^{i\hat{H}_0 t/\hbar}\hat{\rho}(t)e^{-i\hat{H}_0 t/\hbar}, \tag{2.11}$$

$$\tilde{H}_I(t) := e^{i\hat{H}_0 t/\hbar}\hat{H}_I(t)e^{-i\hat{H}_0 t/\hbar} \tag{2.12}$$

and $\hat{H}_0 := \hat{H}_S + \hat{H}_E$, which is assumed to be independent of time. The generically rapid motion generated by $\hat{H}_0$ has therefore been separated out from the slow motion induced by $\hat{H}_I$.

The time evolution of the full system's density operator can be obtained from (2.10). However, we are only interested in the dynamics of the open quantum system S and not of the environment. To achieve this we can average over the possible states of the environmental degrees of freedom. This is equivalent to tracing over the environmental degrees of freedom in the full system's density operator, which leaves behind the so-called reduced density operator of the system $\hat{\rho}_S := \mathrm{Tr}_E\hat{\rho}$. All information that can be extracted by an observer analysing the open system is then contained in its reduced density operator (assuming that the Born rule for quantum probabilities holds). For example, for an observable acting on the open system's Hilbert space, its expectation value is given by:

$$\langle\hat{O}\rangle = \mathrm{Tr}_S(\hat{O}\hat{\rho}_S) \tag{2.13}$$

where $\hat{O}$ is an operator acting on the Hilbert space $\mathcal{H}_S$. The reduced density operator is therefore the quantity that we are most interested in determining as a description of the open quantum system. It does not really represent the state of the open system as that is intimately tied up with the environment, but it is a useful calculational tool for computing the probability distribution for the set of possible outcomes of general measurements on the open system.

The evolution of the reduced density operator (in the interaction picture) can then be calculated from the evolution of the full system's density

operator (2.10):

$$\frac{d}{dt}\tilde{\rho}_S(t) = -\frac{i}{\hbar}\mathrm{Tr}_E[\tilde{H}_I(t), \tilde{\rho}(t)]. \tag{2.14}$$

The dynamics of the reduced system introduced by this equation can, in general, be quite complex. The next sections consider certain approximations that can be made such that the above exact equation for the reduced density can be simplified into a first-order linear differential equation, which is known as the quantum Markovian master equation in Lindblad form. This equation can be derived from purely algebraic means by simply assuming that the density operator evolves under the action of the generator of a quantum dynamical semi-group (see e.g. [32]). However, this approach doesn't appeal to the underlying Hamiltonian dynamics to determine under which physical assumptions the density operator can evolve in this way. The next sections take this latter approach of starting with the underlying Hamiltonian dynamics and then considering what physical assumptions need to be made in order to derive a quantum Markovian master equation in Lindblad form for a general system, and thus a generator of the quantum dynamical semi-group.

2.2.1 The Born Approximation

The master equation for the full system's density operator in the interaction picture (2.10) can be integrated to obtain:

$$\tilde{\rho}(t) = \hat{\rho}(0) - \frac{i}{\hbar}\int_0^t [\tilde{H}_I(t'), \tilde{\rho}(t')]dt'. \tag{2.15}$$

Iterating this solution then results in [30]:

$$\tilde{\rho}(t) = \hat{M}(t)\tilde{\rho}(0) \tag{2.16}$$

where:

$$\hat{M}(t) := \sum_{n=0}^{\infty} \hat{M}_n(t), \tag{2.17}$$

$$\hat{M}_n(t)\rho := \Big(-\frac{i}{\hbar}\Big)^n \int_0^t dt_1 \int_0^{t_1} dt_2 \cdots \times \int_0^{t_{n-1}} dt_n \Big[\tilde{H}_I(t_1), \Big[\tilde{H}(t_2), \ldots [\tilde{H}_I(t_n), \rho]\Big]\Big] \tag{2.18}$$

with $t_0 := t$ and $t_{-1} := 0$ such that $\hat{M}_0(t) = 1$.

The system's density operator can then be determined by tracing over the environment:

$$\tilde{\rho}_S(t) = \hat{N}(t)\tilde{\rho}_S(0) \tag{2.19}$$

where:

$$\hat{N}(t) := \sum_{n=0}^{\infty} \hat{N}_n(t), \tag{2.20}$$

$$\hat{N}_n(t)\rho := \Big(-\frac{i}{\hbar}\Big)^n \mathrm{Tr}_E \int_0^t dt_1 \int_0^{t_1} dt_2 \cdots \times \int_0^{t_{n-1}} dt_n \Big[\tilde{H}_I(t_1), \Big[\tilde{H}(t_2), \ldots [\tilde{H}_I(t_n), \rho_E(0) \otimes \rho]\Big]\Big] \tag{2.21}$$

and the initial state has been assumed to be uncorrelated $\hat{\rho}(0) = \hat{\rho}_S(0) \otimes \hat{\rho}_E(0)$.

The Born approximation is to assume that the coupling between E and S is very weak so that we can ignore higher order perturbation terms. The term $\hat{N}_1$ can in fact be eliminated by assuming that $\mathrm{Tr}_E(\tilde{H}_I\hat{\rho}_E(0)) = 0$, which is guaranteed if the environment operators coupling to S have zero mean in the state $\hat{\rho}_E$, and can always be arranged by including $\mathrm{Tr}_E(\hat{H}_I\hat{\rho}_E(0))$ in the system Hamiltonian [76]. Therefore, in the Born approximation we neglect terms higher than second order in $\tilde{H}_I$ in (2.19). Differentiating this equation then provides an equation of motion for the reduced density

operator in the Born approximation:

$$\frac{d}{dt}\tilde{\rho}_S(t) \approx -\frac{1}{\hbar^2}\int_0^t \mathrm{Tr}_E\big([\tilde{H}_I(t),[\tilde{H}_I(t'),\tilde{\rho}(t')]]\big)dt' \tag{2.22}$$

and $\tilde{\rho}(t) \approx \tilde{\rho}_S(t) \otimes \hat{\rho}_E(0)$ since the reservoir is only negligibly affected by the interaction.

Note that equation (2.22) could also have been obtained by simply plugging (2.15) into (2.14), taking the trace over the environment, and then assuming that $\mathrm{Tr}_E[\tilde{H}_I(t),\hat{\rho}(0)] = 0$ using the assumptions made above i.e. that $\mathrm{Tr}_E(\tilde{H}_I\hat{\rho}_E(0)) = 0$ and that no correlations exist between S and E at the initial time [32].

2.2.2 The Markov Approximation

The Markov approximation assumes that memory effects can be neglected so that the future evolution of $\tilde{\rho}_S(t)$ depends only on its present state. This will be satisfied if the environment is a large system maintained in equilibrium so that it will not preserve the minor changes brought about by its interaction with S long enough to significantly affect the future evolution of S. That is, the Markov approximation relies on the environment correlation time τ_E being much shorter than the time scale τ_R for significant change in S (the relaxation time) [32].

With memory effects neglected $\tilde{\rho}_S(t')$ can be replaced with $\tilde{\rho}_S(t)$. However, the time evolution of $\tilde{\rho}_S$ given by (2.22) will still depend on an explicit choice for the initial preparation at time $t = 0$. To remove this dependence, a change of variable $t' \to t - t'$ is performed and the upper limit of the integral is taken to infinity, which is permissible provided that the integrand disappears sufficiently fast for $\tau \gg \tau_E$ [32]. The equation of motion for the reduced density operator in the Born-Markov approximation is then:

$$\frac{d}{dt}\tilde{\rho}_S(t) = -\int_0^\infty \mathrm{Tr}_E\big([\tilde{H}_I(t),[\tilde{H}_I(t-t'),\tilde{\rho}_S(t)\hat{\rho}_E]]\big)dt'$$

$$= \int_0^\infty \mathrm{Tr}_E\big(\tilde{H}_I(t-t')\tilde{\rho}_S\hat{\rho}_E\tilde{H}_I(t) - \tilde{H}_I(t)\tilde{H}_I(t-t')\tilde{\rho}_S\hat{\rho}_E\big)dt' + h.c. \tag{2.23}$$

where the Hermitian property of $\tilde{H}_I$ has been used and the tensor product has been dropped for convenience.

2.2.3 The Interaction Hamiltonian

The interaction Hamiltonian $\hat{H}_I$ is assumed to be of the form:[2]

$$\hat{H}_I := \sum_i \hat{A}_i \otimes \hat{E}_i \tag{2.24}$$

where $\hat{A}_i$ are eigenoperators of $\hat{H}_S$ belonging to the frequencies $-\omega_i$:

$$[\hat{H}_S, \hat{A}_i] = -\omega_i \hat{A}_i, \tag{2.25}$$

$$\implies [\hat{H}_S, \hat{A}_i^\dagger] = \omega_i \hat{A}_i^\dagger. \tag{2.26}$$

Therefore, the operators $\hat{A}_i$ in the interaction picture are given by:

$$\tilde{A}_i = e^{i\hat{H}_S t/\hbar}\hat{A}_i e^{-i\hat{H}_S t/\hbar} = e^{-\omega_i t/\hbar}\hat{A}_i, \tag{2.27}$$

$$\tilde{A}_i^\dagger = e^{i\hat{H}_S t/\hbar}\hat{A}_i^\dagger e^{-i\hat{H}_S t/\hbar} = e^{+\omega_i t/\hbar}\hat{A}_i^\dagger. \tag{2.28}$$

The interaction Hamiltonian (2.24) in the interaction picture can then be written as:

$$\tilde{H}_I(t) = \sum_i e^{i(\hat{H}_S+\hat{H}_E)t/\hbar}\hat{A}_i \otimes \hat{E}_i e^{-i(\hat{H}_S+\hat{H}_E)t/\hbar} \tag{2.29}$$

$$= \sum_i e^{-i\omega_i t/\hbar}\hat{A}_i \otimes \tilde{E}_i(t) = \sum_i e^{i\omega_i t/\hbar}\hat{A}_i^\dagger \otimes \tilde{E}_i^\dagger(t). \tag{2.30}$$

[2] See [32] for a more general discussion where any $\hat{H}_I$ can be written as $\sum_\alpha \hat{A}_\alpha \otimes \hat{E}_\alpha$ with $\hat{A}_\alpha = \hat{A}_\alpha^\dagger$ and $\hat{E}_\alpha = \hat{E}_\alpha^\dagger$. Then the eigenoperators of $\hat{H}_S$ are formed from the $\hat{A}_\alpha$ operators: $\hat{A}_\alpha = \sum_\omega \hat{A}_\alpha(\omega)$ where $\hat{A}_\alpha(\omega)$ is an eigenoperator of $\hat{H}_S$ with frequency ω. This general Hamiltonian would then cover the case not considered here where there is degeneracy in the eigenfrequencies.

Substituting this into (2.23) results in:

$$\frac{d}{dt}\tilde{\rho}_S(t) = \sum_{ij} e^{i(\omega_i-\omega_j)t/\hbar}\Gamma_{ij}(\omega_j,t)\Big(\hat{A}_j\tilde{\rho}_S(t)\hat{A}_i^\dagger - \hat{A}_i^\dagger\hat{A}_j\tilde{\rho}_S(t)\Big) + \text{h.c.} \quad (2.31)$$

where $\Gamma_{ij}(\omega_j,t)$ is defined in terms of reservoir correlation functions as:

$$\Gamma_{ij}(\omega_j,t) := \frac{1}{\hbar^2}\int_0^\infty dt' e^{i\omega_j t'/\hbar}\langle\tilde{E}_i^\dagger(t)\tilde{E}_j(t-t')\rangle_E. \quad (2.32)$$

2.2.4 The State of the Environment

The state of the environment $\hat{\rho}_E$ is taken to be represented by a product of independent bosonic modes satisfying $\langle\hat{b}_{\boldsymbol{k}}^\dagger\rangle = \langle\hat{b}_{\boldsymbol{k}}\rangle = 0$ where $\hat{b}_{\boldsymbol{k}}^\dagger$ and $\hat{b}_{\boldsymbol{k}}$ are the creation and annihilation operators for each mode, which obey the usual commutation relations for bosons. The operators $\hat{E}_i$ in the interaction Hamiltonian (2.24) will then be functions of the creation and annihilation operators $\hat{b}_i^\dagger$ and $\hat{b}_i$.

The state of the environment is assumed to be a general squeezed thermal state, which reduces to a squeezed vacuum state at $T = 0$ and a thermal state when the squeezing parameter is zero. Unlike a thermal state, this squeezed state is not, in general, a stationary state of the environment i.e. $[\tilde{H}_E, \tilde{\rho}_E] \neq 0$. Given that the environment is in a squeezed thermal state, the correlation function $\Gamma_{ij}(\omega_j,t)$ can be split up into parts that involve rapidly oscillating exponentials $e^{2i\omega_j t/\hbar}$ and those that don't [32]:

$$\Gamma_{ij}(\omega_j,t) = \Gamma_{ij}^{(1)}(\omega_j) + e^{2i\omega_j t/\hbar}\Gamma_{ij}^{(2)}(\omega_j) \quad (2.33)$$

where terms $\Gamma_{ij}^{(1)}(\omega_j,t)$ result from environment correlation functions that contain an equal number of creation operators and annihilation operators, and the terms $\Gamma_{ij}^{(2)}(\omega_j,t)$ vanish for an environment in thermal equilibrium. Note that the correlation function $\Gamma_{ij}(\omega_j,t)$, in general, depends on time for this non-stationary state of the environment. This is in contrast to a thermal state where the corresponding correlation functions are independent of time ($\Gamma_{ij}^{(2)}(\omega_j)$ vanishes) [32].

Inserting the above decomposition of $\Gamma_{ij}(\omega_j, t)$ into the master equation 2.31 results in:

$$\frac{d}{dt}\tilde{\rho}_S(t) = \sum_{ij}\Big(e^{i(\omega_i-\omega_j)t/\hbar}\Gamma_{ij}^{(1)}(\omega_j) + e^{i(\omega_i+\omega_j)t/\hbar}\Gamma_{ij}^{(2)}(\omega_j)\Big) \times \Big(\hat{A}_j\tilde{\rho}_S(t)\hat{A}_i^\dagger - \hat{A}_i^\dagger\hat{A}_j\tilde{\rho}_S(t)\Big) + \text{h.c.} \tag{2.34}$$

As specified in Section 2.2.2, to satisfy the Markov approximation, the reservoir correlation functions must decay in a time τ_E, which is small compared to the relaxation time τ_R. Strictly speaking the decay of the correlations can only be valid for an environment which is infinity large and involves a continuum of frequencies [32].

2.2.5 The Secular Approximation

A typical value for $\omega_i - \omega_j$, where $|\omega_j| \neq |\omega_i|$, defines a typical time scale τ_S for the intrinsic evolution of the system S [32]. If τ_S is large compared to the relaxation time τ_R of the open quantum system then the non-secular terms in (2.34) may be neglected since they will oscillate very rapidly during the time τ_R. This removal of the rapidly oscillating terms from the interaction picture master equation for the reduced density operator is called the secular approximation and is related to the rotating wave approximation which refers to the the removal of the rapidly oscillating terms from the interaction picture Hamiltonian.

With this approximation the master equation for the reduced density operator is given by:

$$\frac{d}{dt}\tilde{\rho}_S(t) = \sum_i \Bigg(\Gamma_{ii}^{(1)}(\omega_i)\Big(\hat{A}_i\tilde{\rho}_S(t)\hat{A}_i^\dagger - \hat{A}_i^\dagger\hat{A}_i\tilde{\rho}_S(t)\Big) + \Gamma_{ij\neq i}^{(2)}(\omega_j)\Big(\hat{A}_i\tilde{\rho}_S(t)\hat{A}_j^\dagger - \hat{A}_i\hat{A}_j^\dagger\tilde{\rho}_S(t)\Big)\Bigg) + \text{h.c.} \tag{2.35}$$

where in the second line j is such that $\hat{A}_j^\dagger = \hat{A}_i$ since $\omega_j = -\omega_i$ for this term.

2.2.6 The Master Equation in Lindblad Form

The Hermitian conjugate terms in (2.35) can be gathered up by rewriting Γ_{ij} as:

$$\Gamma_{ij} := \frac{1}{2}\gamma_{ij} + iS_{ij} \tag{2.36}$$

where S_{ij} and γ_{ij} are Hermitian and positive matrices:

$$S_{ij} := \frac{1}{2i}(\Gamma_{ij} - \Gamma^*_{ji}), \tag{2.37}$$

$$\gamma_{ij} := \Gamma_{ij} - \Gamma^*_{ji}. \tag{2.38}$$

The master equation for the reduced density operator can then be written as:

$$\frac{d}{dt}\tilde{\rho}_S = -\frac{i}{\hbar}[\hat{H}_{LS}, \tilde{\rho}_S(t)] + \mathcal{D}(\tilde{\rho}_S) \tag{2.39}$$

where:

$$\hat{H}_{LS} := \sum_i (S^{(1)}_{ii}\hat{A}^\dagger_i\hat{A}_i + S^{(2)}_{ij\neq i}\hat{A}_i\hat{A}_i), \tag{2.40}$$

$$\mathcal{D}(\tilde{\rho}_S) := \mathcal{D}_T(\tilde{\rho}_S) + \mathcal{D}_S(\tilde{\rho}_S), \tag{2.41}$$

$$\mathcal{D}_T(\tilde{\rho}_S) := \sum_i \gamma^{(1)}_{ii}\Big(\hat{A}_i\tilde{\rho}_S\hat{A}^\dagger_i - \frac{1}{2}\{\hat{A}^\dagger_i\hat{A}_i, \tilde{\rho}_S\}\Big), \tag{2.42}$$

$$\mathcal{D}_S(\tilde{\rho}_S) := \sum_i \gamma^{(2)}_{ij\neq i}\Big(\hat{A}_i\tilde{\rho}_S\hat{A}^\dagger_j - \frac{1}{2}\{\hat{A}^\dagger_j\hat{A}_i, \tilde{\rho}_S\}\Big) \tag{2.43}$$

where again j is such that $\hat{A}^\dagger_j = \hat{A}_i$.

The first part of $\hat{H}_{LS}$ is often called the Lamb shift Hamiltonian since it leads to a Lamb-type renormalization of the unperturbed energy levels induced by the system-reservoir coupling. In general, the renormalization of the system Hamiltonian is induced by the vacuum fluctuations of the

environment and by thermally induced processes. The term $\mathcal{D}(\tilde{\rho}_S)$ on the other hand is called the dissipator. The first term $\mathcal{D}_T(\tilde{\rho}_S)$ in the dissipator represents generalized amplitude damping, while the other terms $\mathcal{D}_S(\tilde{\rho}_S)$ represent phase dependent fluctuations [77].

The master equation (2.39) is of first standard form[3] and, since $\gamma_{ii}^{(1)}$ and $\gamma_{ij}^{(2)}$ are homogeneous in time and thus positive [32], the master equation may be diagonalized to finally obtain the Lindblad equation in diagonal form [32]:

$$\frac{d}{dt}\hat{\rho}_S = -\frac{i}{\hbar}[\hat{H}_{LS}, \hat{\rho}_S] + \sum_l \left(\hat{c}_l \hat{\rho}_S \hat{c}_l^\dagger - \frac{1}{2}\{\hat{c}_l^\dagger \hat{c}_l, \hat{\rho}_S\}\right) \tag{2.45}$$

where $\hat{c}_l$ are called Lindblad operators and are obtained from $\hat{A}_i$, in general, by a unitary transformation.

The Schrödinger picture master equation for the reduced density operator is obtained from (2.45) by simply adding the free Hamiltonian $\hat{H}_S$ to $\hat{H}_{LS}$ [32]:

$$\frac{d}{dt}\hat{\rho}_S = -\frac{i}{\hbar}[\hat{H}, \hat{\rho}_S] + \sum_l \left(\hat{c}_l \hat{\rho}_S \hat{c}_l^\dagger - \frac{1}{2}\{\hat{c}_l^\dagger \hat{c}_l, \hat{\rho}_S\}\right) \tag{2.46}$$

where $\hat{H} = \hat{H}_S + \hat{H}_{LS}$.

This is a first-order linear differential equation for the reduced density operator and was derived from the master equation (2.14) under the approximations and conditions discussed in Sections 2.2.1-2.2.5. The most important of these is the Markov approximation which relied on the time scale of the decay of the environmental correlation functions being much shorter than the time scale for significant change in the open system S. This equation can also be derived without appealing to the underlying Hamiltonian dynamics and instead assuming that the reduced density operator evolves under the action of the generator of a quantum dynamical semi-

[3]That is the dissipator $\mathcal{D}(\tilde{\rho}_S)$ can be written as:

$$\mathcal{D}(\tilde{\rho}_S) = \sum_{i,j=1} \hat{F}_i \tilde{\rho}_S \hat{F}_j^\dagger \tag{2.44}$$

group (see e.g. [32]). The right-hand side of equation (2.46) therefore also represents the most general form for the generator of a quantum dynamical semi-group.

2.3 The Lindblad Master Equation for Phonons of BECs

This section applies the general derivation of a Lindblad master equation, which was performed in the previous section, to the specific case that is of interest to this work, a single phonon mode of a BEC. From the previous chapter, a phonon mode of a BEC will interact with all the other quasi-particle modes via the on-resonance Beliaev and Landau processes as well as certain off-resonance processes. Therefore, in the framework of open quantum systems, the single phonon mode is the open system; the environment is made up of all the other quasi-particle modes; and the interaction Hamiltonian is given by (1.33), which was derived in the previous chapter. The Hamiltonian of the combined system is then:

$$\hat{H} = \hat{H}_S + \hat{H}_E + \hat{H}_I \tag{2.47}$$

where $\hat{H}_S$ and $\hat{H}_E$ derive from (1.26) and respectively describe the free Hamiltonian of the single-mode phonon system and all the other quasi-particle modes:

$$\hat{H}_S := \hbar\omega_q \hat{b}_{\boldsymbol{q}}^\dagger \hat{b}_{\boldsymbol{q}}, \tag{2.48}$$

$$\hat{H}_E := \sum_{\boldsymbol{p}} \hbar\omega_p \hat{b}_{\boldsymbol{p}}^\dagger \hat{b}_{\boldsymbol{p}}, \tag{2.49}$$

and the interaction Hamiltonian $\hat{H}_I$ is defined as:

$$\hat{H}_I = \hat{b}_{\boldsymbol{q}} \hat{Q}^\dagger + \hat{b}_{\boldsymbol{q}}^\dagger \hat{Q} \tag{2.50}$$

where $\hat{Q}$ acts on the Hilbert space of the rest of the quasi-particle modes and is defined in (1.34). The interaction terms between the states of the

large system E in $\hat{H}$ have been ignored considering the environment to be in thermal equilibrium and having a very fast correlation τ_E time since it will form a very large system.

The interaction Hamiltonian (2.50) is already written in the form of (2.24), which was used in the derivation of the Lindblad equation (2.46), since $\hat{b}_{\boldsymbol{q}}$ and $\hat{b}^\dagger_{\boldsymbol{q}}$ are eigenoperators of $\hat{H}_S$ with frequencies $\omega_1 = \omega_{\boldsymbol{q}}$ and $\omega_2 = -\omega_{\boldsymbol{q}}$. Therefore, in the notation of (2.24):

$$\hat{A}_1 = \hat{b}_{\boldsymbol{q}}, \quad \hat{A}_2 = \hat{A}_1^\dagger = \hat{b}^\dagger_{\boldsymbol{q}}, \tag{2.51}$$

$$\hat{E}_1 = \hat{Q}^\dagger, \quad \hat{E}_2 = \hat{E}_1^\dagger = \hat{Q}. \tag{2.52}$$

Assuming that the initial state of the full system is the product state $\hat{\rho}(0) = \hat{\rho}_S(0) \otimes \hat{\rho}_E(0)$, and implementing the Born, Markov and secular approximations (Sections 2.2.1, 2.2.2 and 2.2.5), the reduced density operator of the system will evolve according to the master equation (2.46). Then, further assuming that the environment is in thermal equilibrium and is not squeezed so that the $\mathcal{D}_S$ term vanishes,[4] the reduced density operator will obey the following Schrödinger picture master equation:

$$\begin{aligned}\frac{d}{dt}\hat{\rho}_S = -\frac{i}{\hbar}[\hat{H}, \hat{\rho}_S] + \gamma_{11}\Big(\hat{b}_{\boldsymbol{q}}\hat{\rho}_S\hat{b}^\dagger_{\boldsymbol{q}} - \frac{1}{2}\{\hat{b}^\dagger_{\boldsymbol{q}}\hat{b}_{\boldsymbol{q}}, \hat{\rho}_S\}\Big) \\ +\gamma_{22}\Big(\hat{b}^\dagger_{\boldsymbol{q}}\hat{\rho}_S\hat{b}_{\boldsymbol{q}} - \frac{1}{2}\{\hat{b}_{\boldsymbol{q}}\hat{b}^\dagger_{\boldsymbol{q}}, \hat{\rho}_S\}\Big),\end{aligned} \tag{2.53}$$

which can be written in diagonal form (2.46):

$$\frac{d}{dt}\hat{\rho}_S = -\frac{i}{\hbar}[\hat{H}, \hat{\rho}_S] + \sum_{i=1}^{i=2}\Big(\hat{c}_i\hat{\rho}_S\hat{c}_i^\dagger - \frac{1}{2}\{\hat{c}_i^\dagger\hat{c}_i, \hat{\rho}_S\}\Big) \tag{2.54}$$

where:

$$\hat{c}_1 = \sqrt{\gamma_{11}}\hat{b}_{\boldsymbol{q}}, \tag{2.55}$$

[4] See [78] on how the quasi-particles could occupy squeezed states due to the Beliaev damping process, which is analogous to parametric down conversion in quantum optics.

$$\hat{c}_2 = \sqrt{\gamma_{22}}\hat{b}^\dagger_{\boldsymbol{q}}, \tag{2.56}$$

$$\hat{H} = \hbar\omega'_{\boldsymbol{q}}\hat{b}^\dagger_{\boldsymbol{q}}\hat{b}_{\boldsymbol{q}}, \tag{2.57}$$

$$\omega'_{\boldsymbol{q}} = \omega_{\boldsymbol{q}} + S_{11} + S_{22}. \tag{2.58}$$

It can be easily verified that in the secular (or rotating wave) approximation the non-resonant terms in (2.50), that is $\hat{b}_{\boldsymbol{q}}\hat{A}^\dagger$ and $\hat{b}^\dagger_{\boldsymbol{q}}\hat{A}$, do not contribute to the evolution of the system's reduced density operator. For example, the interaction term $\hat{b}_{\boldsymbol{q}}\hat{b}_{\boldsymbol{k}}\hat{b}_{\boldsymbol{l}}\delta_{-\boldsymbol{q},\boldsymbol{k}+\boldsymbol{l}}$ from $\hat{b}_{\boldsymbol{q}}\hat{A}^\dagger$ involves the rapidly oscillating exponentials $e^{-2i\omega_q t/\hbar}$ in the interaction picture and so are neglected in the rotating wave approximation. These terms will, therefore, not contribute to the rates γ_{11} and γ_{22}.

From, (2.32), the rates γ_{11} and γ_{22} derive from the following expressions:

$$\Gamma_{11} = \frac{1}{\hbar^2}\int_0^\infty dt' e^{i\omega_q t/\hbar}\langle\tilde{E}(t)\tilde{E}^\dagger(t-t')\rangle_E \tag{2.59}$$

$$= \frac{1}{\hbar^2}\int_0^\infty dt' e^{i\omega_q t/\hbar}\Big(\langle\tilde{B}(t)\tilde{B}^\dagger(t-t')\rangle_E + \langle\tilde{B}(t)\tilde{L}^\dagger(t-t')\rangle_E + \langle\tilde{L}(t)\tilde{B}^\dagger(t-t')\rangle_E + \langle\tilde{L}(t)\tilde{L}^\dagger(t-t')\rangle_E\Big), \tag{2.60}$$

$$\Gamma_{22} = \frac{1}{\hbar^2}\int_0^\infty dt' e^{-i\omega_q t/\hbar}\langle\tilde{E}^\dagger(t)\tilde{E}(t-t')\rangle_E \tag{2.61}$$

$$= \frac{1}{\hbar^2}\int_0^\infty dt' e^{-i\omega_q t/\hbar}\Big(\langle\tilde{B}^\dagger(t)\tilde{B}(t-t')\rangle_E + \langle\tilde{B}^\dagger(t)\tilde{L}(t-t')\rangle_E + \langle\tilde{L}^\dagger(t)\tilde{B}(t-t')\rangle_E + \langle\tilde{L}^\dagger(t)\tilde{L}(t-t')\rangle_E\Big) \tag{2.62}$$

where $\tilde{B}$ and $\tilde{L}$ are the Beliaev and Landau operators defined in (1.36) and (1.37) but now in the interaction picture. Since the environment is in thermal equilibrium, any averages in (2.60)-(2.62) that contain different numbers of environmental creation and annihilation operators will vanish (these also vanish under the secular wave approximation), which leaves:

$$\Gamma_{11} = \Gamma_1^B + \Gamma_1^L, \tag{2.63}$$

$$\Gamma_{22} = \Gamma_2^B + \Gamma_2^L \tag{2.64}$$

where:

$$\Gamma_1^B := \frac{1}{\hbar^2}\int_0^\infty dt' e^{i\omega_q t/\hbar}\langle \tilde{B}(t)\tilde{B}^\dagger(t-t')\rangle_E, \tag{2.65}$$

$$\Gamma_2^B := \frac{1}{\hbar^2}\int_0^\infty dt' e^{-i\omega_q t/\hbar}\langle \tilde{B}^\dagger(t)\tilde{B}(t-t')\rangle_E, \tag{2.66}$$

$$\Gamma_1^L := \frac{1}{\hbar^2}\int_0^\infty dt' e^{i\omega_q t/\hbar}\langle \tilde{L}(t)\tilde{L}^\dagger(t-t')\rangle_E, \tag{2.67}$$

$$\Gamma_2^L := \frac{1}{\hbar^2}\int_0^\infty dt' e^{-i\omega_q t/\hbar}\langle \tilde{L}^\dagger(t)\tilde{L}(t-t')\rangle_E. \tag{2.68}$$

The rates γ_{11} and γ_{22} in (2.53) are then given by:

$$\gamma_{11} = \gamma_1^B + \gamma_1^L, \tag{2.69}$$

$$\gamma_{22} = \gamma_2^B + \gamma_2^L \tag{2.70}$$

where the rates $\gamma_1^B, \gamma_1^L, \gamma_2^B$ and γ_2^L derive via (2.36) from the corresponding Γ functions defined in (2.65)-(2.68) above. In fact, since the environment is in thermal equilibrium, the two rates γ_{11} and γ_{22} are not independent but satisfy [27, 32]:

$$\gamma_{11} = e^{\beta_q}\gamma_{22}, \tag{2.71}$$

which can be easily verified after calculating the two rates. The rates are then conveniently characterized by their difference $\gamma = \gamma_{22} - \gamma_{11}$ which is found to be:

$$\gamma = \gamma_B - \gamma_L \tag{2.72}$$

where $\gamma_B := \gamma_2^B - \gamma_1^B$ and $\gamma_L := \gamma_2^L - \gamma_1^L$ characterize the Beliaev and Landau

interactions respectively and can be shown to be given by:

$$\gamma_B := \frac{2g^2 n}{V\hbar^2}\int_0^\infty \pi d\omega_k p_{\omega_k} \mathcal{B}^2_{\omega_k,\omega_l}\delta(\omega_q-\omega_k-\omega_l)(1+N_l^{th}+N_k^{th}), \tag{2.73}$$

$$\gamma_L := \frac{g^2 n}{V\hbar^2}\int_0^\infty \pi d\omega_k p_{\omega_k} \mathcal{L}^2_{\omega_k,\omega_l}\delta(\omega_q+\omega_k-\omega_l)(N_k^{th}-N_l^{th}) \tag{2.74}$$

where $\mathcal{B}_{\omega_k,\omega_l}$ and $\mathcal{L}_{\omega_k,\omega_l}$ are derived from the coupling constants defined in (1.39)-(1.40); and N_k^{th} and N_l^{th} are the thermal occupation numbers of the quasi-particles, defined by (1.31), for the modes k and l respectively. The environment has also been assumed to have an approximate continuum of modes with a density of states p_ω such that $p_\omega d\omega$ gives the number of oscillators with frequencies in the interval ω to $\omega+d\omega$. A detailed derivation of the rates γ_B and γ_L in (2.74)-(2.73) from the functions (2.65)-(2.68) is carried out in Appendix A.

The rates γ_B and γ_L are just the usual Beliaev and Landau dampings rate which have been calculated under various conditions (see [79] for a brief outline of some of the major studies such as [26]). For example, in [70], the Beliaev-Landau damping rate γ is calculated in the Popov approximation for a phonon mode in a uniform BEC. Following [70], a phonon mode has energy $\hbar\omega_q \approx cq$ and so the coefficients u_p and v_p, which characterize the Bogoliubov transformations (1.23) and appear in $\mathcal{L}_{\omega_k,\omega_l}$ and $\mathcal{B}_{\omega_k,\omega_l}$, can be approximated as:

$$u_q \approx \sqrt{\frac{mc_s^2}{2\hbar\omega_q}} + \frac{1}{2}\sqrt{\frac{\hbar\omega_q}{2mc_s^2}}, \tag{2.75}$$

$$v_q \approx -\sqrt{\frac{mc_s^2}{2\hbar\omega_q}} + \frac{1}{2}\sqrt{\frac{\hbar\omega_q}{2mc_s^2}}. \tag{2.76}$$

After substituting these approximations into (2.73) and (2.74), analytical expressions for the damping rates can then be derived by taking the limit $k_BT \ll \hbar\omega_q$ or $k_BT \gg \hbar\omega_q$. The former limit is called the quantum regime and in this regime the thermal occupation of the quasi-particle modes vanishes $N_k \sim e^{-\beta\omega_q} \to 0$ and so $\gamma_B \gg \gamma_L$ since the Believe damping coefficient

$(1+N_l+N_k)$ goes to unity to a very good approximation, whereas, the Landau damping coefficient $(N_l - N_k)$ tends to zero (and there is no Landau damping at zero temperature). Therefore, the Beliaev damping dominates over the Landau damping and is independent of the temperature [70]:

$$\gamma \approx \gamma_B \approx \frac{3}{640\pi}\frac{\hbar}{mnc_s^5}\omega_q^5 \tag{2.77}$$

where n is the (3-dimensional) density of the gas, c_s is the speed of sound defined in (1.30), and γ is in units of one over time. The damping rate has a sensitive dependence on the momentum of the phonon mode since the final state quasi-particles each have an energy lower than the phonon and so the final state phase space is restricted. For the same reason, this damping process cannot occur for the lowest energy modes in trapped Bose gases where the spectrum of states to which the excitation can couple is discrete [70].

In the opposite limit $k_BT \gg \hbar\omega_q$, called the thermal regime, Landau damping dominates over Beliaev damping. This is because the coefficient $\mathcal{L}_{k,l}^2$ is greater than $\mathcal{B}_{k,l}^2$ since the latter contains additional negative contributions from an extra u_kv_l type term and $|u_k| > |v_l|$. At very high temperatures such that $\hbar\omega_q \ll mc_s^2 \ll k_BT$ (where $mc_s^2 = gn = \mu$), the Landau damping rate approximates to [70]:

$$\gamma \approx \gamma_L \approx \frac{3\pi}{8}\frac{k_BTa}{\hbar c_s}\omega_q \tag{2.78}$$

whereas, for temperatures such that $\hbar\omega_q \ll k_BT \ll mc_s^2$, the Landau damping rate approximates to [70]:

$$\gamma \approx \gamma_L \approx \frac{3\pi^3}{8}\frac{(k_BT)^4}{mn\hbar^3c_s^5}\omega_q. \tag{2.79}$$

2.3.1 Comparison with the Quantum Optical Master Equation

The Born-Markov approximation is often used in quantum optical situations since the physical conditions underlying this approximation are usually very

well satisfied [32]. The application of this approximation to such quantum optical situations frequently results in a certain form of master equation called the quantum optical master equation. Since this master equation is well-known, a comparison with the master equation derived here for phonons interacting with the quasi-particle modes of a Bose gas (2.54) should help facilitate a better understanding of the latter master equation.

The quantum optical master equation results from the application of the Born-Markov approximation to the case of a bound quantum system, such as an atom or molecule, interacting with a quantized radiation field which is in thermal equilibrium. The free quantized radiation field will be represented by the following quantum field Hamiltonian [32]:[5]

$$\hat{H}_E = \sum_{\boldsymbol{k}} \sum_{\lambda=1,2} \hbar\omega_k \hat{r}^\dagger_\lambda(\boldsymbol{k}) \hat{r}_\lambda(\boldsymbol{k}) \tag{2.80}$$

where λ labels one of the two transverse polarizations for the wavevector $\boldsymbol{k}$, $\omega_k = c|\boldsymbol{k}|$, and the field operators $\hat{r}_\lambda(\boldsymbol{k})$ and $\hat{r}^\dagger_\lambda(\boldsymbol{k})$ are the annihilation and creation operators for the photons. Note that this Hamiltonian for the environment is similar to that used in the previous sections for the environment of the phonons (see (2.49)).

In the electric dipole approximation the interaction Hamiltonian is given by [32]:

$$\hat{H}_I = -\hat{\boldsymbol{D}} \cdot \hat{\boldsymbol{E}} \tag{2.81}$$

where $\hat{\boldsymbol{D}}$ is the dipole operator the system under consideration, and $\hat{\boldsymbol{E}}$ is the electric field operator in the Schrödinger picture:

$$\hat{\boldsymbol{E}} = i \sum_{\boldsymbol{k}} \sum_{\lambda=1,2} \sqrt{\frac{2\pi\hbar\omega_k}{V}} \boldsymbol{e}_\lambda(\boldsymbol{k}) \Big(\hat{r}_\lambda(\boldsymbol{k}) - \hat{r}^\dagger_\lambda(\boldsymbol{k}) \Big) \tag{2.82}$$

where V is a normalization volume for the field modes and $\boldsymbol{e}_\lambda$ is a unit polarization vector. Note that operator $\hat{\boldsymbol{E}}$ contains a single annihilation or

[5] With an infinite c-number subtracted for the vacuum energy.

creation operator acting on the field models of the environment. This is in contrast to the operators $\hat{Q}$ and $\hat{Q}^\dagger$ in the interaction Hamiltonian for the phonon system (2.50) which contain two annihilation or creation operators that act on the field modes of the environment.

For simplicity, a two-level system for the bound quantum system is assumed such that the dipole operator can be written as:

$$\hat{\boldsymbol{D}} = \boldsymbol{d}\hat{\sigma}_- + \boldsymbol{d}^*\hat{\sigma}_+ \tag{2.83}$$

where $\boldsymbol{d}$ is the transition matrix element of the dipole operator and $\hat{\sigma}_\pm$ are the ladder operators for the two-level system.

Assuming the Born-Markov and secular wave approximations, and taking the radiation field to be in a thermal sate, the quantum master equation for the two-level system can be written in Lindblad form as [32]:

$$\begin{aligned}\frac{d}{dt}\hat{\rho}_S(t) = -\frac{i}{\hbar}[\hat{H}, \hat{\rho}_S] + \gamma_{--}\Big(\hat{\sigma}_-\hat{\rho}_S\hat{\sigma}_-^\dagger - \frac{1}{2}\{\hat{\sigma}_-^\dagger\hat{\sigma}_-, \hat{\rho}_S\}\Big) \\ + \gamma_{++}\Big(\hat{\sigma}_+\hat{\rho}_S\hat{\sigma}_+^\dagger - \frac{1}{2}\{\hat{\sigma}_+^\dagger\hat{\sigma}_+, \hat{\rho}_S\}\Big)\end{aligned} \tag{2.84}$$

where:

$$\gamma_{--} := \frac{4\omega_0^3|\boldsymbol{d}|^2}{3\hbar c^3}(N_0 + 1), \tag{2.85}$$

$$\gamma_{++} := \frac{4\omega_0^3|\boldsymbol{d}|^2}{3\hbar c^3}N_0 \tag{2.86}$$

with ω_0 being the transition frequency of the two-level system, N_0 denoting the Planck distribution at the transition frequency, and $\hat{H}$ the free Hamiltonian of the two-level system including the Lamb and Shark shift contributions.

The above master equation is often called the two-level quantum optical master equation [32]. Its form is very similar to that of the Markov master equation derived for the phonons interacting with an environment of quasiparticle modes (2.53) with σ_- replacing $\hat{b}_{\boldsymbol{q}}$ and σ_+ replacing $\hat{b}_{\boldsymbol{q}}^\dagger$. This is

of course to be expected as the same approximations were used in both cases: the Born-Markov approximation, secular wave approximation, and the assumption that the environment is in a stationary thermal state. The major difference between the two master equations comes in their rates. This is due to the different forms of interaction Hamiltonian where the terms in the optical interaction Hamiltonian (2.81) contain single annihilation or creation operators that act on the environment, whereas, the terms in the phononic interaction Hamiltonian (2.50) contain two. The latter results in much more complicated expressions for the rates γ_{11} and γ_{22} than the γ_{--} and γ_{++} rates of the quantum optical master equation.[6]

As stated in Section 2.3, since the environment of the phonons is in thermal equilibrium, the two rates γ_{11} and γ_{22} are not independent and instead satisfy (2.71). The rates are then conveniently characterized by their difference $\gamma = \gamma_{22} - \gamma_{11}$ which is defined by $\gamma_B - \gamma_L$ where γ_B and γ_L are given by (2.73) and (2.74) respectively.

In the derivation of the quantum optical master equation, the environment was also assumed to be in thermal equilibrium and so the two rates γ_{--} and γ_{++} are also dependent and satisfy an expression analogous to (2.71). Therefore, the two rates are also conveniently characterized by their difference $\gamma_0 := \gamma_{++} - \gamma_{--}$, which is simply given by:

$$\gamma_0 := \frac{4\omega_0^3 |\boldsymbol{d}|^2}{3\hbar c^3}. \tag{2.87}$$

Since $\gamma_{--} = \gamma_0(1 + N_0)$ and $\gamma_{++} = \gamma_0 N_0$, the quantum optical master equation given by (2.84) is often written as:

$$\begin{aligned}\frac{d}{dt}\hat{\rho}_S(t) = -\frac{i}{\hbar}[\hat{H}, \hat{\rho}_S] + \gamma_0\Big[(N_0+1)\Big(\hat{\sigma}_-\hat{\rho}_S\hat{\sigma}_-^\dagger - \frac{1}{2}\{\hat{\sigma}_-^\dagger\hat{\sigma}_-, \hat{\rho}_S\}\Big) \\ + N_0\Big(\hat{\sigma}_+\hat{\rho}_S\hat{\sigma}_+^\dagger - \frac{1}{2}\{\hat{\sigma}_+^\dagger\hat{\sigma}_+, \hat{\rho}_S\}\Big)\Big]\end{aligned} \tag{2.88}$$

illustrating the fact that the rate γ_0 characterizes the evolution of the sys-

[6] The rates γ_{11} and γ_{22} are given by (2.69) and (2.70) where γ_1^B, γ_2^B, γ_1^L, γ_2^L are defined in (A.22), (A.23), (A.19) and (A.20) respectively.

tem.

Note that a simple analytic expression exists for γ_0. This is in contrast to the rate characterizing the evolution of the phonon system γ which is a lot more complicated in general. This is the principal difference between the two-level quantum optical master equation to the master equation for the phonon system (2.50). However, under certain approximations, simple expressions can in fact be used for γ as illustrated by (2.77)-(2.79) but all of these expressions have a different dependence on the system's oscillating frequency compared with γ_0.

2.4 Summary

In conclusion, the evolution of the reduced density operator for a single-mode phonon system has been calculated by considering the phonon system as an open quantum system in the presence of an environment of all other quasi-particle modes of the Bose gas, for which a similar analysis was also performed in [27]. Under the Born-Markov and secular approximations, and assuming the quasi-particles to be in thermal equilibrium, the reduced density operator of the phonon system evolves according to (2.53), which is a Markov master equation in Lindblad form. The difference of the rates that appear in this equation is the usual Landau-Beliaev damping rate for which analytical expressions exist in the limits discussed at the end of Section 2.3. The damping rate of phonons has been observed in various experiments [73]. For example, in [74, 75], the measured damping rate was found to be consistent with the theory of Landau damping [26].

The next Chapter investigates a simplified description of the evolution of the single-mode phonon system by assuming that the state of the system is Gaussian. The system is then fully characterized by two two-dimensional matrices rather than the reduced density operator $\hat{\rho}_S$, which lives in an infinite dimensional space. The evolution of the system is then defined by the evolution of the two characterizing matrices, which derives from the equation of motion for the reduced density operator (2.53). The simple evolution of these two matrices is then used in Chapter 4 to estimate the

relaxation and decoherence times of the single-mode phonon system.

CHAPTER 3

Gaussian Phonon States

The previous chapter treated a single-mode phonon state as an open quantum system and the rest of the quasi-particle modes as its environment. Under realistic assumptions, the reduced density operator of the single-mode phonon state, which lives in an infinite dimensional Hilbert space, was then shown to evolve in time via a Markov master equation that could be written in Lindblad form. In this chapter a further simplification to the description of the evolution of the phonon state is investigated, reducing a problem in an infinite dimensional Hilbert space to a problem that can be solved using the entries of just two two-dimensional matrices. This is achieved by assuming that the phonon state is Gaussian. In this case the time evolution of the phonon state can be fully encoded in the time evolution of the entries of the first and second statistical moments of the state, which can be represented by a two-dimensional vector and square matrix respectively.

Gaussian quantum states are states whose Wigner function is of Gaussian form. They are popular in various areas of theoretical research such as quantum optics, atomic physics, quantum information theory and relativistic quantum information theory since they are convenient to manipulate theoretically. They also frequently arise in experimental physics too. For example, the vacuum state and thermal states of bosonic systems such as the electromagnetic field are Gaussian, and popular manipulations of these states such as ideal beam splitters and squeezers preserve the Gaussianity. Certain non-Gaussian states can also often be well approximated as Gaus-

sian such as states that can arise from a nonlinear squeezing of the vacuum [41].

In quantum information theory Gaussian states are popular tools for continuous variable protocols, playing a leading role in many applications such as quantum communications and quantum metrology [41]. These states enable great simplifications to calculations in information protocols such as analytical derivations of certain state separability thresholds [41, 80]. The loss of entanglement, or decoherence, caused by the influence of the environment is a primary concern in this field and so estimating how Gaussian states decohere is of particular importance.

Gaussian states have also become useful tools of relativistic quantum information theory, particularly in the characterization of bipartite and multipartite entanglement [80, 81]. As discussed in [82, 83], the Gaussian coherent states of non-relativistic quantum mechanics can be generalized to relativistic coherent states of Klein-Gordon and Dirac particles. Recently, Gaussian states were used in techniques formulated for the application of relativity to quantum metrology in order to develop a novel generation of relativistic quantum technologies such as gravimeters, clocks and sensors [17]. For example, the phonon states of a BEC that are used in the relativistic quantum accelerometer and GW detector discussed in [17, 18] and the Introduction are of Gaussian form.

Gaussian states also naturally arise in BECs. For example, the condensate can be thought of as a coherent state[1] and coherent phonon states can be generated by a number of techniques such as Bragg scattering and the modulation of trap frequencies [73, 84]. Furthermore, by suddenly, non-adiabatically perturbing the phonon vacuum, two-mode squeezed phonon states are predicted to be generated, which are also of Gaussian form [37]. This has since been investigated experimentally in [38] although only classical states where observed. Taking the excited single-mode phonon state of Chapters 1 and 2 to be of Gaussian form should, therefore, be a reasonable assumption to make.

[1]If the condensate is a coherent state $|\phi_0\rangle$ then $\hat{a}_0|\phi_0\rangle := \alpha_0|\phi_0\rangle$ and so $\hat{N}|\phi_0\rangle = |\alpha_0|^2|\phi_0\rangle := N_0|\phi_0\rangle$ such that $\langle\hat{a}_0\rangle \sim \sqrt{N_0}$ as required by the symmetry breaking mechanism.

The next section, Section 3.1, introduces the covariance matrix formalism, which is a convenient mathematical framework in phase space for describing Gaussian states and their dynamics. Section 3.2 then looks at how the time evolution of Gaussian states that obey a Markov equation in Lindblad form can be characterized by the evolution of the first and second statistical moments. This is performed for a multi-mode Gaussian state and for a general Lindblad equation. Subsequently, Section 3.3 applies the theory of Section 3.2 to determine the time evolution of a single-mode phonon system when it is taken to be in a Gaussian state. Under general conditions this Gaussianity would be lost in time since the interaction Hamiltonian is is cubic in field operators (it is quadratic in field operators of the environment). However, in the assumed Born-Markov approximation it is shown that the phonon state will persist as a Gaussian state since the master equation then corresponds to a model in which nonlinear terms are effectively not present (there is an effective linearization of the interaction Hamiltonian over the environment field operators). This is important since it means that, under realistic approximations, the simple description of the first two statistical moments fully characterising the state will persist throughout the state's evolution. This simplified version of the evolution of the state is then used in Chapter 4 to estimate the decoherence and relaxation time of a phonon state.

3.1 The Covariance Matrix Formalism

This section introduces the covariance matrix formalism. This incorporates a simple mathematical framework which is used to describe Gaussian states and there transformations. It is frequently used in quantum information with continuous variables where there is, generically, an infinite-dimensional Hilbert space described by observables with continuous eigenspectra.

3.1.1 Phase Space Description of Quantum States

Consider a bosonic field of M independent modes where the creation and annihilation operators for each mode are $\hat{a}_i^\dagger$, $\hat{a}_i$, $i = 1, \ldots, M$, with commu-

tation relations $[\hat{a}_i, \hat{a}_j^\dagger] = \delta_{ij}$. The Hilbert space of the system $\mathcal{H} = \otimes_{i=1}^{M} \mathcal{F}_i$ is the tensor product of the infinite dimensional Fock spaces $\mathcal{F}_i$ of the M modes, each spanned by the number basis $|n\rangle_{m\in\mathbb{M}}$, which are the eigenstates of the number operator $\hat{N} = \hat{a}_i^\dagger \hat{a}_i$. The free Hamiltonian of the system is then given by $\hat{H} = \sum_{i=1}^{M} \hbar\omega_i(\hat{a}_i^\dagger \hat{a}_i + \frac{1}{2})$.

Each mode is analogous to that of a quantum harmonic oscillator where the creation and annihilation operators are analogous to the ladder operators. Similar to the quantum harmonic oscillator, position and momentum-like operators $\hat{q}_i$, $\hat{p}_i$ can be defined in terms of the creation and annihilation operators:

$$\hat{q}_i := \frac{1}{2\kappa_1}(\hat{a}_i + \hat{a}_i^\dagger), \qquad \hat{p}_i := \frac{i}{2\kappa_2}(\hat{a}^\dagger - \hat{a}_i) \tag{3.1}$$

where $\kappa_1 = \kappa_2 := \kappa$ are are taken to be dimensionless constants in contrast to the usual quantum harmonic oscillator operators where $\kappa_1 = \sqrt{\hbar/2m\omega_i}$ and $\kappa_2 = \sqrt{m\omega_i\hbar/2}$. The operators $\hat{q}_i$ and $\hat{p}_i$ are therefore dimensionless operators that represent the quadratures of a single mode i and are similar to the real and imaginary 'parts' of $\hat{a}$. Canonical position and momentum operators are obtained for $\kappa = 2^{-\frac{1}{2}}$, while $\kappa = 1$ is the choice often made in quantum optics [41]. For a general κ, the commutation relations for the quadrature operators are given by:

$$[\hat{q}_i, \hat{p}_j] = \frac{i}{2\kappa^2}\delta_{ij}. \tag{3.2}$$

It is convenient to pair-up these operators and arrange them in a column vector:

$$\hat{\boldsymbol{x}} := \begin{pmatrix} \hat{x}_1 \\ \hat{x}_2 \\ \vdots \\ \hat{x}_{2M-1} \\ \hat{x}_{2M} \end{pmatrix} := \begin{pmatrix} \hat{q}_1 \\ \hat{p}_1 \\ \vdots \\ \hat{q}_M \\ \hat{p}_M \end{pmatrix}. \tag{3.3}$$

The components of $\hat{\boldsymbol{x}}$ then satisfy the commutation relations:

$$[\hat{x}_i, \hat{x}_j] = \frac{i}{\kappa^2}\Omega_{ij} \tag{3.4}$$

where Ω_{ij} are the elements of the symplectic form:

$$\boldsymbol{\Omega} := \bigoplus_{i=1}^{M} \omega, \quad \omega := \begin{pmatrix} 0 & 1 \\ -1 & 0 \end{pmatrix}. \tag{3.5}$$

Other grouping conventions exist such as that where the upper-half of $\boldsymbol{x}$ consists of all the position-like operators and the lower-half all the momentum like operators [41]. Another convention is the so-called complex form of the real symplectic group where, instead of consisting of the quadrature operators, the upper-half of the column vector consists of the annihilation operators, and the lower-half consists of the creation operators of all the modes.

Any quantum state of the bosonic system can be represented in this phase space picture by a quasi-probability distribution function called the Wigner function:[2]

$$W(\boldsymbol{x}) := \int_{\mathbb{R}^{2M}} \frac{d^{2M}\boldsymbol{\xi}}{(2\pi)^{2M}} e^{-i\boldsymbol{x}^T\boldsymbol{\Omega}\boldsymbol{\xi}}\chi(\boldsymbol{\xi}) \tag{3.6}$$

where $\boldsymbol{x} \in \mathbb{R}^{2M}$ are the eigenvalues of the quadrature operators and span a real symplectic space (phase space); $\boldsymbol{\xi} \in \mathbb{R}^{2M}$; $\chi(\boldsymbol{\xi})$ is the symmetric characteristic function:

$$\chi(\boldsymbol{\xi}) := \mathrm{Tr}[\hat{\rho}\hat{D}(\boldsymbol{\xi})]; \tag{3.7}$$

and $\hat{D}(\boldsymbol{\xi})$ is the Weyl (displacement) operator:

$$\hat{D}(\boldsymbol{\xi}) := e^{i\boldsymbol{x}^T\boldsymbol{\Omega}\boldsymbol{\xi}}. \tag{3.8}$$

[2]Quasi-probability means that it is normalized but in general non-positive.

The Wigner function W (and characteristic function χ) offer a representation that is slightly more akin to classical statistical mechanics than the density operator $\hat{\rho} \in \mathcal{H}^{\otimes M}$, which can equivalently also be used to fully characterize any quantum state.

3.1.2 The Displacement Vector and Covariance Matrix

Just as in classical probability theory, the quasi-probability distribution function W can also be characterized by the statistical moments of the quantum state. The first moment is called the displacement vector $\boldsymbol{d}$ and the second moment is the covariance matrix $\boldsymbol{\sigma}$ where the diagonal elements provide the variances of the quadrature operators. The components of these moments are defined as:

$$d_i := \langle \hat{x}_i \rangle \;=\; \mathrm{Tr}(\hat{x}_i \hat{\rho}_S), \tag{3.9}$$

$$\begin{aligned} \sigma_{ij} &:= \frac{1}{2}\langle \{\hat{x}_i, \hat{x}_j\} \rangle - \langle \hat{x}_i \rangle \langle \hat{x}_j \rangle \\ &= \frac{1}{2}\mathrm{Tr}(\{\hat{x}_i - d_i, \hat{x}_j - d_j\}\hat{\rho}_S). \end{aligned} \tag{3.10}$$

The covariance matrix is a real $2M \times 2M$ symmetric matrix which, due to the uncertainty relations among canonical operators, must satisfy [85, 86]:

$$\boldsymbol{\sigma} + \frac{i}{4\kappa^2}\boldsymbol{\Omega} \geq 0, \tag{3.11}$$

which implies the positive definiteness of the matrix. This is in fact the only necessary and sufficient constraint a matrix has to fulfil in order to be the covariance matrix related to a physical state [86].

3.1.3 Gaussian States

Gaussian states are defined as bosonic states whose Wigner function is of Gaussian form:

$$W(\boldsymbol{x}) = \frac{e^{-\frac{1}{2}(\boldsymbol{x}-\boldsymbol{d})^T \boldsymbol{\sigma}^{-1}(\boldsymbol{x}-\boldsymbol{d})}}{(2\pi)^{2M}\sqrt{\det \boldsymbol{\sigma}}} \tag{3.12}$$

where $\boldsymbol{\sigma}$ characterizes the width and $\boldsymbol{d}$ characterizes the centre of the Wigner function. The first two statistical moments are therefore sufficient for a complete description of Gaussian states. In fact, in quantum information theory, often only the covariance matrix is used to characterize the state since first moments don't contribute to informationally relevant properties such as entanglement and entropy [42].

There are four important subclasses of Gaussian states: the vacuum state, coherent states, squeezed states and thermal states. The most important is the vacuum state, which is the state with no bosons. The covariance matrix of the vacuum state is just proportional to the identity:

$$\boldsymbol{\sigma}_{vac} = \frac{1}{4\kappa^2}\boldsymbol{I}. \tag{3.13}$$

Coherent states are displaced vacuum states. That is, they have the same covariance matrix as the vacuum but a non-zero displacement vector. They are defined as the the eigenstates of the annihilation operator $\hat{a}|\alpha\rangle = \alpha|\alpha\rangle$ (the vacuum is the eigenstate with zero eigenvalue) and can be expanded in the number basis as:

$$|\alpha\rangle = e^{-\frac{1}{2}|\alpha|^2}\sum_{n=0}^{\infty}\frac{\alpha^n}{\sqrt{n!}}|n\rangle. \tag{3.14}$$

These states are often said to have a maximal kind of coherence and exhibit a classical kind of behaviour since the behaviour of the states closely resembles that of the oscillatory behaviour of a classical harmonic oscillator. They are also minimum uncertainty states (the uncertainty principle is saturated) and are frequently used in quantum optics. For example, a coherent is the most important state that represents a LASER operating far above threshold [87]

Squeezed states are also minimum uncertainty states. However, whereas the variance of the quadratures is equal for coherent states, this is not the case for squeezed states. Since the uncertainty of a state is equivalent to the area it possesses on phase space, squeezed states form an ellipse on phase space, whereas, the vacuum and coherent states form circles. On going from a coherent state to a squeezed state, the circle on phase space will thus be

squeezed and become an ellipse of identical area. Such a transformation, called the squeezing transformation is, for a single-mode state, given by:

$$S(\xi) = e^{\frac{1}{2}\xi(\hat{a}^\dagger)^2 - \frac{1}{2}\xi^*\hat{a}^2} \tag{3.15}$$

and, when applied to the vacuum, generates the state:

$$|\xi\rangle = \frac{1}{\sqrt{\mu}} \sum_{k=0}^{\infty} \left(\frac{\nu}{2\mu}\right)^k \frac{\sqrt{(2k)!}}{k!} |2k\rangle \tag{3.16}$$

where $\mu := \cosh r$, $\nu := e^{i\phi} \sinh r$ and $\xi := re^{i\phi}$.

Squeezed states of light are considered to be particularly important ingredients in quantum metrology and communication [88]. Squeezing of matter wave fields in BECs has also been considered for such purposes [90]. There have also been investigations into squeezed states of collective excitations of the condensate. For example, in [78], the Beliaev process is treated as parametric down-conversion where two-mode squeezed states of the excitations are created. The acoustic analogue of the dynamical Casimir effect considered in [37, 38] can, in certain cases, also create two-mode squeezed states of the collective excitations. Another method for creating Squeezed states of quantized density oscillations has also been considered in [91].

A thermal state is the state of a system that is in thermodynamic equilibrium. In this case the temperature fully characterizes the system, giving its average energy. By definition, a thermal state maximizes the von Neumann entropy $S = -\mathrm{Tr}(\hat{\rho} \ln \hat{\rho})$ for fixed energy $\mathrm{Tr}(\hat{\rho}\hat{a}^\dagger\hat{a}) = \overline{n}$ where $\overline{n}$ is the mean number of particles in the bosonic mode. It is therefore a maximally mixed state constrained by energy. The density operator of a thermal state is:

$$\hat{\rho}_{th} = \frac{e^{-\hat{H}/k_B T}}{\mathrm{Tr}(e^{-\hat{H}/k_B T})}, \tag{3.17}$$

which, in the number basis, is given by $\hat{\rho}_{th} = \otimes_{i=1}^{M} \hat{\nu}_i$ with:

$$\hat{\nu}_i = \frac{\sum_{n=0}^{\infty} e^{-\hbar\omega_i/k_BT}|n\rangle_{ii}\langle n|}{\mathrm{Tr}\Big[\sum_{n=0}^{\infty} e^{-\hbar\omega_i/k_BT}|n\rangle_{ii}\langle n|\Big]} = \frac{1}{1+N_i^{th}}\sum_{n=0}^{\infty}\Big(\frac{N_i^{th}}{1+N_i^{th}}\Big)^n |n\rangle_{ii}\langle n| \tag{3.18}$$

where N_i^{th} is the average thermal occupation of the bosonic mode i, which comes from the Bose-Einstein distribution for the mode (see (1.31)).

The covariance matrix of this state can be shown to be given by (see e.g. [41]):

$$\boldsymbol{\sigma}_{th} = \frac{1}{4\kappa^2}\mathrm{diag}(1+2N_1^{th}, 1+2N_1^{th}, \ldots, 1+2N_N^{th}, 1+2N_N^{th}) \tag{3.19}$$

and the displacement vector is zero.

Thermal states can be thought of as the most fundamental Gaussian states. This is because, due to Williamson's theorem which shows that every positive-definite real matrix of even dimension can be put in diagonal form by a particular symplectic transformation [92], every Gaussian state can be decomposed into thermal states.

3.1.4 Gaussian Unitaries

A Gaussian unitary describes a unitary operator which preserves the Gaussian character of the state. That is, it is a unitary operator which maps a Gaussian Wigner function into another Gaussian Wigner function. These operations play a major role in the theoretical and experimental manipulation of Gaussian states. For example, ideal beam-splitters, phase shifters and squeezers can be described in terms of a Gaussian unitary [41, 93].

In terms of the quadrature operators, a Gaussian unitary corresponds to the affine map:

$$\hat{\boldsymbol{x}} \to \boldsymbol{S}\hat{\boldsymbol{x}} + \boldsymbol{e} \tag{3.20}$$

where $\boldsymbol{e} \in \mathbb{R}^{2M}$ and $\boldsymbol{S}$ is a $2M \times 2M$ real matrix. This transformation must preserve the commutation relations of (3.4), which is satisfied when

the matrix $\boldsymbol{S}$ is symplectic:

$$\boldsymbol{S}\boldsymbol{\Omega}\boldsymbol{S}^T = \boldsymbol{\Omega}. \tag{3.21}$$

An arbitrary Gaussian unitary is therefore equivalent to an affine symplectic map $(\boldsymbol{S}, \boldsymbol{e})$ acting on the phase space. The symplectic transformations corresponding to the Gaussian unitaries thus act on a $2M$-dimensional phase space and form the (real) symplectic group $\mathrm{Sp}(2M, \mathbb{R})$ [94]. The Lie algebra of this group is given by the set of $2M \times 2M$ (real) Hamiltonian matrices $\mathcal{H}$, which which must satisfy the condition:

$$(\boldsymbol{\Omega}\boldsymbol{\mathcal{H}})^T = \boldsymbol{\Omega}\boldsymbol{\mathcal{H}} \tag{3.22}$$

as can be easily verified from (3.21) when $\boldsymbol{S}(t) = e^{\boldsymbol{\mathcal{H}}t}$. Since they are Hamiltonian matrices, the generators can also be written as $\boldsymbol{\mathcal{H}} = \boldsymbol{\Omega}\boldsymbol{H}$ where $\boldsymbol{H}$ are $2M \times 2M$ (real) symmetric matrices [94]. The generators that are anti-symmetric result in the compact subgroup $\boldsymbol{\mathcal{H}}(M) = \mathrm{Sp}(2M, \mathbb{R}) \cap \mathrm{SO}(2M)$, corresponding to orthogonal symplectic transformations, and constitute 'energy preserving' or passive operations [95]. On the other hand, the symmetric generators result in the non-compact subset of the group, which represents the active transformations such as squeezings [95]. Single-mode transformations can be created from the following set of generators [95]:

$$\boldsymbol{\chi} = \begin{pmatrix} 0 & 1 \\ 1 & 0 \end{pmatrix}, \ \boldsymbol{\Omega} = \begin{pmatrix} 0 & 1 \\ -1 & 0 \end{pmatrix}, \ \boldsymbol{\zeta} = \begin{pmatrix} 1 & 0 \\ 0 & -1 \end{pmatrix} \tag{3.23}$$

for which the corresponding symmetric matrices $\boldsymbol{H}$ are $-\boldsymbol{\zeta}$, $\boldsymbol{\chi}$ and the identity matrix $\boldsymbol{I}$. The identity matrix $\boldsymbol{I}$ generates the compact single-mode rotations, while $\boldsymbol{\zeta}$ and $\boldsymbol{\chi}$ generate single-mode squeezings. A basis of the general generators $\boldsymbol{\mathcal{H}}$ can in fact be built from these generators and those for two mode transformations [95].

The transformation of the quadrature operators induced by a Gaussian unitary (3.20) can be easily shown to result in the following transformations

for the first and second statistical moments (see e.g. [41]):

$$\boldsymbol{d} \to \boldsymbol{S}\boldsymbol{d} + \boldsymbol{e}, \tag{3.24}$$

$$\boldsymbol{\sigma} \to \boldsymbol{S}\boldsymbol{\sigma}\boldsymbol{S}^T. \tag{3.25}$$

It can also be shown that Gaussian unitaries must be generated from Hamiltonians $\hat{H}$ which are second-order polynomials in the field operators [96]:

$$\hat{H} = H_0 + i(\boldsymbol{H}_{1a}\hat{\boldsymbol{a}} + \hat{\boldsymbol{a}}^\dagger \boldsymbol{H}_{2a}\hat{\boldsymbol{a}} + \hat{\boldsymbol{a}}^T \boldsymbol{H}_{2b}\hat{\boldsymbol{a}}) + h.c. \tag{3.26}$$

where H_0 is a constant; $\boldsymbol{H}_{1a}$ is a M-dimensional column-vector; $\boldsymbol{H}_{2a}$ and $\boldsymbol{H}_{2b}$ are $M \times M$ dimensional matrices; $\hat{\boldsymbol{a}} = (\hat{a}_1, \ldots, \hat{a}_M)^T$; $\hat{\boldsymbol{a}}^\dagger = (\hat{a}_1^\dagger, \ldots, \hat{a}_M^\dagger)$; and the corresponding unitary transformation is given by $\hat{U}(t) = e^{-i\hat{H}t/\hbar}$.

3.2 Gaussian States of Open Quantum Systems

This section considers how Gaussian states evolve when the states are treated as those of an open quantum system. In particular, the Gaussian states are treated as open quantum systems interacting with a thermal (and thus Gaussian) environment in the Born-Markov and secular approximations such that the density operator evolves via a Markov master equation in Lindblad form as derived in the previous chapter.

One approach to determining how the Gaussian states evolve is to transform this master equation into a Fokker-Planck equation for the Wigner function [41, 44, 97]. The time evolution of the covariance matrix and displacement vector, which fully characterize a Gaussian state, can then be derived from the time evolution of the Wigner function. Alternatively, the time evolution of these statistical moments can be derived straight from the evolution of the density operator, which, in the Schrödinger picture, is given by (2.46):

$$\frac{d}{dt}\hat{\rho}_S = -\frac{i}{\hbar}[\hat{H}, \hat{\rho}_S] + \mathcal{D}(\hat{\rho}_S) \tag{3.27}$$

where the renormalized Hamiltonian is defined by $\hat{H} = \hat{H}_S + \hat{H}_{LS}$, and the dissipator $\mathcal{D}(\hat{\rho_S})$ is given by:

$$\mathcal{D}(\hat{\rho_S}) = \sum_i \left(\hat{c}_i \hat{\rho}_S \hat{c}_i^\dagger - \frac{1}{2}\{\hat{c}_i^\dagger \hat{c}_i, \hat{\rho}_S\} \right) \tag{3.28}$$

where $\hat{c}_i^\dagger$ are the Lindblad operators, which are obtained from the eigenoperators of the open system by a unitary transformation. The time evolution of the covariance matrix and displacement vector can then be obtained by differentiating their definitions (3.9)-(3.10) and substituting in the differential of the density operator as defined above. By assuming the bosonic system as described in the previous section and rewriting the Markov master equation (3.27) in the phase space picture, simple equation of motions for the statistical moments can then be derived (see Appendix B and [98–100]).

As discussed in the previous Section, Gaussian unitaries are generated by Hamiltonians that are second-order polynomials in the field operators and, therefore, the (renormalized) free Hamiltonian in (3.27) is taken to be of the form of (3.26). In the phase space picture this can be written as $\hat{H} = H_0 + \kappa \hat{\boldsymbol{x}}^T \boldsymbol{H}_1 + \kappa^2 \hat{\boldsymbol{x}}^T \boldsymbol{H}_2 \hat{\boldsymbol{x}}$ where H_0 is a constant; $\boldsymbol{H}_1$ is a $2M$-dimensional column vector; and $\boldsymbol{H}_2$ is a $2M \times 2M$ real, symmetric matrix. Substituting this Hamiltonian into (3.27) and writing the Lindblad operators as linear combinations of quadrature operators (which must be the case since they are linear combinations of creation and annihilation operators), the equation of motion for the displacement vector and covariance matrix is shown in Appendix B to be [98–100]:

$$\frac{d\boldsymbol{d}}{dt} = \boldsymbol{\mathcal{H}}_1 + \boldsymbol{A}\boldsymbol{d}, \tag{3.29}$$

$$\frac{d\boldsymbol{\sigma}}{dt} = \boldsymbol{A}\boldsymbol{\sigma} + \boldsymbol{\sigma}\boldsymbol{A}^{\boldsymbol{T}} + \boldsymbol{D} \tag{3.30}$$

where $\boldsymbol{\mathcal{H}}_1 := \boldsymbol{\Omega}\boldsymbol{H}_1/\hbar$, and the matrix $\boldsymbol{A}$ and symmetric matrix $\boldsymbol{D}$ are referred to as the drift and diffusion matrices respectively [100]. These

matrices are defined as:

$$\boldsymbol{D} := \frac{1}{4\kappa^4}\boldsymbol{\Omega} Re(\boldsymbol{C}^\dagger \boldsymbol{C})\boldsymbol{\Omega}^{\boldsymbol{T}}, \tag{3.31}$$

$$\boldsymbol{A} := \boldsymbol{\mathcal{H}}_2 + \boldsymbol{\mathcal{K}} \tag{3.32}$$

where:

$$\boldsymbol{\mathcal{K}} := \frac{1}{2\kappa^2}\boldsymbol{\Omega} Im(\boldsymbol{C}^\dagger \boldsymbol{C}), \tag{3.33}$$

$$\boldsymbol{\mathcal{H}}_2 := \frac{1}{\hbar}\boldsymbol{\Omega}\boldsymbol{H}_2 \tag{3.34}$$

with the matrix $\boldsymbol{C}$ defined by $\hat{c}_i = C_{ij}\hat{x}_j$.

The general solution of (3.29) is:

$$\boldsymbol{d}(t) = \boldsymbol{X}(t)\boldsymbol{d}_0 + \boldsymbol{Y}(t) \tag{3.35}$$

where, when $\boldsymbol{A}$ is independent of time:

$$\boldsymbol{X}(t) = e^{\boldsymbol{A}t}, \tag{3.36}$$

$$\begin{aligned}\boldsymbol{Y}(t) &= \int_0^t e^{\boldsymbol{A}(t-s)} ds \boldsymbol{H}_1 \\ &= \boldsymbol{A}^{-1}(e^{\boldsymbol{A}t} - 1)\boldsymbol{H}_1.\end{aligned} \tag{3.37}$$

Note that $\boldsymbol{X}(t)$ has to fulfil the condition $\lim_{t\to\infty} \boldsymbol{X}(t) = 0$ and so $\boldsymbol{A}$ must have only eigenvalues with negative parts [98, 101].

The equation of motion for the covariance matrix (3.30) is, in general, a time varying differential Lyapunov matrix equation, of which the general solution is [101]:

$$\boldsymbol{\sigma}(t) = \boldsymbol{X}(t)\boldsymbol{\sigma}_0\boldsymbol{X}^T(t) + \boldsymbol{Z}(t) \tag{3.38}$$

where:

$$\boldsymbol{X}(t) = \boldsymbol{\Phi}(t, 0), \tag{3.39}$$

$$\boldsymbol{Z}(t) = \int_0^t \boldsymbol{\Phi}(t, s)\boldsymbol{D}\boldsymbol{\Phi}^T(t, s)ds. \tag{3.40}$$

When $\boldsymbol{A}$ is independent of time,[3] $\boldsymbol{\Phi}(t, s) = e^{\boldsymbol{A}(t-s)}$ and so the solution to (3.30) can be written as:[4]

$$\boldsymbol{\sigma}(t) = e^{\boldsymbol{A}t}\boldsymbol{\sigma}_0 e^{\boldsymbol{A}^T t} + \int_0^t e^{\boldsymbol{A}(t-s)}\boldsymbol{D}e^{\boldsymbol{A}^T(t-s)}ds \tag{3.41}$$

for which an analytical expression can be obtained when $\boldsymbol{A}$ is diagonalizable [103]. As above, $\boldsymbol{X}(t)$ has to fulfil the condition $\lim_{t\to\infty} \boldsymbol{X}(t) = 0$ for a stable solution and so again $\boldsymbol{A}$ must have only eigenvalues with negative parts [98, 101].

The above solution can also be written as [98, 99, 101]:

$$\boldsymbol{\sigma}(t) = e^{\boldsymbol{A}t}(\boldsymbol{\sigma}_0 - \boldsymbol{\Sigma})e^{\boldsymbol{A}t} + \boldsymbol{\Sigma} \tag{3.42}$$

where $\boldsymbol{\Sigma}$ is time-independent and is the solution of the algebraic matrix Lyapunov equation ($\frac{d\boldsymbol{\sigma}}{dt} = 0$):

$$\boldsymbol{A}\boldsymbol{\Sigma} + \boldsymbol{\Sigma}\boldsymbol{A}^T + \boldsymbol{D} = 0. \tag{3.43}$$

Furthermore, if the following limit exists:

$$\boldsymbol{\sigma}_\infty = \lim_{t\to\infty} \boldsymbol{\sigma}(t), \tag{3.44}$$

then $\boldsymbol{\Sigma} = \boldsymbol{\sigma}_\infty$ [98].

[3] There is no general analytic expression for the transition matrix $\boldsymbol{\Phi}(t, s)$ when $\boldsymbol{A}$ is time dependent and in this case a numerical method is then the only way to obtain a solution [101].

[4] Another option is to convert (3.30) to a vector valued ODE, which can then be readily solved, using vectorization of the matrix $\boldsymbol{\sigma}(t)$ [102].

A connection can be made with the evolution of the displacement vector and covariance matrix generated by a Gaussian unitary (see Section 3.1.4) by neglecting all dissipative effects ($\boldsymbol{D} = 0$, $\boldsymbol{A} = \boldsymbol{\mathcal{H}}_2$). In this case, assuming for convenience that $\boldsymbol{H}_2$ and $\boldsymbol{H}_1$ are independent of time, the solutions (3.35) and (3.38) reduce to:

$$\boldsymbol{d}(t) = e^{\boldsymbol{\mathcal{H}}_2 t}\boldsymbol{d}_0 + \overline{\boldsymbol{\mathcal{H}}}_1(t), \tag{3.45}$$

$$\boldsymbol{\sigma}(t) = e^{\boldsymbol{\mathcal{H}}_2 t}\boldsymbol{\sigma}_0 e^{\boldsymbol{\mathcal{H}}_2^T t} \tag{3.46}$$

where $\overline{\boldsymbol{\mathcal{H}}}_1(t) := \boldsymbol{B}(t)\boldsymbol{\mathcal{H}}_1$ is a real vector with $\boldsymbol{B}(t) := \boldsymbol{\mathcal{H}}_2^{-1}(e^{\boldsymbol{\mathcal{H}}_2 t} - 1)$. By defining $\boldsymbol{S}(t) := e^{\boldsymbol{\mathcal{H}}_2 t}$ it is clear that this is the symplectic transformation corresponding to the free unitary evolution of the system defined by (3.20) and $\overline{\boldsymbol{\mathcal{H}}}_1(t)$ is equivalent to the real vector $\boldsymbol{e}$. The matrix $\boldsymbol{\mathcal{H}}_2 = \boldsymbol{\Omega}\boldsymbol{H}_2/\hbar$ thus forms a symplectic algebra and so, as discussed in Section 3.1.4, $\boldsymbol{\mathcal{H}}_2$ is a (real) Hamiltonian matrix and $\boldsymbol{H}_2$ is a (real) symmetric matrix, which is also required by the Hermitian property of $\hat{H}$.

More generally, when $\boldsymbol{\mathcal{H}}_2$ commutes with $\boldsymbol{\mathcal{K}}$, then the dissipative and free dynamics can be separated out since in this case $e^{\boldsymbol{A}t} = e^{\boldsymbol{\mathcal{H}_2} t}e^{\boldsymbol{\mathcal{K}} t}$. The time-independent solution of the equation of motion for the covariance matrix (3.41) can then be written as:

$$\boldsymbol{\sigma}(t) = \boldsymbol{E}(t)\boldsymbol{\sigma}_S(t)\boldsymbol{E}^T(t) + \int_0^t \boldsymbol{E}(t-s)\boldsymbol{D}_S(t-s)\boldsymbol{E}^T(t-s)ds \tag{3.47}$$

where the subscript S denotes the evolution due to the free dynamics, and $\boldsymbol{E}$ and $\boldsymbol{D}$ constitute the dissipative dynamics:

$$\boldsymbol{\sigma}_S(t) := \boldsymbol{S}(t)\boldsymbol{\sigma}_0\boldsymbol{S}^T(t), \tag{3.48}$$

$$\boldsymbol{D}_S(t) := \boldsymbol{S}(t)\boldsymbol{D}\boldsymbol{S}^T(t), \tag{3.49}$$

$$\boldsymbol{E}(t) := e^{\boldsymbol{\mathcal{K}} t}. \tag{3.50}$$

3.3 Evolution of Gaussian Phonon States

The previous Section looked at how the statistical moments of a general Gaussian state evolve when the state is an open quantum system obeying the general Markov equation in Lindblad form (3.27). In this section the results are specialized to the case of a single-mode phonon state of a BEC.

From Chapter 2, the density operator of the single-mode phonon state obeys the Markov equation in Lindblad form where the Lindblad operators are given by (2.55)-(2.56):

$$\hat{c}_1 = \sqrt{\gamma_{11}}\hat{\boldsymbol{b}}_{\boldsymbol{q}}, \tag{3.51}$$

$$\hat{c}_2 = \sqrt{\gamma_{22}}\hat{\boldsymbol{b}}_{\boldsymbol{q}}^{\dagger}. \tag{3.52}$$

Following (3.3), the quadrature operators for this state are defined as:

$$\hat{\boldsymbol{x}} := \begin{pmatrix} \hat{x}_1 \\ \hat{x}_2 \end{pmatrix} := \frac{1}{2\kappa} \begin{pmatrix} 1 & 1 \\ -i & i \end{pmatrix} \begin{pmatrix} \hat{b}_{\boldsymbol{q}} \\ \hat{b}_{\boldsymbol{q}}^{\dagger} \end{pmatrix} \tag{3.53}$$

and the Lindblad operators can therefore be written as a the following linear combination of the quadrature operators:

$$\hat{\boldsymbol{c}} = \boldsymbol{C}\hat{\boldsymbol{x}} \tag{3.54}$$

where:

$$\hat{\boldsymbol{c}} := \begin{pmatrix} \hat{c}_1 \\ \hat{c}_2 \end{pmatrix}, \tag{3.55}$$

$$\boldsymbol{C} = \kappa \begin{pmatrix} \sqrt{\gamma_{11}} & i\sqrt{\gamma_{11}} \\ \sqrt{\gamma_{22}} & -i\sqrt{\gamma_{22}} \end{pmatrix}. \tag{3.56}$$

The renormalized Hamiltonian for the single-mode phonon state is given by (1.26): $\hat{H} = \hbar\omega'_{\boldsymbol{q}}\hat{\boldsymbol{b}}_{\boldsymbol{q}}^{\dagger}\hat{\boldsymbol{b}}_{\boldsymbol{q}}$ where $\omega'_{\boldsymbol{q}}$ is the renormalized frequency. This can

then be written in the phase space picture as $\hat{H} = \hat{\boldsymbol{x}}^T \boldsymbol{H}_2 \hat{\boldsymbol{x}}$ where:

$$\boldsymbol{H}_2 = \hbar\omega_{\boldsymbol{q}}' \boldsymbol{I} \tag{3.57}$$

and $\boldsymbol{I}$ is the 2×2 identity matrix.

Following Section 3.2, we can then transform the Markov master equation for the phonon state (3.27) to the phase space picture and the displacement vector and covariance matrix will obey the equations of motion (3.29) and (3.30) where the drift and diffusion matrices are given by:

$$\boldsymbol{A} := \omega_q' \boldsymbol{\Omega} - \frac{1}{2}\gamma \boldsymbol{I}, \tag{3.58}$$

$$\boldsymbol{D} = \frac{1}{4\kappa^2}\gamma_T \boldsymbol{I} \tag{3.59}$$

since, from (3.55), $\boldsymbol{C}^\dagger \boldsymbol{C}$ is the following for the single phonon mode:

$$\boldsymbol{C}^\dagger \boldsymbol{C} = \kappa^2 \begin{pmatrix} \gamma_T & -i\gamma \\ i\gamma & \gamma_T \end{pmatrix} \tag{3.60}$$

$$= \kappa^2(\gamma_T \boldsymbol{I} - i\gamma \boldsymbol{\Omega}) \tag{3.61}$$

where $\gamma_T := \gamma_{11} + \gamma_{22}$; $\gamma := \gamma_{22} - \gamma_{11}$; γ_{11} and γ_{22} are defined by (2.69) and (2.70); and $\boldsymbol{\Omega}$ is the symplectic form:

$$\boldsymbol{\Omega} = \begin{pmatrix} 0 & 1 \\ -1 & 0 \end{pmatrix}. \tag{3.62}$$

Substituting the above drift and diffusion matrices for the single-mode phonon system into the general time-independent solutions (3.35) (using (3.36) and (3.37)) and (3.41), the displacement vector and covariance matrix at time t are found to be:

$$\boldsymbol{d}(t) = e^{-\frac{1}{2}\gamma t} \boldsymbol{R}(t) \boldsymbol{d}_0, \tag{3.63}$$

$$\boldsymbol{\sigma}(t) = e^{-\gamma t}\Big(\boldsymbol{R}(t)\boldsymbol{\sigma}_0\boldsymbol{R}^T(t)\Big) + (1 - e^{-\gamma t})\boldsymbol{\sigma}_\infty \tag{3.64}$$

where:

$$\boldsymbol{\sigma}_\infty := \frac{1}{\gamma}\boldsymbol{D} = \frac{1}{4\kappa^2}\frac{\gamma_T}{\gamma}\boldsymbol{I}, \tag{3.65}$$

$$\boldsymbol{R}(t) := e^{\boldsymbol{\Omega}\boldsymbol{H}_2 t/\hbar}. \tag{3.66}$$

The matrix $\boldsymbol{R}(t)$ represents the symplectic transformation corresponding to the free unitary evolution of the single-mode phonon system $U = e^{-iH_S t/\hbar}$ and, since $\boldsymbol{H}_2 = \hbar\omega_q'\boldsymbol{I}$, then $\boldsymbol{R}(t) = \cos(\omega_q t)\boldsymbol{I} + \sin(\omega_q t)\boldsymbol{\Omega}$, which is just the usual symplectic (and in this case rotational) transformation for the phase shift operator. Due to the dissipative effects, this free evolution is now damped by $e^{-\gamma t}$ and the state asymptotically approaches $\boldsymbol{\sigma}_\infty$. If the free evolution can be neglected compared to the dissipative dynamics, then equations (3.63)-(3.64) reduce to the simple expressions [41, 44]:

$$\boldsymbol{d}(t) = e^{-\frac{1}{2}\gamma t}\boldsymbol{d}_0, \tag{3.67}$$

$$\boldsymbol{\sigma}(t) = e^{-\gamma t}\boldsymbol{\sigma}_0 + (1 - e^{-\gamma t})\boldsymbol{\sigma}_\infty. \tag{3.68}$$

As noted in Chapter 2, since the environment is in thermal equilibrium, the two rates γ_{11} and γ_{22} will not be independent but will instead satisfy $\gamma_{11} = e^{\beta_q}\gamma_{22}$ where $\beta_q := \hbar\omega_q/k_B T$ [27, 32]. The rate γ_T can then be written as:

$$\gamma_T := \gamma\coth(\frac{1}{2}\beta_q) = \gamma(1 + 2N_q^{th}) \tag{3.69}$$

where N_q^{th} is the average thermal occupation of a bosonic system, which is given by the Bose-Einstein distribution (see Appendix A for a verification of (A.25) for the single-mode phonon system using the derived expressions

for the rates γ_{11} and γ_{22}). Therefore, the matrix $\boldsymbol{\sigma}_\infty$ is given by:

$$\boldsymbol{\sigma}_\infty = \frac{(1+2N_q^{th})}{4\kappa^2}\boldsymbol{I}, \tag{3.70}$$

which is the covariance matrix of a single-mode thermal state (see e.g. [41]). The excited single-mode phonon state will thus asymptotically approach a thermal sate i.e. it will relax back to thermal equilibrium with the rest of the quasi-particle modes as anticipated.

The form of the equations for the evolution of the statistical moments (3.63)-(3.64) will apply to any single-mode system with free Hamiltonian $\hat{H}_S \propto \hat{b}_q^\dagger \hat{b}_q$ that is interacting in the Born-Markov approximation with an environment that is in thermal equilibrium, and is not just specific to the case of a single-mode phonon state of a BEC. Instead the specific case of a single-mode phonon state is only felt through the damping rate γ and the expected experimental values for ω_q and T. The damping rate γ depends on the environment correlation functions and is, in general, given by (2.72), although analytical expressions can be derived under certain approximations as reviewed in Section 2.3. The fact that it is the characteristic form of the rate γ that separates the single-mode phonon system from other bosonic systems is illustrated in the next section using the specific example of a damped harmonic oscillator in a Gaussian state.

3.3.1 Comparison with Previous Studies

Studies of Gaussian states of open quantum systems have principally considered a bosonic system coupled to an environment modeled by a large number of external modes and with an interaction Hamiltonian that is bilinear in field operators. Such an interaction Hamiltonian is given, for example, by:

$$\hat{H}_I = \sum_i \left(g_i \hat{a}_i \hat{r}_i^\dagger + g_i^* \hat{a}_i^\dagger \hat{r}_i \right) \tag{3.71}$$

where $\hat{a}_i$ and $\hat{a}_i^\dagger$ represent the annihilation and creation operators of the open system, g_i denotes the coupling strength, and $\hat{r}_i$ and $\hat{r}_i^\dagger$ represent the

annihilation and creation operators of the environment.

Taking just a single-mode system, (3.71) represents the interaction Hamiltonian of a damped harmonic oscillator, which could, for example, describe the damping of an electromagnetic field mode inside a cavity [32]. After a rotating wave approximation in the interaction picture has been applied, the interaction Hamiltonian is also similar to that used for the optical system considered in Section 2.3.1, which was used to derive the two-level quantum optical master equation (2.84).

In the Born-Markov approximation, and assuming that the environment is in a thermal state, a Lindblad master equation can be derived for the single-mode bosonic system [30, 32, 76]:

$$\frac{d}{dt}\hat{\rho}_S = -\frac{i}{\hbar}[\hat{H}, \hat{\rho}_S] + \gamma^a_{11}\Big(\hat{a}\hat{\rho}_S\hat{a}^\dagger - \frac{1}{2}\{\hat{a}^\dagger\hat{a}, \hat{\rho}_S\}\Big) + \gamma^a_{22}\Big(\hat{a}^\dagger\hat{\rho}_S\hat{a} - \frac{1}{2}\{\hat{a}\hat{a}^\dagger, \hat{\rho}_S\}\Big), \tag{3.72}$$

which is analogous to the master equation derived for the phonon system interacting with an environment of quasi-particle modes (2.53) since the same approximations were used in its derivation. However, the two master equations contain different rates due to the different interaction Hamiltonians. Analogous to the optical system case considered in Section 2.3.1, the rates γ^a_{11} and γ^a_{22} of the master equation for the damped harmonic oscillator are given by [30, 32, 76]:

$$\gamma^a_{11} := \frac{4\omega_a^3|g|^2}{3\hbar c^3}(1 + N_a), \tag{3.73}$$

$$\gamma^a_{22} := \frac{4\omega_a^3|g|^2}{3\hbar c^3}N_a \tag{3.74}$$

where ω_a is the frequency of the system's mode, and N_a is the thermal occupation of the mode. These expressions are in contrast to the much more complicated expressions for the rates γ_{11} and γ_{22} for the single-mode phonon system (see (2.69) and (2.70)).

By assuming an initial Gaussian state and following the same steps car-

ried out in the previous section, the covariance matrix and displacement vector of the damped harmonic oscillator can be shown to satisfy the following once the free dynamics have been neglected [41, 44]:

$$\boldsymbol{d}_a(t) = e^{-\frac{1}{2}\gamma_a t}\boldsymbol{d}_0, \tag{3.75}$$

$$\boldsymbol{\sigma}_a(t) = e^{-\gamma_a t}\boldsymbol{\sigma}_0 + (1 - e^{-\gamma_a t})\boldsymbol{\sigma}^a_\infty, \tag{3.76}$$

$$\boldsymbol{\sigma}^a_\infty := \frac{1}{4\kappa^2}\frac{\gamma^a_T}{\gamma_a}\boldsymbol{I} \tag{3.77}$$

where $\gamma_a := \gamma^a_{22} - \gamma^a_{11}$ and $\gamma^a_T := \gamma^a_{11} + \gamma^a_{22}$. These expressions are of course analogous to those of (3.67),(3.68) and (3.65) due to the analogy of the master equations for the damped harmonic oscillator and single-mode phonon systems.

Just as for the single-mode phonon system, since the environment of the bosonic system is in thermal equilibrium, the two rates γ^a_{11} and γ^a_{22} are not independent but instead satisfy [32]:

$$\gamma^a_{11} = e^{\hbar\omega_a/k_BT}\gamma^a_{22} \implies \frac{\gamma^a_T}{\gamma_a} = 1 + 2N_a, \tag{3.78}$$

which is of course clearly satisfied by (3.73)-(3.74) since, from these expressions, $\gamma_a = 4\omega_a^3|g|^2/3\hbar c^3$ and $\gamma^a_T = (4\omega_a^3|g|^2/3\hbar c^3)(1 + 2Na)$. Substitution of (3.78) into (3.77) then illustrates that $\boldsymbol{\sigma}^a_\infty$ is the covariance matrix of the thermal state with frequency ω_a. The fact that $\gamma_T/\gamma = 1 + 2N_{\boldsymbol{q}}$ equally holds in the single-mode phonon system was also used to show that the final state for that system is similarly the thermal state of the mode $\boldsymbol{q}$. In that case the verification of the expression $\gamma_T/\gamma = 1 + 2N_{\boldsymbol{q}}$ using the definitions of γ_{22} and γ_{11} is a little more complicated but still involves simple algebra (see Appendix A).

From (3.75)-(3.76), the dissipation of the damped harmonic oscillator system is characterized by the rate γ_a, which is defined by $\gamma^a_{22} - \gamma^a_{11}$. Similarly, from (3.67)-(3.68), the dissipation of the single-mode phonon system is characterized by the rate γ, which is defined by $\gamma_{22} - \gamma_{11}$ and this was already anticipated in Section 2.3. As discussed in Section 2.3.1, the rate γ,

given by (2.72), is, in general, a lot more complicated than the simple rate γ_a for the damped harmonic oscillator, or equivalently the two-level system of Section 2.3.1. However, as illustrated in Section 2.3, simple expressions can be used for γ when certain approximations are assumed such as low or high temperatures. These expressions are given by (2.77)-(2.79), none of which have the same frequency dependence as γ_a. This is the essential difference between the single-mode phonon system in a Gaussian state and the damped harmonic oscillator system in a Gaussian state, or equivalently the two-level system of Section 2.3.1, and arises from the different types of interaction Hamiltonians. Two other parameters that characterize the evolution of the different systems are the frequency of the mode and the temperature of the environment, which will, in practice, likely be quite different for the optical and phonon systems. As well as contributing to the dissipation rate γ, the frequency of the system also characterizes the free dynamics of the systems, which will, in general, contribute to their evolution. However, in Chapter 4 it is shown that the free dynamics are unimportant to the quantifies of interest here, the relaxation and decoherence times. The temperature also contributes to the dissipation rate γ as well as characterizing the final state of the system through $\boldsymbol{\sigma}_\infty$.

3.4 Gaussian Channels

Knowing how the covariance matrix and displacement vector evolve for the single-mode state will only be useful if they continue to fully characterize the state. That is, if the Gaussian state remains Gaussian throughout the interaction with the environment. One way to verify this is by studying the Fokker-Planck equation for the Wigner function that derives from a Markov master equation for the density operator. It can be shown that, for a multi-mode Gaussian state obeying a quantum optical master equation, the Wigner function continues to be Gaussian [41] and so the first and second statistical moments persist in characterizing the state. It is straightforward to apply this to the case of a Markov master equation for the single-mode phonon state (2.54) and to show that the first and second

statistical moments will persist in characterizing the phonon state. The evolution of a Gaussian single-mode phonon state can thus be defined by the transformations of the covariance matrix and displacement vector.

More generally, the Gaussianity of a state is preserved by a quantum operation if it can be represented as Gaussian channel, which is a trace-preserving completely positive map that maps Gaussian trace-class operators onto Gaussian trace-class operators [104]. A Gaussian channel acts on the first and second statistical moments through equations of the form (3.35) and (3.38) where complete positivity requires that:[5]

$$\boldsymbol{Z}(t) + i\boldsymbol{\Omega} - i\boldsymbol{X}^T(t)\boldsymbol{\Omega}\boldsymbol{X}(t) \geq 0, \tag{3.79}$$

which for single-mode channels reduces to:

$$\boldsymbol{Z}(t) \geq 0, \;\; \det \boldsymbol{Z}(t) \geq (\det \boldsymbol{X}(t) - 1)^2. \tag{3.80}$$

Markovian and non-Markovian noisy channels can both preserve Gaussianity [41, 105].[6] A Markovian channel is divisible, that is, for all intermediate times the the evolution can be decomposed into two successive, independent, completely positive maps. A necessary and sufficient criterion for the non-Markovianity of Gaussian channel is then that there exists an intermediate map that violates (3.79) [107].

The evolution of a Gaussian state in the Markov approximation is generally analysed for an interaction Hamiltonian that is bilinear in the field operators (e.g. see [41]). However, the case of a single-mode phonon state of a BEC emphasises that this isn't a necessary condition for the preservation of Gaussianity since the interaction Hamiltonian is cubic in field operators (see (1.33)). With the Markov approximation dropped it is expected that the Gaussianity of the state will not, in general, be preserved and so, in practice, it is anticipated that the state will not persist as a Gaussian

[5]Note that the vector $\boldsymbol{Y}$ in (3.35) just corresponds to a displacement in phase space.

[6]In fact any channel of the form (3.38) and satisfying (3.79) can be shown to correspond to the reduction of a symplectic (unitary) evolution acting on a larger Hilbert space, and the converse is also true [95, 106].

state. However, if the Markov approximation is valid for the BEC setup, the evolved state should be well approximated as Gaussian.

3.5 Summary

By assuming a Gaussian state, the description of the evolution of an excited single-mode phonon state has been reduced down from the evolution of the density operator in an infinite dimensional Hilbert space (2.54), to the evolution of just the entries of two two-dimensional matrices, the covariance matrix and the displacement vector. Furthermore, the form of the evolution of these two matrices for the single-mode phonon state allows for simple analytic solutions (3.63)-(3.64). These analytic expressions will be used in the next chapter to estimate how quickly the excited state will decohere and relax back to equilibrium with the rest of the Bose gas.

CHAPTER 4

Decoherence of a Single-Mode Phonon State in a BEC

The previous chapter considered how the evolution of an excited single-mode phonon state is mathematically simplified when it is assumed that the state is Gaussian. In this case the evolution of the single-mode state is fully determined by two analytical expressions for the evolution of the entries of the state's two-dimensional covariance matrix and displacement vector. These simple expressions are now used in this chapter to estimate the time taken for the phonon state to decohere and relax back to thermal equilibrium with the Bose gas. Following [44], the loss of coherence is quantified by certain global entropic measures and nonclassical indicators of Gaussian states. Once determined, the evolution of these quantities is then compared to that of the average occupation, which is used as a measure of relaxation. Since the phonon state of interest is a single-mode state, the squeezing of the state is also investigated since this, together with the average occupation and one of the decoherence measures, fully defines a single-mode state.

The following section reviews popular entropic and nonclassical measures of Gaussian states, which can be used to quantify the decoherence of the state, as well as certain properties of the state such as its average occupation and squeezing. The evolution of each of these quantities is investigated for a single-mode phonon state using the calculated evolution of the covariance matrix and displacement vector from the previous chapter. Section 4.2 then illustrates each quantity's evolution for specific BEC setups and compares

the estimates for the decoherence time to those for the relaxation time.

4.1 Quantifiers of Decoherence and Relaxation of Gaussian States

4.1.1 Purity

The purity of a quantum state $\mu = \mathrm{Tr}(\hat{\rho}^2)$ is a measure of how pure a quantum state is: for pure states (states for which there is complete information on the state vector) $\mu = 1$, whereas, for maximally mixed states $\mu = 1/d$ where d is the dimension of the space. It is directly related to the $p = 2$ case of the Schatten p-norms [108]:

$$\|\hat{\rho}\|_p := (\mathrm{Tr}|\hat{\rho}|^p)^{\frac{1}{p}} = (\mathrm{Tr}\hat{\rho}^p)^{\frac{1}{p}},\ p \in (1, \infty), \tag{4.1}$$

which are invariant under unitary operations.

The p-norms are multiplicative on tensor product states and determine the family of Rényi entropies S_p^R [109] and Bastiaans-Tsallis entropies S_p^{BT} [110] by:

$$S_p^R := \frac{-\ln \mathrm{Tr}\rho^p}{p-1}, \tag{4.2}$$

$$S_p^{BT} := \frac{1 - \mathrm{Tr}\rho^p}{p-1}. \tag{4.3}$$

These quantify the degree of mixedness of the state ρ, which is related to its coherence.[1]

As stated above, the purity of a quantum state is conserved for unitary transformations of a closed system, which can be readily verified from the von Neumann master equation:

$$\frac{d\mu}{dt} = \frac{\mathrm{Tr}(\rho^2)}{dt} = 2\mathrm{Tr}(\frac{d\rho}{dt}\rho) = -2i\mathrm{Tr}([H,\rho]\rho) = -2i\mathrm{Tr}(H[\rho,\rho]) = 0. \tag{4.4}$$

[1] See [111] for an investigation into the relationship between coherence and mixedness in a finite dimensional system where it is shown that the amount of quantum coherence in a state is restricted by the amount of mixedness.

However, this need not be the case for an open quantum system. For example, for a Markov master equation in Lindblad form, the purity of the quantum state evolves according to:

$$\frac{1}{2}\frac{d\mu_S(t)}{dt} = \mathrm{Tr}(\mathcal{D}(\hat{\rho}_S(t))\hat{\rho}_S(t)) \tag{4.5}$$

where $\mathcal{D}(\hat{\rho}_S(t))$ is the dissipator.

The purity of state is easily computable from the Wigner function and, for an m-mode Gaussian state, is simply related to the determinant of the covariance matrix [41]:

$$\mu = \frac{1}{(2\kappa)^{2m}\sqrt{\det \boldsymbol{\sigma}}}. \tag{4.6}$$

Therefore, for a single-mode state, the purity is given by:

$$\mu = \frac{1}{4\kappa^2\sqrt{\det \boldsymbol{\sigma}}} = \frac{1}{4\kappa^2 s} \tag{4.7}$$

where s is the symplectic eigenvalue of the state (the modulus of the eigenvalues of $i\boldsymbol{\Omega\sigma}$).

From computing the evolution of $\det \boldsymbol{\sigma}$ one can then determine the evolution of μ in the particular quantum channel. For a Markov channel the covariance matrix evolves according to (3.30) and the evolution of the determinant can be calculated from this using Jacobi's formula:

$$\frac{d}{dt}\det \boldsymbol{\sigma} = \mathrm{Tr}\Big(\mathrm{adj}\boldsymbol{\sigma}\frac{d\boldsymbol{\sigma}}{dt}\Big). \tag{4.8}$$

Substituting in (3.10) for $d\boldsymbol{\sigma}/dt$ provides the following equation of motion for $\det \boldsymbol{\sigma}$ in a Markov channel:

$$\frac{d}{dt}\det \boldsymbol{\sigma}(t) = \det \boldsymbol{\sigma}(t).\mathrm{Tr}\Big(\frac{1}{\kappa^2}\boldsymbol{\Omega}Im(\boldsymbol{C}^\dagger\boldsymbol{C}) + \boldsymbol{\sigma}(t)^{-1}\boldsymbol{D}\Big). \tag{4.9}$$

For the single-mode phonon case described in Section 3.3, the matrices $\boldsymbol{C}$

and $\boldsymbol{D}$ are given by (3.55) and (3.59), and so the above equation of motion simplifies to:[2]

$$\frac{d}{dt}\det\boldsymbol{\sigma}(t) = \gamma\det\boldsymbol{\sigma}(t)\Big(\boldsymbol{\sigma}_\infty \mathrm{Tr}[\boldsymbol{\sigma}(t)] - 1\Big) \tag{4.10}$$

where, from (3.64), $\mathrm{Tr}[\boldsymbol{\sigma}(t)]$ is given by:

$$\mathrm{Tr}[\boldsymbol{\sigma}(t)] = e^{-\gamma t}\mathrm{Tr}[\boldsymbol{R}(t)\boldsymbol{\sigma}_0\boldsymbol{R}^T(t)] + (1-e^{-\gamma t})\mathrm{Tr}\boldsymbol{\sigma}_\infty \tag{4.11}$$

$$= e^{-\gamma t}\mathrm{Tr}[\boldsymbol{\sigma}_0] + (1-e^{-\gamma t})\mathrm{Tr}[\boldsymbol{\sigma}_\infty] \tag{4.12}$$

and $\boldsymbol{R}\boldsymbol{R}^T = \boldsymbol{I}$ since $\boldsymbol{R}$ is a rotation matrix. Therefore, using (4.10), the evolution of μ can be computed for the single-mode phonon state. Note that in this special case the evolution of μ is only dependent on the dissipative effects and not on the free dynamics of the single-mode phonon state.

As stated in Section 3.1.3, due to a theorem by Williamson [92], every covariance matrix can be diagonalized by a symplectic transformation and thus written in terms of a covariance matrix for a thermal state. For a single-mode state this results in any covariance matrix being written as the application of a squeezing transformation to a thermal state [41, 112]:

$$\boldsymbol{\sigma} = \boldsymbol{\Sigma}_\xi \boldsymbol{\sigma}_\nu^T \boldsymbol{\Sigma}_\xi \tag{4.13}$$

where $\boldsymbol{\sigma}_\nu$ is the covariance matrix of a thermal state and $\boldsymbol{\sigma}_\nu$ is the single-mode symplectic squeezing matrix corresponding to the unitary operator for single-mode squeezing $\hat{U}_S$:

$$\hat{U}_S = \exp\Big\{\frac{1}{2}\xi(\hat{a}^\dagger)^2 - \frac{1}{2}\xi^*\hat{a}^2\Big\}, \tag{4.14}$$

$$\implies \boldsymbol{\Sigma}_\xi = \begin{pmatrix} \cosh r + \sinh r\cos\psi & \sinh r\sin\psi \\ \sinh r\sin\psi & \cosh r - \sinh r\cos\psi \end{pmatrix} \tag{4.15}$$

[2]The principle assumptions that result in the simplification are that the free renormalized Hamiltonian is of the form of that for a simple harmonic oscillator, and the state of the environment is a non-squeezed thermal state.

where $\xi = re^{i\psi}$. The matrix version of (4.13) can be written as:

$$\boldsymbol{\sigma} = \frac{1}{4\kappa^2\mu}\begin{pmatrix} \cosh(2r)+\sinh(2r)\cos(\psi) & \sinh(2r)\sin(\psi) \\ \sinh(2r)\sin(\psi) & \cosh(2r)-\sinh(2r)\cos(\psi) \end{pmatrix} \tag{4.16}$$

where μ is the purity of the state, and κ comes from the definitions of the quadrature operators (3.1). Every single-mode covariance matrix can be written as the above matrix and is, therefore, fully defined by the purity and the squeezing of the state.[3] The displacement vector of a single-mode Gaussian state can also be written in a general form:

$$\boldsymbol{d} = \frac{1}{\kappa}\begin{pmatrix} Re(\alpha) \\ Im(\alpha) \end{pmatrix} \tag{4.17}$$

where α is the eigenvalue of the annihilation operator.

The general expression for the covariance matrix can be substituted into (4.10) to obtain the equation of motion for the purity of a single-mode phonon state [113]:

$$\frac{d\mu}{dt} = \gamma\mu\Big(1 - \frac{\mu}{\mu_\infty}\cosh(2r(t))\Big) \tag{4.18}$$

where $\mu_\infty := (1+2N_q)^{-1} = \tanh(\hbar\omega_q/2k_BT)$ is the purity of the asymptotic state $\boldsymbol{\sigma}_\infty$. The matrix (4.16) can also be substituted into the equation that determines the covariance matrix of single-mode phonon state at time t (3.64) to find the purity of the state at that time [113]:[4]

$$\det\boldsymbol{\sigma}(t) = e^{-2\gamma t}(\det\boldsymbol{\sigma}_0) + e^{-\gamma t}\sigma_\infty \mathrm{Tr}(\boldsymbol{\sigma}_0) + (1-e^{-\gamma t})^2\sigma_\infty^2 \tag{4.19}$$

[3]Equivalently, instead of the purity, the symplectic eigenvalue of the state or the average occupation of the thermal state $\boldsymbol{\sigma}_\nu$ could be used in addition to the squeezing since these are all directly related to each other.

[4]Or, alternatively, (4.18) can be solved together with the corresponding differential equation for r (see Section 4.1.3) [41, 113].

$$\implies \mu(t) = \mu_0\Big(e^{-2\gamma t} + \frac{\mu_0^2}{\mu_\infty^2}(1-e^{-\gamma t})^2 + \frac{2\mu_0}{\mu_\infty}e^{-\gamma t}(1-e^{-\gamma t})\cosh(2r_0)\Big)^{-1/2}. \tag{4.20}$$

The purity of the state as defined by (4.20) can exhibit a local minimum when $r_0 > \max(\mu_0/\mu_\infty,\ \mu_\infty/\mu_0)$ [44, 113]. If this is satisfied then the minimum is reached at the following time [44, 113]:

$$t_{min} = \frac{1}{\gamma}\ln\left(\frac{\frac{\mu_0}{\mu_\infty} + \frac{\mu_\infty}{\mu_0} - 2\cosh(2r_0)}{\frac{\mu_0}{\mu_\infty} - \cosh(2r_0)}\right). \tag{4.21}$$

The time t_{min} can provide a good characterization of the decoherence time of such squeezed states [44, 113]. Any increase in the purity after that time just reflects the state being driven towards the state of the environment. This characterization of the decoherence time will be used in Section 4.2 for an estimate of the decoherence time of a single-mode phonon state in several BEC setups. Note that as $r_0 \to \infty$ the minimum time t_{min} tends towards $\frac{1}{\gamma}\ln 2$. This minimum time is also obtained for an initially pure state at $T = 0$ (as long $r_0 > 1$). On the other hand, as $T \to \infty$ then $t_{min} \to 0$.

The above decoherence time has been derived from a Born-Markov master equation, which assumed that the full state of the system (the single-mode phonon system and its environment) remains a separable state (see Section 2.2.1). Therefore, the loss of coherence is not arising from the generation of entanglement between the environment and the open system, which differs to some decoherence processes [32].

For a more general discussion on the evolution of purity, where the environment is taken to be a thermal squeezed state and the free dynamics are ignored from the outset, see [44, 113].

4.1.2 Von Neumann Entropy

The von Neumann entropy S_V is determined by the p-norms as [114]:

$$\lim_{p\to 1+} S_p^R = -\mathrm{Tr}(\rho\ln\rho) = S_V. \tag{4.22}$$

It is an important measure of the mixedness of a quantum state with $S_V = 0$ corresponding to pure states. For the case of a single-mode Gaussian state, S_V simplifies to [104, 115]:

$$S_V = f(\sqrt{\det \boldsymbol{\sigma}}) \tag{4.23}$$

where:

$$f(x) := (x + \frac{1}{4\kappa^2}) \ln(x + \frac{1}{4\kappa^2}) - (x - \frac{1}{4\kappa^2}) \ln(x - \frac{1}{4\kappa^2}). \tag{4.24}$$

The von Neumann entropy provides the same characterization of mixedness for a single-mode Gaussian state as the linear entropy, which is defined as $S_L := (1 - \mu)$ and, from (4.3), is given by the $p = 2$ case of the Bastiaans-Tsallis entropies S_p^{BT}. The equation of motion for the von Neumann entropy can thus be obtained from that for purity using the relation:

$$\frac{d}{dt} S_V(t) = \frac{1}{4\kappa^2 \mu(t)} \ln\Big(\frac{1 - \mu(t)}{1 + \mu(t)}\Big) \frac{d}{dt}\mu(t), \tag{4.25}$$

which is derivable from (4.23). From this relation it is clear that, as would be expected, if the purity of a single-mode state has a minimum then the von Neumann entropy undergoes a maximum at the same time.

4.1.3 Squeezing

From (4.16), the covariance matrix of a general single-mode state is fully defined by its purity and squeezing.[5] Therefore, computing the evolution of the squeezing and purity completely determines the evolution of the covariance matrix. In fact, since the squeezing parameter ψ can be shown to remain a constant for a non-squeezed environment [41, 113], only the evolution of r and μ needs to be considered, with the latter already being computed in Section 4.1.1.

From (4.16), the squeezing of a general single-mode covariance matrix

[5]Equivalently, a single-mode state in an environment in thermal equilibrium is also fully defined by its nonclassical depth and purity (see (4.31)).

can be calculated at any time using:

$$\cosh(2r(t)) = 2\kappa^2\mu\mathrm{Tr}(\boldsymbol{\sigma}(t)). \tag{4.26}$$

For a single-mode phonon state, the trace of the covariance matrix evolves as (4.11), and so the equation of motion for r can be derived as [113]:

$$\frac{dr(t)}{dt} = -\frac{\gamma}{2}\frac{\mu(t)}{\mu_\infty}\sinh(2r(t)). \tag{4.27}$$

After integrating this equation together with the corresponding equation of motion for μ, which is given by (4.18), or equivalently, after substituting (4.16) into (3.64) and using (4.26), the value of r at time t is found from [113]:

$$\cosh(2r(t)) = \mu(t)\Big(e^{-\gamma t}\frac{\cosh(2r_0)}{\mu_0} + \frac{1-e^{-\gamma t}}{\mu_\infty}\Big). \tag{4.28}$$

Note that, as was also the case with the purity, the above equation illustrates that the squeezing evolves independently of the free dynamics for the single-mode phonon case. The evolution of r is also calculated in [41, 44, 113] for a squeezed Markovian environment with the free dynamics ignored from the start.

4.1.4 Nonclassical Depth

A popular measure for quantifying the nonclassicality of a quantum state has been the nonclassical depth introduced in [116]. This has the physical meaning of the number of thermal photons necessary to destroy the nonclassical nature of the quantum state [117]. For a general quantum state $\hat{\rho}$, the nonclassical depth is defined as:

$$\tau_\rho := \frac{1-\mathcal{S}_\rho}{2} \tag{4.29}$$

where $\mathcal{S}_\rho$ is the supremum of the set of values s for which the Wigner function function can be regarded as a (positive semidefinite and non singular) probability distribution. For a coherent state $\tau_\rho = 0$, whereas, for a Fock state $\tau_\rho = 1$. This quantity is easily computed for a general Gaussian state since it is given by:

$$\tau = \max\Big[\frac{1-2u}{2}, 0\Big] \tag{4.30}$$

where u is the smallest eigenvalue of $\boldsymbol{\sigma}$. In this case the nonclassical depth τ detects the state as nonclassical if a canonical quadrature exists whose variance is below 1/2 [44], and τ cannot be greater than 1/2. For a single-mode Gaussian state the smallest eigenvalue is given by $u = \exp\{-2r/\mu\}$ and so:

$$\tau_\rho = \max\Big[\frac{1}{2}\Big(1 - \frac{e^{-2r}}{\mu}\Big), 0\Big] \tag{4.31}$$

where the maximum value of τ is reached when $r = \infty$.

From the time evolution of the covariance matrix (3.64), the nonclassical depth τ of the single-mode can be shown to evolve as [44]:

$$\tau(t) = \frac{\mu_0(\mu_\infty - 1) + e^{-\gamma t}(\mu_0 - \mu_\infty e^{-2r_0})}{2\mu_0\mu_\infty} \tag{4.32}$$

$$= \frac{1}{2}\bigg(1 - \frac{1}{\mu_\infty} + e^{-\gamma t}\Big(\frac{1}{\mu_\infty} - \frac{e^{-2r_0}}{\mu_0}\Big)\bigg). \tag{4.33}$$

The time at which the state becomes classical i.e. when $\tau_\rho = 0$ (if this can occur) is then found to be:

$$t_0 = \frac{1}{\gamma}\ln\left(\frac{1 - \frac{\mu_\infty}{\mu_0}e^{-2r_0}}{1 - \mu_\infty}\right). \tag{4.34}$$

For high squeezing $r_0 \gg 1$ (and assuming $\mu_\infty < \mu_0$) this time can be

approximated as:

$$t_0 \approx \frac{1}{\gamma} \ln\Big(\frac{1}{1-\mu_\infty}\Big), \tag{4.35}$$

which is independent of the initial purity. For high temperatures on the other hand t_0 tends to zero, and for low temperatures t_0 tends to infinity, in contrast to the time at which a minimum of purity is achieved (see Section 4.1.1). The maximisation of the evolution of τ_ρ is considered in [44] where it is shown from numerical analysis that the nonclassical depth increases with increasing squeezing r_0 and purity μ_0.

4.1.5 Coherence Measures

Recently a rigorous framework for the quantification of coherence has been introduced by adopting the viewpoint of coherence as a physical resource [118]. Intuitive and easily computable measures of coherence can then be put on a sound footing following the approach that has already been established for entanglement [119]. This is in contrast to a wide variety of measures of coherence that tend to be justified principally on the grounds of physical intuition [118].

In [118] a set of properties that every proper measure of coherence should satisfy were introduced, and the relative entropy of coherence and the l_1-norm of coherence were identified as the most general and easy-to-use quantifiers of coherence. The l_1-norm is a widely used quantifier of coherence and is intuitively defined in terms of the off-diagonal elements of a density matrix ρ in the chosen reference basis:

$$C_{l_1}(\hat{\rho}) := \sum_{i \neq j} |\hat{\rho}_{ij}|. \tag{4.36}$$

The relative entropy of coherence on the other hand is a distance-based coherence monotone defined by:

$$C_{re}(\hat{\rho}) := S_V(\hat{\rho}_{diag}) - S_V(\hat{\rho}) \tag{4.37}$$

where $\hat{\rho}_{diag} := \sum_i \rho_{ii}|i\rangle\langle i|$ only contains the leading diagonal elements of $\hat{\rho} := \sum_{ij} \rho_{ij}|i\rangle\langle j|$ in the reference basis, and $S_V(\hat{\rho})$ is the von-Neumann entropy.

Decoherence could be quantified by considering the evolution of the above coherence monotones. This would potentially provide a more intuitive description of decoherence and would be similar to the approach used where the decoherence time is derived from the decoherence function $\Gamma_{nm}(t)$, which describes the behaviour of the off-diagonals of the reduced density matrix [32]. However, the above quantifiers implicitly assume the finite dimensional setting [118], whereas the case of interest here is infinite dimensional. Hence, a quantum theory of coherence in infinite dimensional systems is needed. This would likely follow the the development of entanglement quantification [118] where problems concerning continuity can be addressed by requiring energy constraints [120] or by considering special, experimentally relevant, subclasses such as Gaussian states [121]. In fact a connection between entanglement and coherence has recently been found where any degree of coherence with respect to some reference basis can be converted to entanglement via incoherent operations [122]. This has allowed for the development of a general class of measures of coherence for a quantum system in terms of the maximum bipartite entanglement that can be generated via incoherent operations applied to the system and an incoherent ancilla. The resulting measures are then valid coherence monotones satisfying all the requirements dictated by the resource theory of quantum coherence and will potentially provide powerful advances for the operational quantification of coherence [122].

4.1.6 Average Occupation

The average occupation of a general state is defined by $N := \sum_i N_i := \sum_i \langle \hat{a}_i^\dagger \hat{a}_i \rangle$ where i labels the different modes. In general, this quantity depends on the first as well as the second statistical moment of a Gaussian

state:

$$N = \sum_i \langle \hat{a}_i^\dagger \hat{a}_i \rangle \tag{4.38}$$

$$= \kappa^2 \sum_i \langle \hat{q}_i^2 + \hat{p}_i^2 + i[\hat{q}_i, \hat{p}_i] \rangle \tag{4.39}$$

$$= \kappa^2 \sum_i (\langle \hat{q}_i^2 \rangle + \langle \hat{p}_i^2 \rangle) - \frac{1}{2} \tag{4.40}$$

$$= \kappa^2 \Big(Tr(\boldsymbol{\sigma}) + \boldsymbol{d}^T \boldsymbol{d} \Big) - \frac{1}{2}. \tag{4.41}$$

Using (4.16), for a general single-mode Gaussian state i, the average occupation is given by:[6]

$$N_i = \frac{1}{2\mu} \cosh(2r) + |\alpha|^2 - \frac{1}{2}. \tag{4.42}$$

The time evolution of the average occupation can, therefore, be calculated from the evolution of squeezing parameter r and purity μ. However, it is simpler to calculate it from the quantum Markov master equation for the density operator of the state (2.46) (see Appendix C). From (C.5), and using $\hat{O} = \hat{N}_i = \hat{b}_{\boldsymbol{q}}^\dagger \hat{b}_{\boldsymbol{q}}$, the average occupation at time t for a single-mode phonon state is shown to be given by:

$$N_q(t) = (N_q(0) - N_q^{th}) e^{-\gamma t} + N_q^{th} \tag{4.43}$$

where:

$$N_q^{th} := \frac{1}{(\gamma_{11}/\gamma_{22}) - 1}. \tag{4.44}$$

[6] Since μ is inversely proportional to the symplectic eigenvalue of the state, the average occupation can also be defined in terms of that or the average occupation of the thermal state obtained from Williamson's theorem.

Since the environment is in thermal equilibrium the two rates γ_{11} and γ_{22} are related via (2.71) and so:

$$N_q^{th} = \frac{1}{e^{\beta\omega_q} - 1}, \tag{4.45}$$

which is just the the average (thermal) occupation of the environment.

Note that this evolution is independent of the free evolution of the system since $\hat{H} \propto \hat{N}_q$. This can also be observed from its above definition in terms of the covariance matrix and displacement vector since $Tr(\boldsymbol{\sigma})(t)$ is independent of the free evolution as discussed in Section 4.1.1, and $\boldsymbol{d}^T(t)\boldsymbol{d}(t) = \boldsymbol{d}_0^T \boldsymbol{A}^T \boldsymbol{A}\boldsymbol{d}_0 = e^{-\gamma t}\boldsymbol{d}_0^T\boldsymbol{d}_0$.

The relaxation time is the time scale required for the approximate vanishing of the populations of quantum states [30, 31] and thus the evolution of the average occupation provides information on this time scale. From (4.43), the time at which the the original populations vanish and the mode is completely occupied by the thermal population is never actually reached theoretically. Typically the relaxation time is instead given by the inverse of a typical relaxation rate such as the damping rate [32]. However, this choice of time scale cannot be compared well against the time scales for decoherence derived in Sections 4.1.1 and 4.1.4 since these are given by the occurrence of an exact event (the minimum of purity or the vanishing of nonclassicality) rather than the inverse of a rate. Alternative characterisations of the relaxation time, which can be better compared to the decoherence times of Section 4.1.1 and 4.1.4, are the time at which the original and thermal populations only differ by one quanta, or when the population of the state reaches a certain percentage of the fixed point thermal population.[7] Experimentally of course there will be a limit to what can be differentiated. In this case, to determine if the state has reached a thermal state, the method of state discrimination could be used. Then perfect unit fidelity is not required and one tolerates that the quantum state arrives within a small fidelity distance from the target, fixed a priori. This could

[7]Another option would be to just compare the rate at which the purity goes to a minimum (or the nonclassical depth goes to zero) to the rate at which the populations decay to zero, rather than attempting to calculate actual time scales.

be achieved in this case, for example, by considering the fidelity distance between the covariance matrix of the phonon state and the environment. Then one characterizes the relaxation time as the minimal time required for the initial state to freely reach the target state within a given error parameter. For example, in [77], the minimal time required for an initial state $\boldsymbol{\sigma}_0$ to freely reach the target $\boldsymbol{\sigma}_\infty$ within a fixed fidelity $1-\epsilon$ was found to be $|\ln\epsilon|/2\gamma$ where γ is the damping rate.

4.2 Decoherence of Phonons in Realistic BEC Setups

This section investigates the time evolution of the above global entropic measures and nonclassical indicators for particular BEC setups. The setups that will be considered are: (i) the setup for the GW detector based on concepts from RQIT that was discussed in the Introduction and developed in [18], (ii) the setup used to observe Landau damping in the MIT experiment with Sodium atoms [64], and (iii) the setup that will be discussed in Chapter 5 which is the setup that is currently being investigated in Nottingham to measure the experimental decoherence of phonons.

As discussed in Sections 4.1.1 and 4.1.4, it is possible to extract an estimate for the decoherence time of the phonons from the evolution of the purity and nonclassical depth. Furthermore, from the time evolution of the average occupation, it is possible to extract an estimate for the relaxation time as discussed in Section 4.1.6.

Each BEC setup will be discussed in turn in the following three sections. The time evolution of the entropic measures and nonclassical indicators are evaluated for high and low temperatures and for three different initial Gaussian phonon states: a coherent state, vacuum squeezed state, and thermal squeezed state (thermalized to the given temperature). All these initial states are chosen such that the initial average occupation is the same.

4.2.1 RQIT Gravitational Wave Detector

The setup of the GW detector introduced in [18] is based on a uniform ^{87}Rb BEC with a speed of sound of $c_s \sim 1\times10^{-2}$ ms^{-1} and angular frequency

of the excitatory phonon mode $\omega_q \sim 2\pi \times 5000$ Hz. As discussed in Section 2.3, there are two temperature regimes of interest called the quantum and thermal regimes, which are characterized by $k_B T \ll \hbar\omega_q$ and $k_B T \gg \hbar\omega_q$ respectively. In the former regime Beliaev damping dominates, whereas, in in the latter regime it is Landau damping that dominates. These two regimes will be investigated in turn in the Sections 4.2.1.1 and 4.2.1.2 respectively.

4.2.1.1 Quantum Regime

For a temperature of 0.5nK the BEC will be in the quantum regime where Beliaev damping dominates. Figure 4.1 illustrates the time evolution of the purity, nonclassical depth, squeezing, and average occupation of a single-mode phonon state with angular frequency $\omega_q \sim 2\pi \times 5000$ Hz. From Figure 4.1 the squeezed states undergo a minimum of purity before asymptomatically relaxing to the purity of the environment, which is approximately the vacuum. From Section 4.1.1, the time t_{min} at which the minimum is attained is given by (4.21) and provides a good characterization of the decoherence time of the squeezed states [44]. In this quantum regime, it is approximately given by $t_{min} \approx \ln 2/\gamma$ where γ is the Beliaev damping rate. This is to be compared with the time at which the nonclassical depth reaches zero, which is approximately given by $t_{\tau=0} = 2\beta_q/\gamma$ and will thus only asymptotically approach zero when $T = 0$. The decoherence time characterized by the time at which the purity of squeezed states reaches its minimum is of order $6s$, whereas, the time at which $e^{-\gamma t} = 1\%$ is of order $40s$ for this particular BEC setup. The latter time is taken to be a rough guide to the comparative relaxation time of the system.[8] Note that the ratio of the two scales is independent of γ and so is not explicitly dependent on intrinsic BEC parameters such as the density and atomic mass, but it is dependent on certain properties of the phonon state such as the initial squeezing and average occupation.

The time of $6s$ for pure squeezed states to reach a minimum of purity could be taken as a rough estimate of the decoherence time of the phonons

[8]This equivalent to taking $\epsilon = (0.01)^2$ for the error parameter used in quantum discrimination as discussed in Section 4.1.6.

in the proposed GW detector. Such a decoherence time, although much smaller than the expected lifetime of the BEC, is still anticipated to provide the relativistic quantum technological device with a better accuracy than the current state of the art [18]. A more accurate determination of the decoherence time would need to generalize the results to two modes and the effects from gravity and motion would also need to be included. This is discussed in more detail in Chapter 7.

4.2.1.2 Thermal Regime

Although the GW detector has been designed for a BEC in the quantum regime, this section looks at the behaviour of the measures in the thermal regime to illustrate the dependence of the measures on the temperature of the BEC and angular frequency of the phonon mode. For a temperature of 100nK and phonon angular frequency of $\omega_q = 2\pi \times 500\text{Hz}$, the BEC will be in the thermal regime where Landau damping dominates and obeys (2.79) since $\hbar\omega_q \ll k_B T \ll mc_s^2$. Figure 4.2 illustrates the time evolution of the purity, nonclassical depth, squeezing, and average occupation of a single-mode phonon state in this regime. The squeezed states still undergo a minimum of purity but now the nonclassical depth goes to zero in around the same time scale. The time at which this occurs is of order $5 \times 10^{-2}s$ whereas the time taken for $e^{-\gamma t}$ to reach 1% is of order $1.7s$.

When $k_B T \gg \mu$ the damping rate γ is approximately linear in T (see (2.78)). This is the case when $T = 100\text{nK}$ and the phonon frequency is $\omega_q = 2\pi \times 500\text{Hz}$ as in the previous section, but now the speed of sound is taken to be $c_s = 2.5 \times 10^{-3}\text{ms}^{-1}$. The time evolution of the purity, nonclassical depth, squeezing and average occupation for this regime is illustrated in Figure 4.3. In this regime the purity of realistically squeezed states still undergo a minimum but the nonclassical depth degrades to zero in a time that is an order of magnitude shorter. The time at which this occurs is approximately given by $t_\tau \approx \beta/\gamma$ and is of order $10^{-4}s$ for the chosen BEC setup. On the other hand, the time taken for the $e^{-\gamma t}$ to reach 1% is of order $4 \times 10^{-3}s$.

4.2.2 MIT Sodium BEC Setup

This section investigates the decoherence of a single-mode phonon state for a BEC setup inspired by that used to observe Landau damping in [64], which used a Sodium Bose gas. As with the GW detector, the evolution of the entropic and nonclassical measures will be investigated for different energy regimes, and the same three different initial Gaussian phonon states will be used. It should be emphasized that the derivation of the decoherence and relaxation times assumed a uniform BEC whereas this experiment used an harmonic trap. However, estimates for the damping rate using a uniform BEC were still found to be applicable to this experiment [26].

4.2.2.1 Quantum Regime

The BEC setup assumed in this and the following section is a uniform Sodium BEC with speed of sound $c_s = 5 \times 10^{-3}\text{ms}^{-1}$ and an excited phonon mode with angular frequency $2\pi \times 510\text{Hz}$.[9] For a temperature of 0.5nK the BEC will be in the quantum regime where Beliaev damping dominates.[10] Figure 4.4 illustrates the time evolution of the purity, nonclassical depth, squeezing, and average occupation of the single-mode phonon state. The squeezed states undergo a minimum of purity before asymptomatically relaxing to the purity of the environment, which is approximately the vacuum. From Section 4.1.1, the time t_{min} at which the minimum is attained is given by (4.21) and provides a good characterization of the decoherence time of the squeezed states [44]. In this quantum regime, it is approximately given by $t_{min} \approx \ln 2/\gamma$. This is to be compared with the time at which the nonclassical depth reaches zero, which is approximately given by $t_{\tau=0} = 2\beta_q/\gamma$ and will thus only asymptotically approach zero when $T = 0$.

[9] The actual experiment used a trapped Bose gas but the theoretical calculations performed in this work are for a uniform BEC.

[10] Note that this temperature wasn't achieved in the experiment of [64] and is just used for illustrative purposes. In fact, since the experiment used a trap, Beliaev damping wouldn't have been active for the lowest energy modes.

4.2.2.2 Thermal Regime

For a temperature of 50nK and phonon angular frequency of $\omega_q = 2\pi \times$ 510Hz, the BEC will be in the thermal regime where Landau damping dominates and obeys (2.79) since $\hbar\omega_q \ll k_B T \ll mc_s^2$. Figure 4.5 illustrates the time evolution of the purity, nonclassical depth, squeezing, and average occupation of a single-mode phonon state in this regime.

For $T = 150$nK the condition $k_B T \gg \mu$ is satisfied and the damping rate γ is approximately linear in T (see (2.78)). The time evolution of the purity, nonclassical depth, squeezing and average occupation for this regime is illustrated in Figure 4.6. In this regime the purity of realistically squeezed states still undergo a minimum but the nonclassical depth degrades to zero in a time that is an order of magnitude shorter.

4.2.3 Nottingham Lithium BEC Setup

This section investigates the decoherence of a single-mode phonon state for a BEC setup inspired by the experiment currently being investigated in Nottingham that uses a Lithium BEC and is planned to be used to experimentally observe decoherence (see Chapter 5 for more detail). As with the previous two setups, the evolution of the entropic and nonclassical measures will be investigated for different energy regimes, and the same three different initial Gaussian phonon states will be used.

4.2.3.1 Quantum Regime

The BEC setup used in this and the following section is a uniform molecular Lithium BEC with speed of sound $c_s \sim 5 \times \times 10^{-3}\text{ms}^{-1}$ and an excited phonon mode with angular frequency $2\pi \times 100$Hz.[11] For a temperature of 0.5nK the BEC will be in the quantum regime where Beliaev damping dominates. [12] Figure 4.7 illustrates the time evolution of the purity, nonclassical depth, squeezing, and average occupation of the single-mode phonon state.

[11] The actual experiment uses a trapped Bose gas but the theoretical calculations performed in this work are for a uniform BEC.

[12] Note that this temperature may not be achievable in the experiment and is instead just used for illustrative purposes. In fact, since the experiment used a trap, Beliaev damping wouldn't have been active for the lowest energy modes.

The squeezed states undergo a minimum of purity before asymptomatically relaxing to the purity of the environment, which is approximately the vacuum. From Section 4.1.1, the time t_{min} at which the minimum is attained is given by (4.21) and provides a good characterization of the decoherence time of the squeezed states [44]. In this quantum regime, it is approximately given by $t_{min} \approx \ln 2/\gamma$. This is to be compared with the time at which the nonclassical depth reaches zero, which is approximately given by $t_{\tau=0} = 2\beta_q/\gamma$ and will thus only asymptotically approach zero when $T = 0$.

4.2.3.2 Thermal Regime

For a temperature of 25nK and phonon angular frequency of $\omega_q = 2\pi \times$ 100Hz, the BEC will be in the thermal regime where Landau damping dominates and obeys (2.79) since $\hbar\omega_q \ll k_B T \ll mc_s^2$. Figure 4.8 illustrates the time evolution of the purity, nonclassical depth, squeezing, and average occupation of a single-mode phonon state in this regime.

For $T = 100$nK the condition $k_B T \gg \mu$ is satisfied and the damping rate γ is approximately linear in T (see (2.78)). The time evolution of the purity, nonclassical depth, squeezing and average occupation for this regime is illustrated in Figure 4.9. In this regime the purity of realistically squeezed states still undergo a minimum but the nonclassical depth degrades to zero in a time that is an order of magnitude shorter.

4.3 Summary

In this chapter the times in which a single-mode phonon state of a BEC decoheres and relaxes to equilibrium have been estimated for certain examples of BEC setups. In particular, in the BEC setup that is inspired by the GW detector [18], the decoherence time at $T = 0.5$nK for a squeezed vacuum state was estimated to be around $6s$, and a rough estimate for the relaxation time was $40s$. A BEC setup based on that which is planned to be used to experimentally measure decoherence was also considered. For example, at a temperature of around $T = 25$nK, it was estimated that a thermal squeezed state would decohere in around $0.9 - 2.5 \times 10^{-4}s$, and relax to equilibrium

in around $3 \times 10^{-3} s$ (see Figure 4.8). These estimations for the decoherence and relaxation times are the culmination of the theoretical calculations of Part I of this work, which have involved treating the phonons of BECs as open quantum systems and as Gaussian states such that the times can be extracted from the evolution of some of the properties of these states.

Part II of this work considers how these decoherence and relaxation times could be extracted from experiments. This will, in particular, involve investigating strongly-interacting BECs and how their absorption images can be understood in order to extract these times from the experiments.

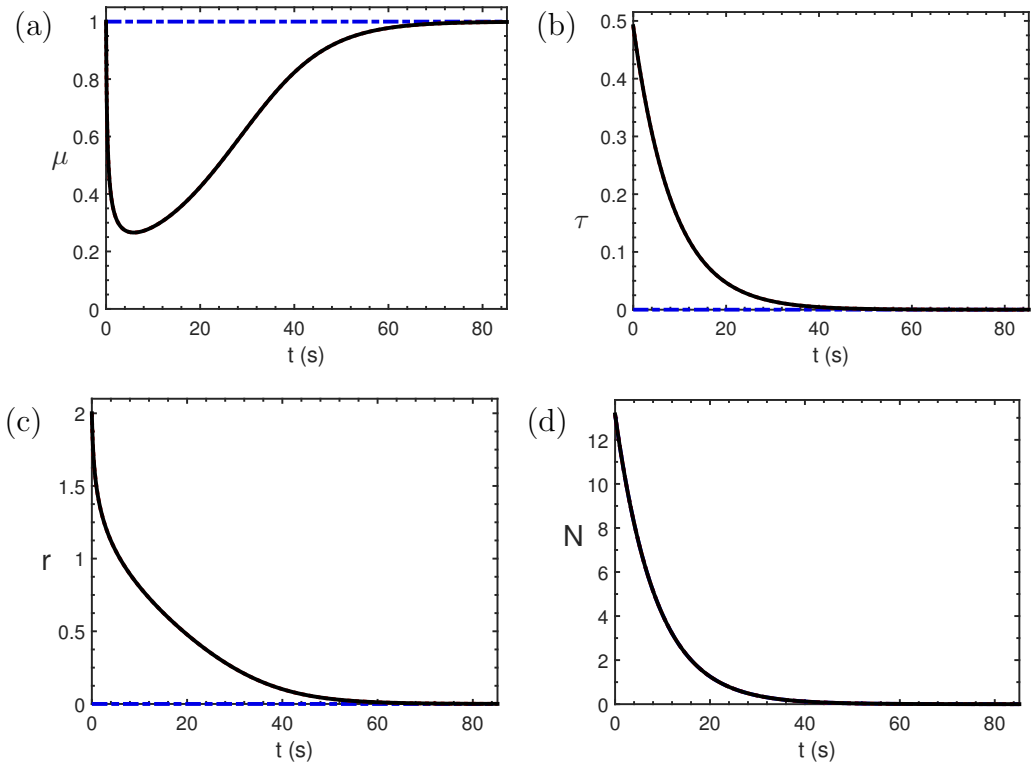

Figure 4.1: Time evolution of (a) Purity μ; (b) Nonclassical depth τ; (c) Squeezing r; (d) Average occupation N. The BEC setup assumed in [18] was used (a uniform ^{87}Rb BEC with $c_s \sim 10^{-2}\text{m}^{-1}$) with a temperature of 100nK and angular frequency $\omega_q = 2\pi \times 5000\text{Hz}$. The blue dot-dash line is an initial coherent state, the red dotted line (behind the black line) is an initial thermal squeezed state with $r = 2$, and the black solid line is an initial vacuum squeezed state with $r = 2$. The initial thermal squeezed state is approximately a vacuum squeezed state at this temperature. All initial states were chosen such that the initial average occupation is the same. These graphs, and all the proceeding graphs in this chapter, were generated by a MATLAB package developed by R. Howl.

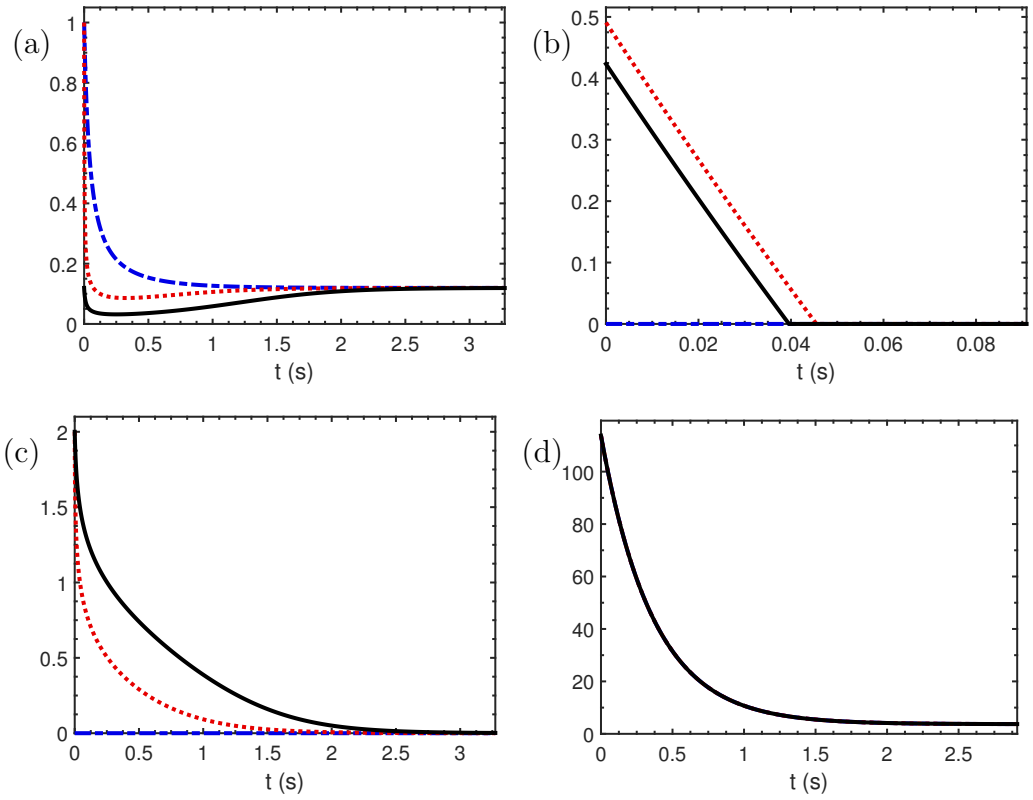

Figure 4.2: Time evolution of (a) Purity μ; (b) Nonclassical depth τ; (c) Squeezing r; (d) Average occupation N. The BEC setup assumed in [18] was used (a uniform ^{87}Rb BEC with $c_s \sim 10^{-2}\text{m}^{-1}$) with a temperature of 100nK and angular frequency $\omega_q = 2\pi \times 500\text{Hz}$. The blue dot-dash line is an initial coherent state, the red dotted line is an initial thermal squeezed state with $r = 2$, and the black solid line is an initial vacuum squeezed state with $r = 2$. All initial states were chosen such that the initial average occupation is the same.

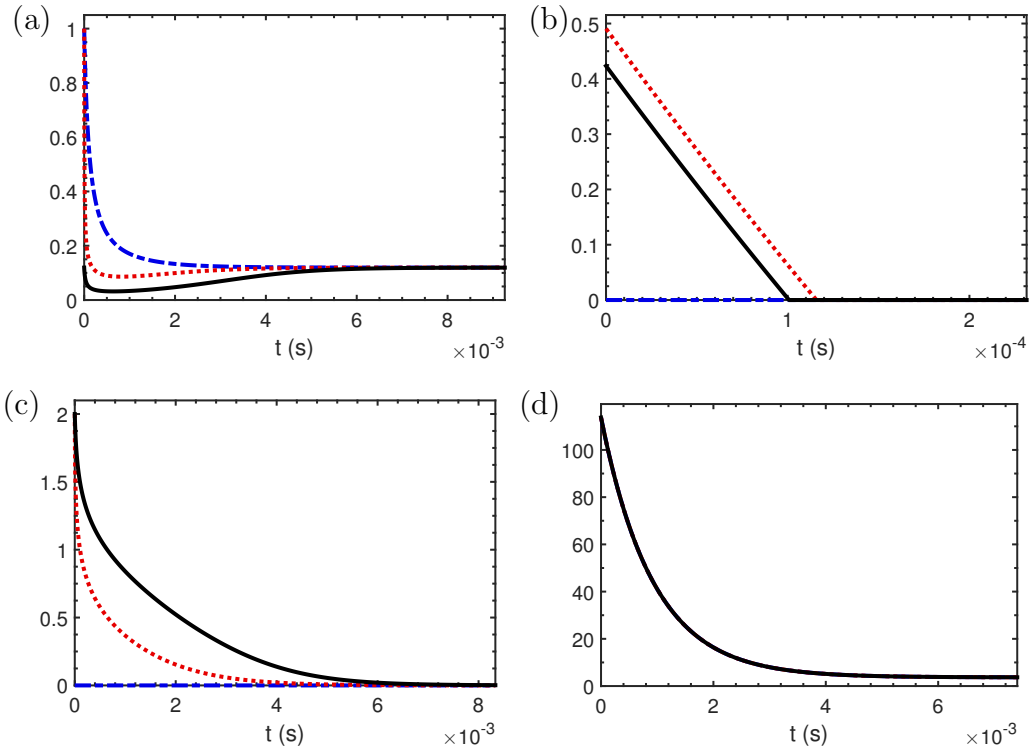

Figure 4.3: Time evolution of (a) Purity μ; (b) Nonclassical depth τ; (c) Squeezing r; (d) Average occupation N. The BEC setup assumed in [18] was used (a uniform ^{87}Rb BEC with $c_s 2.5\times \sim 10^{-3}\mathrm{m}^{-1}$) with a temperature of 100nK and angular frequency $\omega_q = 2\pi \times 500\mathrm{Hz}$. The blue dot-dash line is an initial coherent state, the red dotted line is an initial thermal squeezed state with $r = 2$, and the black solid line is an initial vacuum squeezed state with $r = 2$. All initial states were chosen such that the initial average occupation is the same.

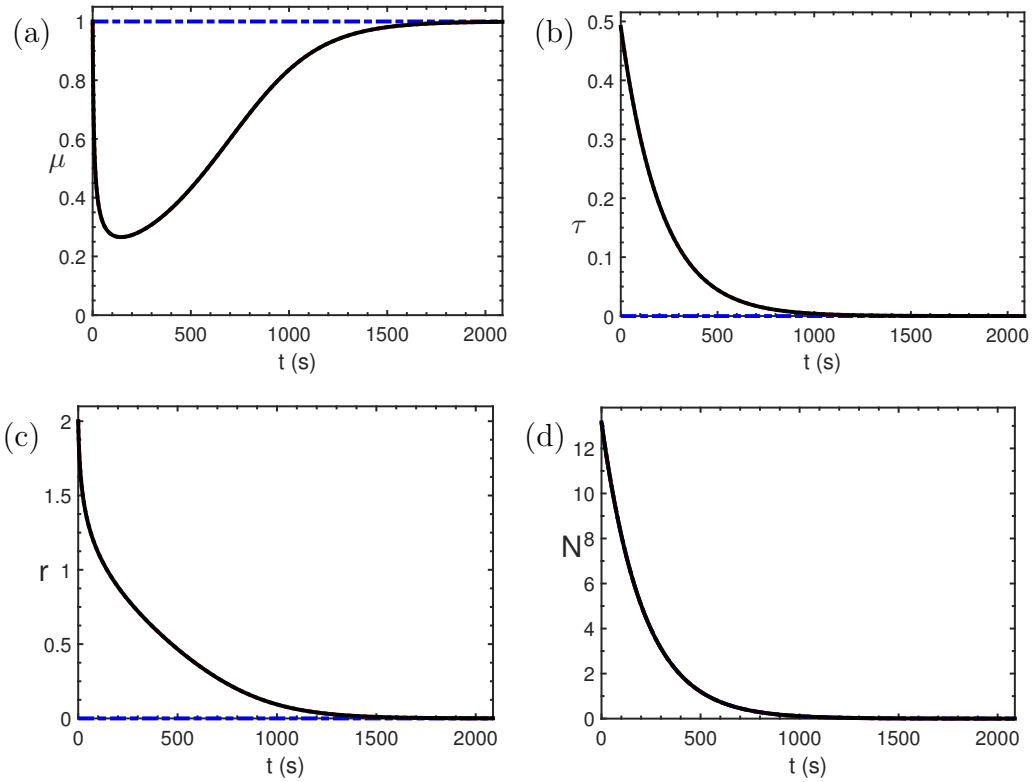

Figure 4.4: Time evolution of (a) Purity μ; (b) Nonclassical depth τ; (c) Squeezing r; (d) Average occupation N. BEC parameters similar to [64] were used with a temperature of 0.5nK and angular frequency $\omega_q = 2\pi \times$ 510Hz. The blue dot-dash line is an initial coherent state, the red dotted line (behind the black line) is an initial thermal squeezed state with $r = 2$, and the black solid line is an initial vacuum squeezed state with $r = 2$. The initial thermal squeezed state is approximately a vacuum squeezed state at this temperature. All initial states were chosen such that the initial average occupation is the same.

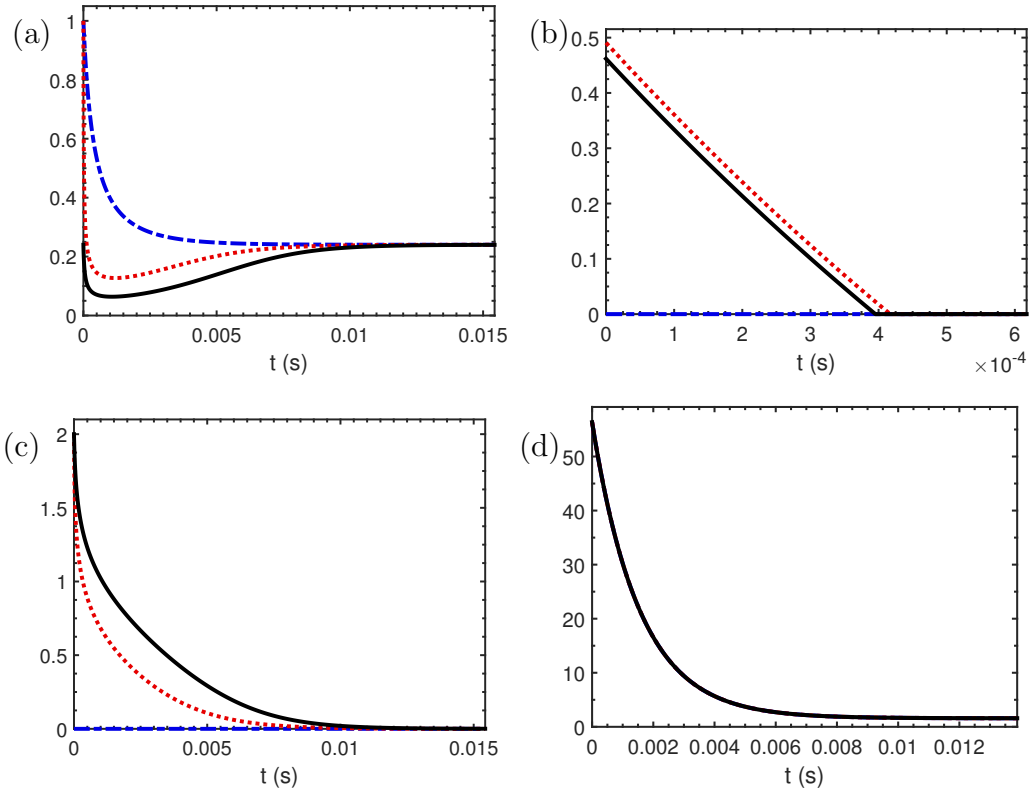

Figure 4.5: Time evolution of (a) Purity μ; (b) Nonclassical depth τ; (c) Squeezing r; (d) Average occupation N. BEC parameters similar to [64] were used with a temperature of 50nK and angular frequency $\omega_q = 2\pi \times$ 510Hz. The blue dot-dash line is an initial coherent state, the red dotted line (behind the black line) is an initial thermal squeezed state with $r = 2$, and the black solid line is an initial vacuum squeezed state with $r = 2$. The initial thermal squeezed state is approximately a vacuum squeezed state at this temperature. All initial states were chosen such that the initial average occupation is the same.

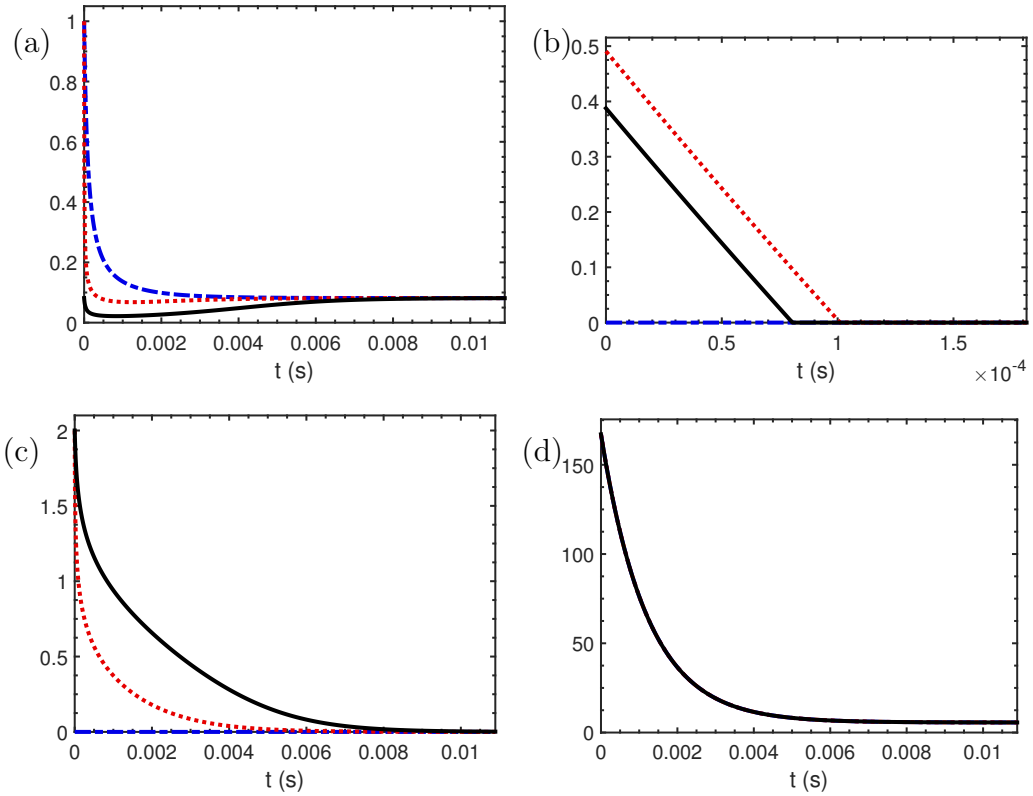

Figure 4.6: Time evolution of (a) Purity μ; (b) Nonclassical depth τ; (c) Squeezing r; (d) Average occupation N. BEC parameters similar to [64] were used with a temperature of 150nK and angular frequency $\omega_q = 2\pi \times$ 510Hz. The blue dot-dash line is an initial coherent state, the red dotted line (behind the black line) is an initial thermal squeezed state with $r = 2$, and the black solid line is an initial vacuum squeezed state with $r = 2$. The initial thermal squeezed state is approximately a vacuum squeezed state at this temperature. All initial states were chosen such that the initial average occupation is the same.

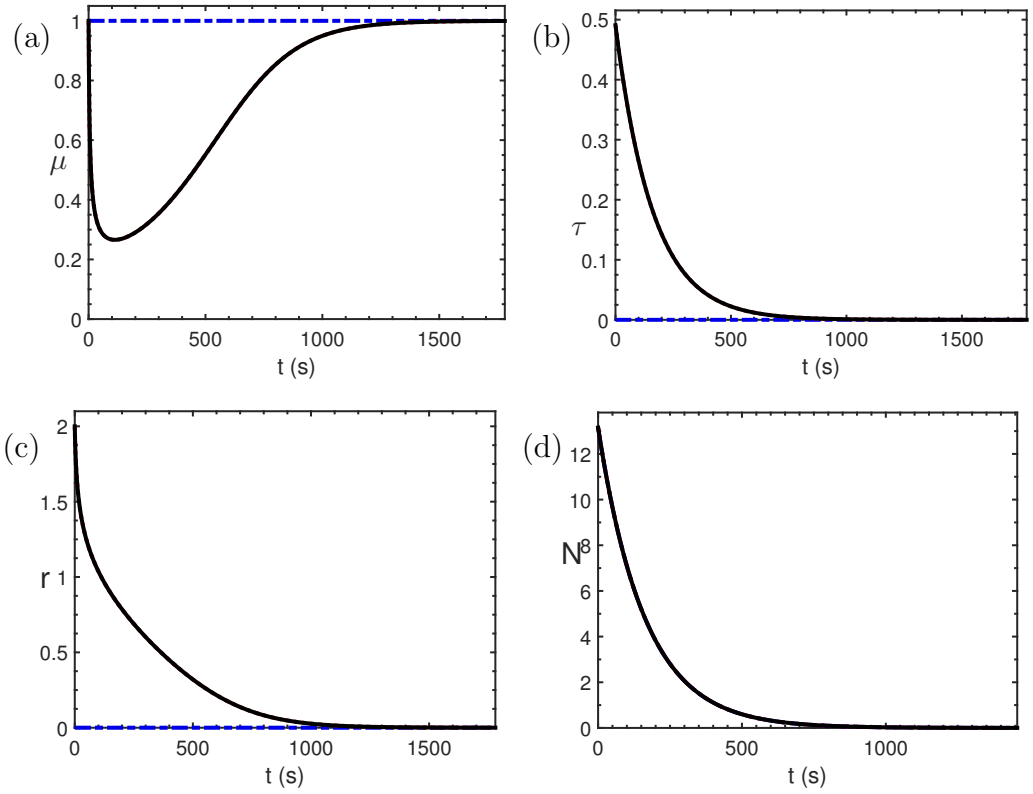

Figure 4.7: Time evolution of (a) Purity μ; (b) Nonclassical depth τ; (c) Squeezing r; (d) Average occupation N. BEC parameters discussed in Section were used with a temperature of 0.5nK and angular frequency $\omega_q = 2\pi\times 100$Hz. The blue dot-dash line is an initial coherent state, the red dotted line (behind the black line) is an initial thermal squeezed state with $r = 2$, and the black solid line is an initial vacuum squeezed state with $r = 2$. The initial thermal squeezed state is approximately a vacuum squeezed state at this temperature. All initial states were chosen such that the initial average occupation is the same.

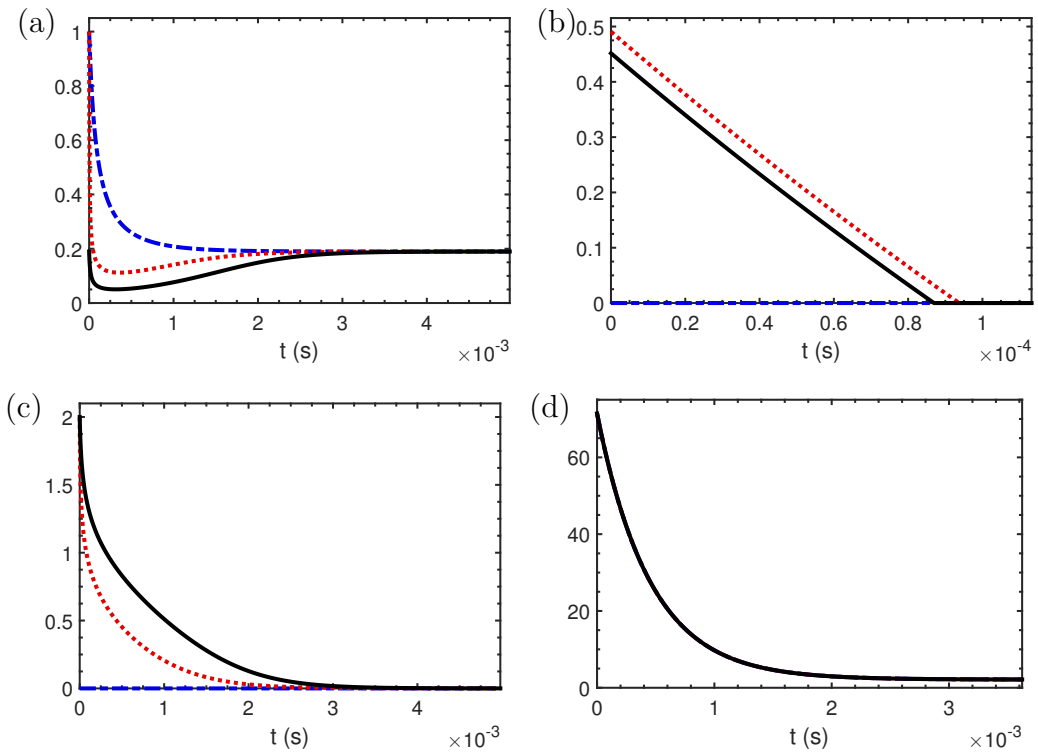

Figure 4.8: Time evolution of (a) Purity μ; (b) Nonclassical depth τ; (c) Squeezing r; (d) Average occupation N. BEC parameters discussed in Section were used with a temperature of 25nK and angular frequency $\omega_q = 2\pi \times 100$Hz. The blue dot-dash line is an initial coherent state, the red dotted line (behind the black line) is an initial thermal squeezed state with $r = 2$, and the black solid line is an initial vacuum squeezed state with $r = 2$. The initial thermal squeezed state is approximately a vacuum squeezed state at this temperature. All initial states were chosen such that the initial average occupation is the same.

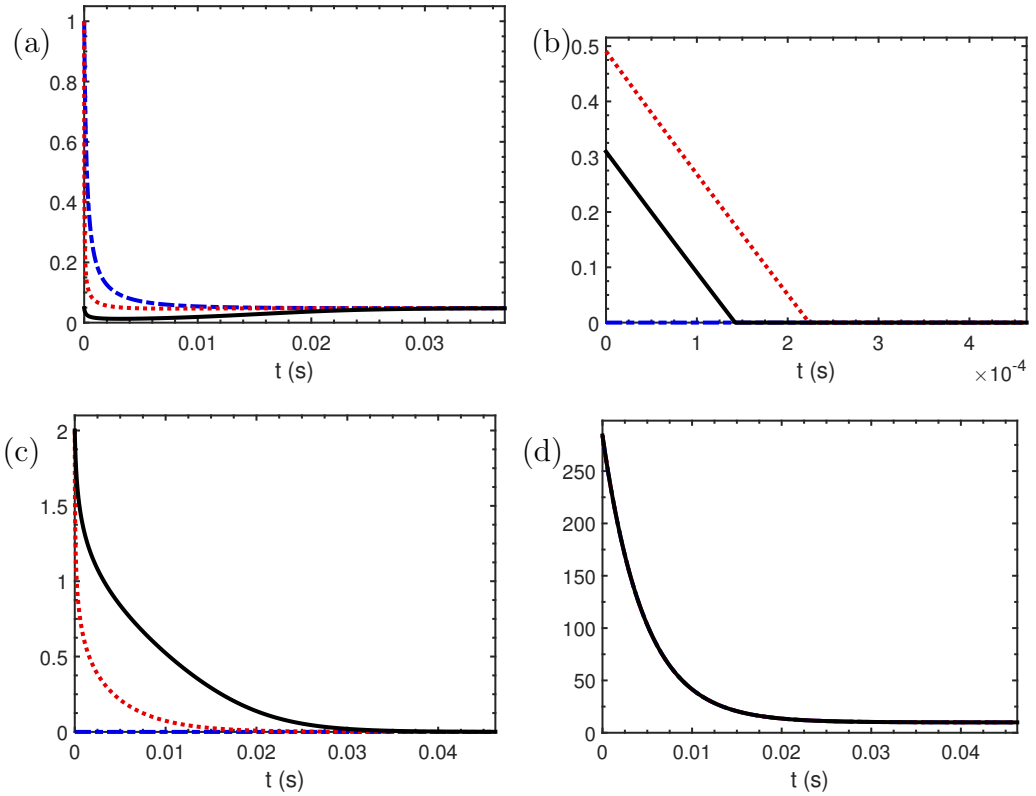

Figure 4.9: Time evolution of (a) Purity μ; (b) Nonclassical depth τ; (c) Squeezing r; (d) Average occupation N. BEC parameters discussed in Section were used with a temperature of 100nK and angular frequency $\omega_q = 2\pi\times 100$Hz. The blue dot-dash line is an initial coherent state, the red dotted line (behind the black line) is an initial thermal squeezed state with $r = 2$, and the black solid line is an initial vacuum squeezed state with $r = 2$. The initial thermal squeezed state is approximately a vacuum squeezed state at this temperature. All initial states were chosen such that the initial average occupation is the same.

Part II

Measuring the Decoherence of Phonons in BECs and Strongly-Interacting Bose Gases

CHAPTER 5

Measuring the Decoherence of Phonons using a Strongly-Interacting BEC

The previous part of this work concerned the estimation of the theoretical decoherence and relaxation time of an excited single-mode phonon state of a Bose condensed gas [25]. In this second part, the progress with the experimental verification of these predictions is considered. The part comprises two chapters where this chapter discusses how the decoherence could be measured and the BEC setup that is planned to be used, while the following chapter considers the progress that is being made in analysing the BEC, which will facilitate the experimental observation of the decoherence of phonons.

This chapter starts with a discussion on how phonons are excited and analysed in BEC experiments. Section 5.2 then considers what quantities need to be measured in experiments, such as purity and density, in order to determine the decoherence and relaxation times of the phonons. The BEC setup that is planned to be used is then introduced in Section 5.3. This BEC is a strongly-interacting BEC and this type of BEC is not as well understood as its weakly-interacting counterpart. In particular, in-situ absorption images of this strongly-interacting BEC are expected to differ significantly from those of a weakly-interacting BEC, and these must be properly understood in order to measure the decoherence of phonons. Chapter 6 investigates how in-situ absorption images of a strongly-interacting BEC could be modelled and discusses the current progress with modelling the images

of our BEC at various scattering lengths and temperatures [51]. Once the in-situ absorption images can be modeled effectively, the decoherence of the phonons will be investigated experimentally [45].

5.1 Phonons in the Lab

In a Bose-Einstein context, phonons are defined as the quanta of long-wavelength oscillations (sound waves) of the condensate. In Chapter 1 these phonons were derived as quantum excitations (quasi-particles) involving the noncondensate. However, the phonons can also be derived in a more classical way which emphasizes the connection to condensate oscillations. This more classical derivation is presented in Appendix D where the wave function of the condensate is treated as a classical field in analogy with the transition from quantum electrodynamics to the classical description of electromagnetism. There it is also shown that the spectrum of the condensate density oscillations is in fact identical to that of the quasi-particles (1.29). This is a characteristic signature of Bose-Einstein condensation that is valid at zero and finite temperatures, and can be understood from the symmetry-breaking mechanism of the condensation [50].

Long-wavelength oscillations of condensed Bose gases were observed shortly after the first demonstrations of Bose-Einstein condensation in alkali gases [74, 75]. These experiments used trapped atomic gases and measured the oscillations in a classical way: they induced an oscillation of the condensate by modulating an external parameter which, in this case, was achieved by applying a small, sinusoidal, time-dependent perturbation to the transverse trap potential. Unlike a uniform BEC where the condensed and normal components overlap everywhere, in a trapped BEC the density of the condensate varies in space and has a finite size. In these systems the oscillations that have a wavelength comparable to the size of the condensate result in collective shape oscillations of the condensate. These were the oscillations observed in [74, 75, 123, 124] and were soon followed by the observation of smaller wavelength oscillations (much smaller than axial size of the cloud [125] but still larger than the healing length, which varies in

space in a trapped BEC). These smaller wavelength oscillations appear as hydrodynamic ripples spreading across the surface of the condensate at the speed of sound.

Since the Bose gases are trapped in these experiments, at non-zero temperatures the condensed and noncondensed components are spatially distinct, which facilitates the use of absorption imaging for the identification of the condensed fraction and its oscillations. This imaging technique is a destructive method that involves shining light onto the gas and using the shadow from the absorption to cast its image [63]. In the experiments that first observed condensate oscillations, after the cloud was set to oscillate by the sudden perturbation to the trap potential, the cloud was then allowed to freely oscillate until the trap potential was turned off so that the cloud suddenly expanded and could be imaged by the above technique. The oscillations were then identified by the apparent time-dependent changes to the shape of the condensate in the absorption images. In the experiments that observed shorter wavelengths [125], the localized density perturbations on the condensate surface were similarly studied by allowing the condensate to expand adiabatically but then taking a rapid sequencing of non-destructive phase contrast images.

Rather than perturbing the transverse trap potential as in the early experiments [74, 75, 123], the experiments that observed shorter wavelengths generated localized density perturbations using a focused far-off-resonant laser beam [125]. In fact several methods have since been adopted to perturb the condensate to create long-wavelength oscillations. These include modulating the trap potential of the gas as discussed above, modulating the scattering length [126], and using Bragg spectroscopy where laser beams coherently impart an energy to the condensate and optically "imprint" phonons into the gas (see e.g. [125, 127]). In the limit of low excitation amplitude, the spectrum of low-lying collective excitations corresponds exactly to the Bogoliubov quasi-particle spectrum as discussed above [84, 128] and the collective condensate response to the perturbation, in the limit of low amplitude, is simply a coherent state of these elementary excitations [129].

Another, more quantum, method to create phonons was proposed in [37] where the scattering length is modulated at a rapid rate. In this case the system is not able to adiabatically follow the instantaneous ground state, and non-adiabatic processes result in the creation of correlated pairs of excitations out of the vacuum state [130]. This is an acoustic analogue to the dynamical Casimir effect of quantum field theory, which has been experimentally confirmed using superconducting circuits [131], where the vacuum can generate real particles whenever the boundary conditions, dispersion law, or background of the quantum field are quickly varied in time. The result can in fact be similar to that of parametric down-conversion [72] in quantum optics where a two-mode squeezed state of photons can be created.

This more quantum method of creating phonons has been investigated experimentally in [38] where the trap stiffness was changed rather than the atomic scattering length. This has a similar effect since changing the scattering length is analogous to changing the optical index as the speed of sound changes, and this also occurs when the trap stiffness changes since the density changes (see (1.30) which was derived for a uniform BEC). When the confining potential was modulated in time a pair of elementary excitations were produced in both the phonon and particle regimes, which were then examined in momentum space.[1] In the phonon regime the phonons were adiabatically converted into single atoms of the same momentum during the release of the trap in a process referred to as 'phonon evaporation' [133] and the momentum of these atoms was then measured. However, due to the high temperature, the pairs in this case came from the thermal noise rather than the vacuum and so no quantum correlations were observed.

Note that this method of generating phonons can be used to create two-mode squeezed states of phonons as the process can be analogous to parametric down conversion [37, 38]. Such a state was utilized in [18] to develop a theoretical GW detector and so it is vital to understand the decoherence of this state. This technique is, therefore, the technique that

[1] Interestingly, such a fast modulation of the confining potential was also studied from a purely classical point of view in Faraday wave experiments [132] where the radial trapping potential was modulated. In fact modulations of the scattering length have also been considered in this classical context [132].

we plan to use to generate phonons in our BEC to study the decoherence. However, as discussed in further detail in Section 5.3, we intend to modulate the scattering length rather than the trap stiffness.

5.2 Measuring Decoherence and Relaxation

5.2.1 Measuring Relaxation

The first observations of condensate oscillations [73] revealed oscillations with almost no damping, which is in good agreement with the zero temperature Gross-Pitaevskii equation (see Appendix D). Since then various experiments have been performed illustrating the damping of oscillations [73]. For example, in [73] the original experiments were carried out at higher temperatures where an exponentially decaying amplitude of the oscillations in the radial cloud width was observed in agreement with Landau damping [70, 134] and, in [135–138], Beliaev damping was observed.

The experiments are usually performed using a harmonic trapping potential, whereas, the theory of damping derived in Section 1.3 was based on a uniform Bose gas. This uniform-BEC theory can be extended to various types of traps [139], but the uniform case can still work quite well [70, 140]. A principle difference between trapped and homogeneous systems is that the Beliaev damping is not active for the lowest energy modes in the former case because of the discretization of levels [70, 134].

From the observed damping rate one can, in principle, estimate the relaxation rate (see Section 4.1.6). Alternatively quantum discrimination could be used where, for Gaussian states, a fidelity distance between the covariance matrix of the system, or some of its properties such as purity, and the environment can be computed (see Section 4.1.6 for more detail). For example, in [77], the minimal time required for an initial state $\boldsymbol{\sigma}_0$ to freely reach the target $\boldsymbol{\sigma}_\infty$ within a fixed fidelity $1-\epsilon$ was found to be $|\ln\epsilon|/2\gamma$. This is equivalent to the time taken for relaxation in Section 4.2 if $\epsilon = \alpha^2$ with $\alpha = 1\%$. This quantum discrimination would of course involve determining the full covariance matrix or some of its properties. In principle, the covariance matrix can be constructed from the joint detection of two conju-

gate quadratures, say position and momentum. Similar to quantum optics, phonon evaporation[2] could be performed and then homodyne detection of the atoms called be carried out [30, 113, 143]. However, as discussed in [35], another, potentially simpler, method would be to measure the Fourier component of the atomic density fluctuations corresponding to the phonon mode. An example, of a particular setup to measure the covariance matrix in this way is presented in [35] where an optical cavity couples to the condensate and the phonon's quadratures can be reconstructed from particular measurements of the optical mode shift.

5.2.2 Measuring Decoherence

From Section 4.1.1, one possible way to measure the decoherence time of a squeezed single-mode phonon state would be to determine the time at which the state's purity reaches a minimum. Purity is a non-linear function of the state's density operator and so is not related to the expectation value of a single-system hermitian operator or a single-system probability distribution that would be obtained from a positive operator-valued measure [113]. On the other hand, if the full quantum state of the system is known then the purity can be determined. For example, this could be performed using quantum tomography [144]. For Gaussian states this would mean just having to determine their first two statistical moments, which can be measured by the joint detection of two conjugate quadratures (see the discussion in the previous section).[3] However, this can be simplified further since, for Gaussian states, the purity is a simple function of the determinant of the covariance matrix as discussed in Section 4.1.1. The measurement of the Q–function can then be shown to provide the optimal minimal measurement for the purity for Gaussian states since it requires the minimum number of

[2] Phonon evaporation is the adiabatic conversion of phonons (and other quasi-particles) into a single atom/molecule of the same momentum during the release of the Bose gas from the trap [141, 142]. When the trapping potential is turned off, all the interaction energy is transformed into kinetic energy during a short acceleration period. The free particles that the quasi-particles are transformed into can then be imaged by resonant absorption imaging.

[3] In fact, since Gaussian states are fully characterized by the first and second moments, it suffices to measure only the rotated quadrature $\hat{x}_\theta = (\hat{a}^\dagger e^{i\theta} + \hat{a}e^{-i\theta})/\sqrt{2}$ for three different values of θ [113].

observables to be measured [113]. By measuring the purity of the phonons at various different stages in their free propagation (which would likely involve repeating the same experiment several times unless no destructive techniques were used [91]), it should be possible to extract the evolution of the purity of the states and thus their decoherence.

Several strategies have been proposed to directly measure the purity of a state. For example, in [145, 146] a simple quantum network is proposed in the context of a discrete system, and in [147] a setup is proposed that needs only beam splitters and single-photon detectors which could also be experimentally implemented in atom-field cavity or trapped ions experiments [146]. The latter scheme can also be used to measure the squeezing of Gaussian states [147], which, together with the purity, is enough to determine the nonclassicality of single-mode states.[4] This quantity could also be used as a quantifier of decoherence as discussed in Section 4.1.4.

A quantity unique to multi-partite systems is entanglement. Interactions with the environment can lead to rapid loss of entanglement, which is of primary importance in fields such as quantum information theory. Extending the theoretical framework of the previous chapters for the decoherence of a single-mode phonon state to the loss of entanglement in multi-mode systems will be the subject of future work [33]. Entangled phonons should, in principle, occur in the acoustic analogue of Hawking radiation in analogue gravity setups as well as other setups such as the acoustic analogue of the dynamical Casimir effect discussed above where a two-mode squeezed state is created [23, 37, 148–152]. A popular measure of entanglement is the Peres-Horedecki measure [153, 154], which has been extended to the continuous variable case of present interest [155, 156]. For two-mode Gaussian states this measure is easily calculated from the covariance matrix, and its application to phonon modes of a BEC has been discussed in [34–36, 157]. In particular, in [157] it was shown that, in the context of analogue gravity setups at low temperatures, violation of this inequality could be measured from the density-density correlation function extracted from in-

[4] Other methods for observing squeezing of phonons of BECs are considered in [78].

situ imaging.[5] At the time of writing, entanglement, and thus the loss of entanglement, is yet to be observed in phonons of BECs but this is expected to be achieved in the very near future.[6][7] Such a signature would be a clear sign of the quantumness of the systems, and measuring its loss would be vital in determining the application of such systems to relativistic quantum information science [17, 18, 40, 158] and potentially to quantum gravity theories. Note that this entanglement is of a very different nature to that observed in two-component BECs where it is atoms rather than phononic excitations that are entangled [159, 160].

Another nonclassical indicator that has been explored experimentally in BECs is the Cauchy-Schwarz inequality [161]. This has been measured for two-component BECs [162] but has yet to be violated using phononic excitations. For example, the acoustic analogue experiment of the dynamical Casimir effect investigated the Cauchy-Schwarz inequality but found no violation at the high temperature of the experiment. The violation and satisfaction of this inequality could also be used as a potential measure of the decoherence of the system. Furthermore, in [163], a violation of the Cauchy-Schwarz inequality was also considered to be a sign of entanglement of the BEC system in [162].

5.3 BEC Setup: A Strongly-Interacting BEC

5.3.1 Experimental Setup

Decoherence of phonons will be measured using a molecular ^{6}Li Bose gas. Bose-Einstein condensation has been demonstrated with this gas in the lab and was achieved in the following way: after leaving an oven, the technique of Zeeman slowing [164–166] is used to reduce the velocity of the gas so

[5] We are also currently looking at whether purity could be measured in a similar way [45].

[6] Subsequent to the submission of this thesis a measurement of the entanglement of high-frequency acoustic Hawking radiation was reported in [39]. This measurement opens the door to investigations into measuring the decoherence of phonons of BECs.

[7] As well as analogue gravity studies investigating entanglement of phonons in BECs, the generation of entanglement of phonons of BECs has also been considered in other contexts such as Beliaev decay and measurement backaction of a far-detuned light field [78, 91].

that it can be captured and cooled in an magneto-optical trap (MOT) [167]. After the MOT stage, the gas is then transferred to and trapped in a far off-resonance optical dipole trap [168]. The gas is then further cooled using the technique of evaporative cooling. This removes the molecules with the highest energies and allows those remaining to re-thermalize through elastic collisions.

Absorption imaging is used as the primary tool for observing the Bose gas. An on-resonance probe beam is sent through the cloud and the shadow corresponding to the light absorbed by the cloud is imaged on a camera. This destroys the atomic cloud but is simple to implement and produces a large signal-to-noise ratio. In our setup, the cloud can be imaged in-situ or after a time-of-flight.

5.3.2 Generating Phonons

As reviewed in Section 5.1, there are a number of ways in which condensate oscillations can be induced such as perturbing the potential, modulating the scattering length and using the technique of Bragg scattering. Of these options, modulating the scattering length has the advantage that, at finite temperatures, the thermal component would not be excited by this technique [126]. It can also be used to create special states such as a two-mode squeezed state as discussed in Section 5.1. For ^{6}Li, the Feshbach resonances make it possible to modulate the scattering length by the modulation of an external magnetic field.[8]

One method that is used to observe long-wavelength oscillations, of which phonons are the quanta, is through absorption imaging as discussed in Section 5.1 [74, 75, 123, 125]. For in-situ imaging the condensate is usually modelled as being constrained to an inverted parabolic region, which comes from assuming the Thomas-Fermi approximation where, for dense and large clouds, the kinetic energy of the particles is neglected when compared to interparticle interaction energy (see Chapter 6 for more detail). At finite temperatures there will also be a thermal cloud, which is usually

[8]Feshbach resonances occur when the energy associated with an elastic scattering process comes close to the energy of a bound state. See e.g. [58] for more detail.

modelled as an ideal gas and thus its density profile occupies a Gaussian profile. From fitting the condensate and noncondensate clouds various thermodynamic properties can be estimated such as the temperature, chemical potential and condensate fraction. This particular fitting technique where the extent of condensate is modelled as a parabola and the thermal cloud as a Gaussian, is often called the bi-modal or ideal gas fit. Once the clouds can be fit to, any perturbations can be identified and measured, which will facilitate the quantification of relaxation and decoherence using the methods discussed in Section 5.2.

5.3.3 Effects from Strong Interactions

The simple bi-modal fitting technique discussed in the previous section assumes negligible interactions between the condensate and the thermal cloud as well as within the thermal cloud. However, experiments have shown evidence of the mutual interaction between the condensate and thermal component [172]. This causes the condensate to be compressed by the thermal cloud and its shape to deviate from that predicted by the bi-modal model. The shape of the thermal cloud will also differ to that predicted by the bi-modal model since the condensate will act back on the thermal cloud and their will be repulsive interactions between thermal particles. These interaction effects become more prominent at higher temperatures as the thermal cloud grows in size. They will also be enhanced in more strongly-interacting gases such as ^{6}Li which has a greater coupling constant than other alkali gases such as ^{23}Na, ^{41}K and ^{87}Rb. Therefore, at low, and especially high, temperatures we expect to see a greater effect from the thermal cloud interactions than in previous studies and, unless modelled correctly, this will result in inaccurate measurements taken from in-situ (and time-of-flight) absorption imaging.

We are currently in the process of modelling in-situ images using more sophisticated methods than the bi-modal model. The next chapter reviews these alternative models, which are all based on mean-field theory, and discusses the current progress with modelling the ^{6}Li Bose gas. As well as facilitating the experimental measurement of the decoherence and relaxation

time of phonons, this analysis is also expected to inform the BEC community on the validity of the generically used bi-modal model for modelling strongly-interacting Bose gases as well as the effects of the mutual interaction between the condensed and noncondensed components. The Feshbach resonances of ^{6}Li also make it possible to vary the scattering length by adjusting an external parameters such as the magnetic field and this will provide more information on the applicability of the bi-modal model. If the interaction strength is high enough then beyond mean-field theory effects may also be seen. These occur when the dilute condition $na^3 \ll 1$ breaks down and interactions are no longer only dominated by two-body encounters [58]. This will also be discussed in further detail in the next chapter.

CHAPTER 6

Modelling Absorption Images of a Strongly-Interacting Gas

6.1 Introduction

This chapter investigates three different models that can be used to fit the density profile from an in-situ absorption image of a strongly-interacting BEC. These three models are referred to as the bi-modal, semi-ideal [52] and Hartree-Fock models [46, 47, 173]. In the previous chapter it was argued that the bi-modal model, where the (three-dimensional) condensate density profile is an inverted parabola and the noncondensate profile is a Gaussian, would not represent an accurate model for a strongly-interacting BEC since all inter-particle interactions are ignored in this model except those involving only condensate particles. The semi-ideal model, which was first formulated in [52], represents a more accurate model since it includes the interaction that the condensate imparts on the thermal cloud in a mean-field description. As with the bi-modal model, the semi-ideal model can be formulated as independent analytical expressions for the condensate and noncondensate density profiles, and is a simple model to fit the density profiles to. The third model that will be investigated is the Hartree-Fock model which improves on the semi-ideal model by including all interactions within a mean-field approximation. However, this model is more complicated to use compared to the other two models since the two density profiles are coupled and must be solved numerically.

The next section derives all three models from the quantum field Hamiltonian of a Bose gas (1.8). This derivation relies on the assumption that the temperature of the gas is high $k_B T \gg \mu$. However, at low temperatures the thermal cloud should be negligible and so any additional interaction effects beyond those of the bi-modal model would unlikely be seen in realistic absorption images at those temperatures. The subsequent section, Section 6.3, then considers how the three models can be used to fit the line density profiles of an absorption image of a BEC in a cylindrical trap. In particular, in Section 6.3.4, absorption images of the ^{6}Li BEC that was introduced in the previous chapter are used to illustrate these fits, and current progress with the experiment is discussed. Finally, in Section 6.4, the validity of the models is examined and beyond-mean-field theory effects are considered.

6.2 Derivation of the Hartree-Fock, Semi-Ideal and Bi-Modal Models

All three fitting models can be derived from the quantum field Hamiltonian of a rarefied interacting Bose gas, which is given by (1.8). Taking the temperature of the gas to be below the critical temperature so that there is sufficiently low-energy and the gas is dilute, the potential $\mathcal{U}(\boldsymbol{r}' - \boldsymbol{r})$ can be approximated to be short-range and given by the contact potential $g\delta(\boldsymbol{r}' - \boldsymbol{r})$ where, in the s-wave approximation, $g = 4\pi\hbar^2 a/m$.[1] This results in the Hamiltonian:

$$\hat{H} = \int d\boldsymbol{r} \Big(-\hat{\psi}^\dagger(\boldsymbol{r}) \frac{\hbar^2}{2m} \boldsymbol{\nabla}^2 \hat{\psi}(\boldsymbol{r}) + \mathcal{V}(\boldsymbol{r}) \hat{\psi}^\dagger(\boldsymbol{r}) \hat{\psi}(\boldsymbol{r}) + \frac{g}{2} \hat{\psi}^\dagger(\boldsymbol{r}) \hat{\psi}^\dagger(\boldsymbol{r}) \hat{\psi}(\boldsymbol{r}) \hat{\psi}(\boldsymbol{r}) \Big). \tag{6.1}$$

[1] In principle, the assumption of a contact potential is only really consistent in a first-order approximation where the physical quantities are evaluated to first order in the interaction (see Chapter 1 and [66] for more detail). Any additional effects are neglected in this chapter.

By analogy with (1.11), the field operator is then split up into its condensate and noncondensate components:

$$\hat{\psi}(\boldsymbol{r}) = \psi_0(\boldsymbol{r})a_0 + \sum_{i\neq 0}\psi(\boldsymbol{r})\hat{a}_i \tag{6.2}$$

$$:= \Phi(\boldsymbol{r}) + \delta\hat{\psi}(\boldsymbol{r}) \tag{6.3}$$

where, in the Bogoliubov approximation (see (1.11)), $\Psi(\boldsymbol{r})$ behaves as a classical-field since $\hat{a}_0$ is now a c-number. On substituting (6.2) into (6.1), the Hamiltonian of the gas becomes:

$$\begin{aligned}\hat{H} = \int d\boldsymbol{r}\Big[&\Phi^*(\boldsymbol{r})\Big(-\frac{\hbar^2}{2m}\boldsymbol{\nabla}^2 + \mathcal{V}(\boldsymbol{r}) + \frac{1}{2}g|\Phi(\boldsymbol{r})|^2\Big)\Phi(\boldsymbol{r}) \\ &+ \delta\hat{\psi}^\dagger(\boldsymbol{r})\Big(-\frac{\hbar^2}{2m}\boldsymbol{\nabla}^2 + \mathcal{V}(\boldsymbol{r})\Big)\delta\hat{\psi}(\boldsymbol{r}) \\ &+ \hat{H}_2^I + \hat{H}_3^I + \hat{H}_4^I\Big]\end{aligned} \tag{6.4}$$

where the interaction Hamiltonians are given by:

$$\hat{H}_2^I := \frac{g}{2}|\Phi(\boldsymbol{r})|^2[\delta\hat{\psi}(\boldsymbol{r})\delta\hat{\psi}(\boldsymbol{r}) + 4\delta\hat{\psi}^\dagger(\boldsymbol{r})\delta\hat{\psi}(\boldsymbol{r}) + \delta\hat{\psi}^\dagger(\boldsymbol{r})\delta\hat{\psi}^\dagger(\boldsymbol{r})], \tag{6.5}$$

$$\hat{H}_3^I := g[\Phi^*(\boldsymbol{r})\delta\hat{\psi}^\dagger(\boldsymbol{r})\delta\hat{\psi}(\boldsymbol{r})\delta\hat{\psi}(\boldsymbol{r}) + \Phi(\boldsymbol{r})\delta\hat{\psi}^\dagger(\boldsymbol{r})\delta\hat{\psi}^\dagger(\boldsymbol{r})\delta\hat{\psi}(\boldsymbol{r})], \tag{6.6}$$

$$\hat{H}_4^I := \frac{g}{2}\delta\hat{\psi}^\dagger(\boldsymbol{r})\delta\hat{\psi}^\dagger(\boldsymbol{r})\delta\hat{\psi}(\boldsymbol{r})\delta\hat{\psi}(\boldsymbol{r}), \tag{6.7}$$

which are analogous to (1.14)-(1.16) but in position space. In the self-consistent mean-field approximation, the terms in $\hat{H}_I^3$ and $\hat{H}_4^I$ are approximated into various terms involving the normal average $\langle\delta\hat{\psi}^\dagger\delta\hat{\psi}\rangle$, and the anomalous averages $\langle\delta\hat{\psi}^\dagger\delta\hat{\psi}^\dagger\rangle$ and $\langle\delta\hat{\psi}\delta\hat{\psi}\rangle$ [174]. In the Hartree-Fock-Bogoliubov approximation the averages that include three or more operators are then neglected:

$$\delta\hat{\psi}^\dagger\delta\hat{\psi}\delta\hat{\psi} \approx 2\langle\delta\hat{\psi}^\dagger\delta\hat{\psi}\rangle\delta\hat{\psi} + \langle\delta\hat{\psi}\delta\hat{\psi}\rangle\delta\hat{\psi}^\dagger, \tag{6.8}$$

$$\delta\hat{\psi}^\dagger\delta\hat{\psi}^\dagger\delta\hat{\psi} \approx 2\langle\delta\hat{\psi}^\dagger\delta\hat{\psi}\rangle\delta\hat{\psi}^\dagger + \langle\delta\hat{\psi}^\dagger\delta\hat{\psi}^\dagger\rangle\delta\hat{\psi}, \tag{6.9}$$

$$\delta\hat{\psi}^\dagger\delta\hat{\psi}^\dagger\delta\hat{\psi}\delta\hat{\psi} \approx 4\langle\delta\hat{\psi}^\dagger\delta\hat{\psi}\rangle\delta\hat{\psi}^\dagger\delta\hat{\psi} + \langle\delta\hat{\psi}^\dagger\delta\hat{\psi}^\dagger\rangle\delta\hat{\psi}\delta\hat{\psi} + \langle\delta\hat{\psi}\delta\hat{\psi}\rangle\delta\hat{\psi}^\dagger\delta\hat{\psi}^\dagger. \tag{6.10}$$

Note that the origin of the factor of 2 in the above equations is due to the identicality of the Hartree and Fock exchange terms in the zero-range interaction approximation [174]. Substituting (6.8)-(6.10), and dropping the terms that do not conserve momenta, the Hamiltonian of (6.4) is then given by:

$$\begin{aligned}\hat{H} = \int d\boldsymbol{r}\Big[&\hat{\Phi}_0^*(\boldsymbol{r})\Big(-\frac{\hbar^2}{2m}\boldsymbol{\nabla}^2 + \mathcal{V}(\boldsymbol{r}) + \frac{1}{2}gn_0\Big)\hat{\Phi}_0(\boldsymbol{r}) \\ &+ \delta\hat{\psi}^\dagger(\boldsymbol{r})\Big(-\frac{\hbar^2}{2m}\boldsymbol{\nabla}^2 + \mathcal{V}(\boldsymbol{r}) + 2gn_0(\boldsymbol{r}) + 2gn_T(\boldsymbol{r})\Big)\delta\hat{\psi}(\boldsymbol{r}) \\ &+ \frac{1}{2}gm^*(\boldsymbol{r})\delta\hat{\psi}(\boldsymbol{r})\delta\hat{\psi}(\boldsymbol{r}) + \frac{1}{2}gm(\boldsymbol{r})\delta\hat{\psi}^\dagger(\boldsymbol{r})\delta\hat{\psi}^\dagger(\boldsymbol{r})\Big]\end{aligned} \tag{6.11}$$

where:

$$n_0(\boldsymbol{r}) := |\Phi(\boldsymbol{r})|^2, \tag{6.12}$$

$$n_T(\boldsymbol{r}) := \langle\delta\hat{\psi}^\dagger(\boldsymbol{r})\delta\hat{\psi}(\boldsymbol{r})\rangle, \tag{6.13}$$

$$m(\boldsymbol{r}) := \Phi(\boldsymbol{r})^2 + \langle\delta\hat{\psi}(\boldsymbol{r})\delta\hat{\psi}(\boldsymbol{r})\rangle, \tag{6.14}$$

$$m^*(\boldsymbol{r}) := \Phi(\boldsymbol{r})^{*2} + \langle\delta\hat{\psi}^\dagger(\boldsymbol{r})\delta\hat{\psi}^\dagger(\boldsymbol{r})\rangle. \tag{6.15}$$

Comparing (6.11) to the Hamiltonian obtained in the Bogoliubov approximation (1.22) in Section 1.2.1, the interaction terms that were cubic in $\delta\hat{\psi}$, which are responsible for Landau and Beliaev damping of phonons, have again vanished, but terms from $\hat{H}_4^I$ have been kept. The Bogoliubov approximation is a good description of a weakly interacting dilute Bose gas at low temperatures because the depletion of the condensate is very small. However, as the gas becomes denser or the temperature becomes higher, the interactions between the noncondensate particles become more important and the Bogoliubov model loses its validity. The Hartree-Fock-Bogoliubov

approximation thus upgrades the Bogoliubov interactions by taking into account the contributions from interactions between the noncondensate particles [66]. Analogous to the case of the Bogoliubov approximation, the Hamiltonian (6.11) can again be diagonalized by a Bogoliubov transformation resulting in quasi-particles similar to the Bogoliubov quasi-particles but now 'dressed' by the mean-field effects on noncondensate particles [66].

6.2.1 Noncondensate Equation of Motion

The equations of motion for the operators $\delta\hat{\psi}$ and $\delta\hat{\psi}^\dagger$ in the Heisenberg picture are by definition:

$$i\hbar\frac{\partial\delta\hat{\psi}}{\partial t} = [\delta\hat{\psi}, \hat{H}] \quad \text{and} \quad i\hbar\frac{\partial\delta\hat{\psi}^\dagger}{\partial t} = [\delta\hat{\psi}^\dagger, \hat{H}], \tag{6.16}$$

which, upon substitution of $\hat{H}$ from (6.11), become:

$$\begin{aligned} i\hbar\frac{\partial\delta\hat{\psi}(\boldsymbol{r},t)}{\partial t} = \Big(-\frac{\hbar^2}{2m}\boldsymbol{\nabla}^2 + \mathcal{V}(\boldsymbol{r}) + 2gn_0(\boldsymbol{r},t) + 2gn_T(\boldsymbol{r},t)\Big)\delta\hat{\psi}(\boldsymbol{r},t) \\ + gm(\boldsymbol{r},t)\delta\hat{\psi}^\dagger(\boldsymbol{r},t) \end{aligned} \tag{6.17}$$

and:

$$\begin{aligned} i\hbar\frac{\partial\delta\hat{\psi}^\dagger(\boldsymbol{r},t)}{\partial t} = \Big(-\frac{\hbar^2}{2m}\boldsymbol{\nabla}^2 + \mathcal{V}(\boldsymbol{r},t) + 2gn_0(\boldsymbol{r},t) + 2gn_T(\boldsymbol{r},t)\Big)\delta\hat{\psi}^\dagger(\boldsymbol{r},t) \\ + gm^*(\boldsymbol{r},t)\delta\hat{\psi}(\boldsymbol{r},t). \end{aligned} \tag{6.18}$$

These equations of motion can be solved by carrying out a transformation analogous to the Bogoliubov transformations given by (1.23):

$$\delta\hat{\psi}(\boldsymbol{r},t) = \sum_{i\neq 0}\Big(u_i(\boldsymbol{r})\hat{b}_i e^{-i\epsilon_i t/\hbar} - v_i^*(\boldsymbol{r})\hat{b}_i^\dagger e^{+i\epsilon_i t/\hbar}\Big) \tag{6.19}$$

where $u_i(\boldsymbol{r},t)$ and $v_i(\boldsymbol{r},t)$ are given by the solutions of the coupled Hartree-Fock-Bogoliubov equations [174]:

$$\Big(-\frac{\hbar^2}{2m}\boldsymbol{\nabla}^2+\mathcal{V}(\boldsymbol{r})+2gn(\boldsymbol{r})-\epsilon_i\Big)u_i(\boldsymbol{r})-gm(\boldsymbol{r})v_i(\boldsymbol{r})=0, \tag{6.20}$$

$$\Big(-\frac{\hbar^2}{2m}\boldsymbol{\nabla}^2+\mathcal{V}(\boldsymbol{r})+2gn(\boldsymbol{r})+\epsilon_i\Big)v_i(\boldsymbol{r})-gm^*(\boldsymbol{r})u_i(\boldsymbol{r})=0 \tag{6.21}$$

with $n(\boldsymbol{r}):=n_0(\boldsymbol{r})+n_T(\boldsymbol{r})$. Here the condensate and noncondensate have been assumed to both be in static thermal equilibrium so that the time dependence of various terms can be dropped. Note that these equations are similar to the Bogoliubov-de-Genes equations [175] and can be derived using a variety of methods (see [173, 174] for more detail).

Once the eigenvalues ϵ_i and the associated solutions u_i and v_i have been determined, the operator $\hat{H}$ may be expressed in these terms so that $\hat{H}=\sum_{i\neq 0}\epsilon_i\hat{b}_i^\dagger\hat{b}_i+\text{constant}$ [58] where, for a uniform BEC with n_T ignored, ϵ_i is just given by (1.29) from Chapter 1. As discussed in Section 1.2.1, if the temperature is high then the excitations are dominated by free particles and the effects from the phonon-like excitations can be neglected. This is equivalent to neglecting the $\delta\hat{\psi}\delta\hat{\psi}$ and $\delta\hat{\psi}^\dagger\delta\hat{\psi}^\dagger$ terms in $\hat{H}_2^I$ and means that $v\approx 0$ in (6.20)-(6.21). The anomalous averages $\langle\delta\hat{\psi}\delta\hat{\psi}\rangle$ and $\langle\delta\hat{\psi}^\dagger\delta\hat{\psi}^\dagger\rangle$ will also vanish in this high temperature limit so that (6.20) and (6.21) reduce to just:

$$\Big(-\frac{\hbar^2}{2m}\boldsymbol{\nabla}^2+\mathcal{V}(\boldsymbol{r})+2gn_0(\boldsymbol{r})+2gn_T(\boldsymbol{r})\Big)u_i(\boldsymbol{r})=\epsilon_i u_i(\boldsymbol{r}) \tag{6.22}$$

where $\delta\hat{\psi}(\boldsymbol{r})=\sum_i u_i(\boldsymbol{r})\hat{b}_i$. This equation describes the noncondensate component of the gas in the so-called Hartree-Fock approximation. In deriving this equation, the only interaction terms that have been kept are then those from the terms $\Phi^*\delta\hat{\psi}^\dagger\Phi\delta\hat{\psi}$ (the so-called Hartree term), $\Phi^*\delta\hat{\psi}^\dagger\delta\hat{\psi}\Phi$ (the so-called Fock term) and $\delta\hat{\psi}^\dagger\delta\hat{\psi}^\dagger\delta\hat{\psi}\delta\hat{\psi}$, which are all illustrated in Figure 6.1. This suggests that an alternative derivation of (6.22) is to assume high temperatures $k_BT\gg\mu$ from the start and that such high temperatures results in all excitations being particle-like (no phononic contributions). All the

terms in (6.4) would then be assumed to vanish except the Hermitian terms in $\delta\psi$ and Φ, and with $\hat{H}_4^I$ replaced by (6.10) as before. This illustrates that the wave function of the excitations must have the form of a product of single-particle states symmetrized with respect to interchange of particles.

The equilibrium distribution of the excitations can be derived from (6.22) by maximizing the entropy with the the condition that the total energy and the total number of particles are fixed. The excitations here just correspond to adding a single particle to a gas and thus, in maximizing the entropy, one must introduce the chemical potential term to maintain the particle number at a constant value [58]. This is unlike the case for quasi-particles in Section 1.2.1 where the chemical potential for the uniform gas $\mu = gn$ is contained in the solutions (the constraint on the particle number has been implemented explicitly) which, for the above derivation, would have meant starting with the grand canonical operator $\hat{K} = \hat{H} - \mu\hat{N}$ [58].

In the semi-classical approximation the typical de Broglie wavelengths of particles are small compared with the length scales over which the trapping potential and the particle densities vary significantly [58]. For a cylindrical trap this requires that $k_b T \gg \hbar\omega_r$, where ω_r is the radial frequency of the trap, so that the cloud of thermal atoms has a spatial extent much larger than the oscillator length. The properties of the excitations may then still be described semi-classically when the particles interact provided that spatial variations occur over distances large compared with the wavelengths of typical excitations. In this approximation, the density of noncondensed particles is then given by (see, for example, [48, 58]):

$$n_T(\boldsymbol{r}) = \int \frac{d\boldsymbol{p}}{(2\pi\hbar)^3} \frac{1}{e^{(\epsilon_p - \mu)/k_B T} - 1} = \frac{1}{\lambda_T^3} g_{3/2}(z(\boldsymbol{r})) \tag{6.23}$$

where λ_T is the thermal de Broglie wavelength:

$$\lambda_T = \left(\frac{2\pi\hbar^2}{m k_B T}\right)^{\frac{1}{2}}; \tag{6.24}$$

the function $g_{3/2}(z)$ is defined by:

$$g_{3/2}(z(\boldsymbol{r})) := \sum_{l=1}^{\infty} \frac{z(\boldsymbol{r})^l}{l^{3/2}}, \tag{6.25}$$

$$z(\boldsymbol{r}) := e^{(\mu - 2gn_T(\boldsymbol{r}) - 2gn_0(\boldsymbol{r}) - \mathcal{V}(\boldsymbol{r}))/k_BT}; \tag{6.26}$$

and the energies ϵ_p are continuous and derive from (6.22):

$$\epsilon_p = \frac{p^2}{2m} + \mathcal{V}(\boldsymbol{r}) + 2g(n_0(\boldsymbol{r}) + n_T(\boldsymbol{r})). \tag{6.27}$$

Equation (6.23) describes a density profile of the noncondensed particles. This will be referred to as the Hartree-Fock density profile of the noncondensed particles. Note that this equation contains $n_T(\boldsymbol{r})$ on both the left and the right.

6.2.2 Condensate Equation of Motion

The previous section derived an expression for the density profile of the noncondensate particles by starting with the quantum field Hamiltonian of the Bose gas and assuming high temperatures. In this section the same assumptions are applied to derive the density profile of the condensate component.

For the quantum field Hamiltonian (6.1), the grand canonical operator $\hat{K} = \hat{H} - \mu\hat{N}$ is given by:

$$\hat{K} = \int \Big[\hat{\psi}^\dagger(\boldsymbol{r})\Big(-\frac{\hbar^2}{2m}\boldsymbol{\nabla}^2\hat{\psi}(\boldsymbol{r}) + \mathcal{V}(\boldsymbol{r}) - \mu\Big)\hat{\psi}(\boldsymbol{r}) + \frac{g}{2}\hat{\psi}^\dagger(\boldsymbol{r})\hat{\psi}^\dagger(\boldsymbol{r})\hat{\psi}(\boldsymbol{r})\hat{\psi}(\boldsymbol{r})d\boldsymbol{r}\Big]. \tag{6.28}$$

The equation of motion for the operator $\hat{\psi}$ in the Heisenberg picture is then:

$$i\hbar\frac{\partial\hat{\psi}(\boldsymbol{r},t)}{\partial t} = \Big(-\frac{\hbar^2}{2m}\boldsymbol{\nabla}^2 + \mathcal{V}(\boldsymbol{r}) - \mu\Big)\hat{\psi}(\boldsymbol{r},t) + g\hat{\psi}^\dagger(\boldsymbol{r},t)\hat{\psi}(\boldsymbol{r},t)\hat{\psi}(\boldsymbol{r},t) \tag{6.29}$$

since:

$$i\hbar\frac{\partial\hat{\psi}}{\partial t} = [\hat{\psi}, \hat{K}]. \tag{6.30}$$

As in the previous section, the field operator $\hat{\psi}$ is split up into its condensate and noncondensate parts (see (6.2)), and so $\langle\hat{\psi}\rangle = \Phi$ since $\langle\delta\hat{\psi}\rangle = 0$. Therefore, the equation of motion for the condensate is given by:

$$i\hbar\frac{\partial\Phi(\boldsymbol{r},t)}{\partial t} = \Big(-\frac{\hbar^2}{2m}\boldsymbol{\nabla}^2 + \mathcal{V}(\boldsymbol{r}) - \mu\Big)\Phi(\boldsymbol{r},t) + g\langle\hat{\psi}^\dagger(\boldsymbol{r},t)\hat{\psi}(\boldsymbol{r},t)\hat{\psi}(\boldsymbol{r},t)\rangle. \tag{6.31}$$

Using (6.2), the last term in (6.31) can be expanded as:

$$\hat{\psi}^\dagger\hat{\psi}\hat{\psi} = |\Phi|^2\Phi + 2|\Phi|^2\delta\hat{\psi} + \Phi^2\delta\hat{\psi}^\dagger + \Phi^*\delta\hat{\psi}\delta\hat{\psi} + 2\Phi\delta\hat{\psi}^\dagger\delta\hat{\psi} + \delta\hat{\psi}^\dagger\delta\hat{\psi}\delta\hat{\psi}$$

and, following the previous section, in the Hartree-Fock-Bogoliubov mean-field approximation, $\delta\hat{\psi}^\dagger\delta\hat{\psi}\delta\hat{\psi}^\dagger \approx 2\langle\delta\hat{\psi}^\dagger\delta\hat{\psi}\rangle\delta\hat{\psi} + \langle\delta\hat{\psi}\delta\hat{\psi}\rangle\delta\hat{\psi}^\dagger$ so that this terms vanishes on evaluating its expectation value. The condensate equation of motion can then be approximated as:[2]

$$i\hbar\frac{\partial\Phi(\boldsymbol{r},t)}{\partial t} = \Big(-\frac{\hbar^2}{2m}\boldsymbol{\nabla}^2 + \mathcal{V}(\boldsymbol{r}) + gn_0(\boldsymbol{r},t) + 2gn_T(\boldsymbol{r},t) - \mu\Big)\Phi(\boldsymbol{r},t) + g\langle\delta\hat{\psi}(\boldsymbol{r},t)\delta\hat{\psi}(\boldsymbol{r},t)\rangle\Phi^*(\boldsymbol{r},t) \tag{6.32}$$

where, as before, $n_0(\boldsymbol{r},t) = |\Phi(\boldsymbol{r},t)|^2$ and $n_T(\boldsymbol{r},t) = \langle\hat{\psi}^\dagger(\boldsymbol{r},t)\hat{\psi}(\boldsymbol{r},t)\rangle$.

In the limit of high temperatures the anomalous density $\langle\delta\hat{\psi}(\boldsymbol{r},t)\delta\hat{\psi}(\boldsymbol{r},t)\rangle$ in the above equation vanishes since the excitations are particle-like as discussed in the previous section. Ignoring all time dependence, the equation

[2]Note that this equation almost reduces to the well-used ($T = 0$) Gross-Pitaevskii equation when the noncondensate component is neglected such that the anomalous and normal density terms for this component vanish. The only reason it doesn't quite reduce to the Gross-Pitaevskii is that the latter is derived from the Hamiltonian rather than the grand canonical and so there is no μ term.

of motion for the condensate then reduces to:

$$\Big(-\frac{\hbar^2}{2m}\boldsymbol{\nabla}^2 + \mathcal{V}(\boldsymbol{r}) + gn_0(\boldsymbol{r}) + 2gn_T(\boldsymbol{r})\Big)\Phi(\boldsymbol{r}) = \mu\Phi(\boldsymbol{r}) \tag{6.33}$$

where the absence of a factor of two compared to (6.22) reflects the fact that there is no exchange term for two particles in the same state.

A further approximation that can usually be successfully applied to a trapped Bose gas is the Thomas-Fermi approximation where the kinetic energy associated with the condensate in (6.33) is ignored, which is equivalent to neglecting the quantum pressure term in the hydrodynamic version of the equation (the Madelung description). By comparing the kinetic and potential energy terms, this can be shown to be valid for a cylindrical trap when [176]:[3]

$$\frac{N_0 a}{a_{ho}} \gg 1 \tag{6.34}$$

where:

$$a_{ho} := \Big(\frac{\hbar}{m\omega_{ho}}\Big)^{1/2}, \quad \omega_{ho} := (\omega_x\omega_y\omega_z)^{1/3}. \tag{6.35}$$

This approximation is therefore valid when there are sufficiently high numbers of condensate particles. With this approximation the equation of motion for the condensate then simplifies to:

$$\Big(\mathcal{V}(\boldsymbol{r}) + gn_0(\boldsymbol{r}) + 2gn_T(\boldsymbol{r})\Big)\Phi(\boldsymbol{r}) = \mu\Phi(\boldsymbol{r}) \tag{6.36}$$

and so the density profile of the condensate is given by:

$$n_0(\boldsymbol{r}) = \frac{1}{g}\Big(\mu - \mathcal{V}(\boldsymbol{r}) - 2gn_T(\boldsymbol{r})\Big)\theta(\mu - \mathcal{V}(\boldsymbol{r}) - 2gn_T(\boldsymbol{r})) \tag{6.37}$$

[3]Note that this can be satisfied at the same time as the condition for dilute gases $n|a|^3 \ll 1$.

where $\theta(x)$ is the step function:

$$\theta(x) = \begin{cases} 1 & \text{if } x > 0 \\ 0 & \text{if } x < 0 \end{cases} \tag{6.38}$$

6.2.3 The Hartree-Fock Model

The coupled density equations (6.23) and (6.37) will be referred to as the Hartree-Fock model of the Bose gas [46, 47, 173]. In this mean-field model the noncondensate component is treated as a 'non-interacting' gas of density that experiences a self-consistent mean-field interaction potential from the noncondensate and condensate components $2gn(\boldsymbol{r})$ [177]. That is, a mean-field description is used which treats excited particles as independent and evolving in a self-consistent static potential. Numerical schemes must be employed to solve the condensate and noncondensate densities of this model [46]. For example, a transcendental equation method can be used by substituting (6.37) into (6.23) such that a transcendental-type equation is obtained for the noncondensate density [178]. Other alternatives include iterative schemes such as a Newton-Raphson method.

Note that an improved description of the gas would be to include the collective (phononic) effects that were neglected in the derivation. However, it has been demonstrated that low-energy, collective excitations cause a minute change in the thermodynamic properties of the system even at relatively low temperatures[179–181]. In fact, in trapped Bose gases, the Hartree-Fock model provides a good approximation down to much lower temperatures than in the case of a uniform Bose gas [50].

6.2.4 The Semi-Ideal Model

The Hartree-Fock model can be simplified by neglecting the mean-field repulsion from noncondensed particles in (6.37) and (6.23). This results in the uncoupled equations:

$$n_0(\boldsymbol{r}) = \frac{1}{g}\Big(\mu - \mathcal{V}(\boldsymbol{r})\Big)\theta(\mu - \mathcal{V}(\boldsymbol{r})) \text{ and} \tag{6.39}$$

$$n_T(\boldsymbol{r}) = \frac{1}{\lambda_T^3} g_{3/2}(z(\boldsymbol{r})) \tag{6.40}$$

where:

$$z(\boldsymbol{r}) = e^{(\mu - 2gn_0(\boldsymbol{r}) - \mathcal{V}(\boldsymbol{r}))/k_B T} \tag{6.41}$$

$$= e^{\mu/k_B T}\ \theta(|\boldsymbol{r}| - R_{TF}) + e^{(\mathcal{V}(\boldsymbol{r}) - \mu)}\ \theta(R_{TF} - |\boldsymbol{r}|) \tag{6.42}$$

and R_{TF} is the radius of the condensate in the Thomas-Fermi approximation.

Equations (6.39)-(6.40) form the so-called semi-ideal model [52]. The condensate density profile in this case is that which derives from the Gross-Pitaevskii equation in the Thomas-Fermi approximation and is thus the density of a zero temperature Bose gas in a trap with a significant number of condensate particles. On the other hand, the density of the noncondensed component is that of an ideal gas of bosons confined in the combination of the external trapping potential and the repulsive mean-field potential of the condensate particles. Its wide range of validity has been confirmed by numerical analysis [182].

6.2.5 The Bi-Modal Model

A further simplification is to neglect the mean-field potential of the condensate particles in (6.40) and assume that the temperature of the gas is high enough such that the majority of the noncondensate particles have energies much larger than μ. The noncondensate particles then follow a Boltzmann distribution rather than a Bose-Einstein distribution:

$$n_T(\boldsymbol{r}) = \frac{1}{\lambda_T^3} e^{(\mu - \mathcal{V}(\boldsymbol{r}))/k_B T}. \tag{6.43}$$

This together with the condensate density given by (6.40) defines the bi-modal model. It is the simplest of the three models and the one that is used most frequently in BEC experiments. The principle assumption in its derivation is that the temperature is high enough such that the kinetic

energy of the noncondensate particles is much larger than the mean-field energy and thus deviations from ideal gas behaviour are small [74, 75, 137, 183]. However, it also assumes the Thomas-Fermi approximation for the condensate component which might not be particularity accurate at such high temperatures since the condensate will be more depleted than at low temperatures.

6.3 Fitting Absorption Images

The above models can be used to fit in-situ absorption images of a Bose gas to extract certain thermodynamic properties such as the chemical potential, temperature, atom number and condensate fraction. The Lithium BEC that was discussed in Chapter 5 uses a cylindrical trapping potential and the images that will be fit are line density images. Therefore, the three models will need to be fit to a line density absorption image of a BEC from a cylindrical trap. Sections 6.3.1-6.3.3 derive the expressions for the line densities of the condensate and noncondensate component of a Bose gas in a cylindrical trap for the bi-modal, semi-ideal and Hartree-Fock models respectively. These can then be used to fit an in-situ absorption image of a Bose gas in a cylindrical trap. To illustrate this, Section 6.3.4 provides examples of in-situ absorption images of the strongly-interacting ^{6}Li BEC and how these three models can be used to fit to them.

6.3.1 Bi-Modal Line Densities

The potential of a cylindrical trap is defined as:

$$\mathcal{V}(\boldsymbol{r}) = \frac{1}{2}m(\omega_\rho^2\rho^2 + \omega_z^2 z^2) \tag{6.44}$$

where z is the axial direction; $\rho^2 = x^2 + y^2$ is the radial direction; and $\omega_\rho = \omega_x = \omega_y$, or more generally, $\omega_\rho = \sqrt{\omega_x\omega_y}$. The three-dimensional condensate density profile of (6.39) therefore corresponds to an inverted parabola extending from the potential minimum up to the Thomas-Fermi radius. The line density of the condensate and noncondensate can be found

by radially integrating (6.39) and (6.43):

$$n_0(z) = \frac{\pi}{gm\omega_\rho^2}\Big(\mu - \frac{1}{2}m\omega_z^2 z^2\Big)^2 \theta(\mu - \frac{1}{2}m\omega_z^2 z^2), \tag{6.45}$$

$$n_T(z) = \frac{1}{\lambda_T^5}\Big(\frac{2\pi\hbar}{m\omega_\rho^2}\Big)^2 e^{(\mu - \frac{1}{2}m\omega_z^2 z^2)/k_B T}. \tag{6.46}$$

These equations can then be fit to line density images of a BEC in a cylindrical trap. Note that the total number of particles for each component is easily obtained by integrating over the remaining coordinate:

$$N_0 = \Big(\frac{2\mu}{\hbar\omega_{ho}}\Big)^{5/2}\frac{a_{ho}}{15a_s}, \tag{6.47}$$

$$N_T = \Big(\frac{k_B T}{\hbar\omega_{ho}}\Big)^3 e^{\mu/k_B T}. \tag{6.48}$$

6.3.2 Semi-Ideal Line Densities

Cylindrical coordinates can be used to calculate the line and radial densities of the condensate and noncondensate components [52]. Concentrating on just the line densities, these are given by:

$$n_0(z) = \frac{\pi}{gm\omega_\rho^2}\Big(\mu - \frac{1}{2}m\omega_z^2 z^2\Big)^2 \theta(\mu - \frac{1}{2}m\omega_z^2 z^2), \tag{6.49}$$

$$\begin{aligned} n_T(z) = \frac{1}{\lambda_T^5}\Big(\frac{2\pi\hbar}{m\omega_\rho^2}\Big)^2 \Big[& g_{5/2}(e^{(\mu - \frac{1}{2}\omega_z^2 z^2)/k_B T})\theta(\mu - \frac{1}{2}m\omega_z^2 z^2) \\ & + \Big(2\zeta(5/2) - g_{5/2}(e^{(\frac{1}{2}m\omega_z^2 z^2 - \mu)/k_B T})\Big)\theta(\frac{1}{2}m\omega_z^2 z^2 - \mu)\Big] \end{aligned} \tag{6.50}$$

where $n_0(z)$ is the same as for the bi-modal model.

Note that, as with the bi-modal model, the density profiles for the two gases can still be solved separately. However, a simple geometric series now needs to be evaluated for the Bose gas (see (6.40)), which converges quickly.

6.3.3 Hartree-Fock Line Densities

In the Hartree-Fock model the densities of the condensed and thermal clouds are given by the coupled equations (6.37) and (6.23):

$$n_0(\boldsymbol{r}) = \frac{1}{g}\Big(\mu - \mathcal{V}(\boldsymbol{r}) - 2gn_T(\boldsymbol{r})\Big)\theta(\mu - \mathcal{V}(\boldsymbol{r}) - 2gn_T(\boldsymbol{r})) \text{ and} \tag{6.51}$$

$$n_T(\boldsymbol{r}) = \frac{1}{\lambda_T^3} g_{3/2}(z(\boldsymbol{r})),\ z(\boldsymbol{r}) = e^{(\mu - \mathcal{V}(\boldsymbol{r}) - 2gn_T(\boldsymbol{r}) - 2gn_0(\boldsymbol{r}))/k_B T} \tag{6.52}$$

where, for a cylindrical trap, $\mathcal{V}(\boldsymbol{r})$ is given by (6.44). These equations must be solved numerically and integrated to determine the line densities. For example, (6.51) can be substituted into (6.52) to obtain an equation that only depends on the noncondensate density:

$$n_T(\boldsymbol{r}) = \frac{1}{\lambda_T^3} g_{3/2}(e^{\pm X(\boldsymbol{r})})\theta(\mp X(\boldsymbol{r})) \tag{6.53}$$

where $X(\boldsymbol{r}) := \mu - \mathcal{V}(\boldsymbol{r}) - 2gn_T(\boldsymbol{r})$. This equation can then be solved using an iterative scheme such as a Newton-Raphson method or using a transcendental equation method as discussed in Section 6.2.3. The solution is then substituted into (6.51) to determine the condensate density, and the line densities are obtained upon integrating over the radial coordinates.

Unlike the bi-modal and semi-ideal models, the shape of the condensate is no longer solely determined by the trap potential, and is instead influenced by the thermal cloud. This will result in the condensate being more compressed as the temperature increases, which is in contrast to the other models where the condensate maintains the same width for all temperatures while the chemical potential is kept constant.

6.3.4 Absorption Image Fits

The models have been fit to trial absorption images of the strongly-interacting ^{6}Li BEC in a cylindrical trap by minimising χ^2 using the unknown parameters μ and T.[4] In particular, C++ and MATLAB programs were developed

[4]Other unknown parameters included the centre of the trap.

that utilized minimization packages and numerical solvers to determine the best fit for all the models. Figures 6.2 and 6.3 illustrate how the models can be used to the fit the line density data from two particular absorption images of the ^{6}Li BEC. Note that these images are only for illustrative purposes as they are examples of trial absorption images from the experiment and will, therefore, not form part of the publication [45]. The two images were taken with different cameras, with the camera used for 6.3 being of higher resolution but potentially used with a poorer calibrated BEC setup.

Preliminary results from the experiment suggest that, as expected, the Hartree-Fock provides the best fits, closely followed by the semi-ideal model, and the bi-modal model provides the poorest fits.[5] However, at the time of writing, it is too early to draw any conclusions from the experiment as it is still in operation and numerous sections of parameter space have yet to be explored. For example, future in-situ absorption images of the ^{6}Li BEC will be taken for different effective interaction strengths by utilizing the Feshbach resonances. Once all the data has been collected, the three models will then be used to extract thermodynamic properties, such as the condensate fraction, and will be compared to one another (for example, by comparing the best values of χ^2). That is, parameter fitting and hypothesis testing will be carried out for all the absorption images.

A similar analysis has been carried out in [53]. There the ideal, semi-ideal and Hartree-Fock models were all fitted to time of flight absorption images of a ^{87}Rb BEC in a harmonic trap at finite temperatures.[6] Unambiguous deviations from ideal-gas thermodynamics were observed and good agreement with the Hartree-Fock model was found. The experiment was carried out for a range of temperatures and primarily investigated the condensed fraction and release energy. However, unlike [53] our study will look at a strongly-interacting BEC using a range of interaction strengths and will use in-situ absorption images in an attempt to circumnavigate the issue of

[5]However, at distances far from the centre of the trap, the models all agreed well since the thermal cloud behaves like an ideal gas in this region. This region is in fact often used to extract the temperature of the gas but, in our case, had a small signal-to-noise ratio for preliminary images.

[6]Note that the ideal model in [53] slightly differs to the bi-modal model used here.

there being a lack of theory to understand the expansion of a mixed cloud (which could lead to systematic errors [53]).

Deviations from ideal gas behaviour at finite temperatures were also measured in [184, 185] for a ^{39}K BEC where the scattering length can also be varied. In particular, the effects of interactions on the mechanism of condensation were investigated, namely the saturation of the excited states where the semi-ideal model appears to have been used. The effects of interactions on the critical temperature were also investigated and experimental results were compared to both mean-field and beyond-mean-field theories. Again time-of-flight expansion from the trap was used but the interactions were rapidly turned off at the beginning by tuning the Feshbach field to the $a = 0$ point.

Studies have also been performed to investigate the effect of temperature on the radius of a Bose–Einstein condensate [177], which have also demonstrated deviations from ideal gas behaviour. In [177] an approximation to the Hartree-Fock model was made such that the interactions within the thermal cloud were neglected. The resulting model is slightly more complex than the semi-ideal model discussed here since the influence of the thermal cloud has on the condensate is still kept. By assuming the quantitative equivalence between the chemical potential and the interaction the thermal cloud feels from the condensate, an analytical model can then be derived for this model. However, this assumes that, no matter where the thermal particles are in the trap, they feel the same interaction with the condensate. This simplified Hartree-Fock model showed good agreement with the data, and the standard parabola prediction of the semi-ideal and bi-modal models was clearly excluded, confirming that the thermal cloud's mean-field energy affects the condensed atoms.

6.4 Beyond Mean-Field Theory

Since a ^{6}Li Bose gas is strongly-interacting, it is possible that beyond mean-field theory effects will be observable at high interaction strengths. Such effects are expected to occur when the diluteness condition $na^3 \ll 1$ breaks

down i.e. when the number of particles in a "scattering volume" is no longer very small (note that this does not imply necessarily that the interaction effects themselves are small). In [186] it was demonstrated that this can occur when $na^3 \sim 10^{-3}$, which might be reached for high values of a for our BEC.

The above models also begin to lose their validity when the Thomas-Fermi approximation breaks down. As discussed in Section 6.2.2, this breaks down for a cylindrical trap when:

$$\frac{N_0 a}{a_{ho}} \gg 1 \tag{6.54}$$

which is equivalent to $R_{TF} \gg \lambda_T$. Note that it is possible for this to be violated but the diluteness condition still to be satisfied. However, both conditions are satisfied for the gas used to generate the absorption images in Figures 6.2 and 6.3.

The Hartree-Fock model will also no longer be a good approximation when finite size effects are sufficiently large; the condensate is not macroscopically occupied (since the Bogoliubov approximation of treating the condensate field as a classical field can no longer be made); and, as discussed in its derivation, when the temperature of the gas is not too small such that collective effects need to be taken into account and the semi-classical approximation is no longer valid. However, in the latter case the thermal cloud may be so small that the signal-to-noise ratio may prevent an accurate fit to the corresponding data from an absorption image.

The calculation carried out in Part I for the decoherence and relaxation time of phonons was based on mean-field theory concepts and assumed dilute gases. It would, therefore, be interesting to determine whether there are significant deviations from these time estimates in a beyond mean-field theory regime. Experimental measurements of the times in this regime would also potentially facilitate a better theoretical understanding of decoherence when mean-field theory breaks down. One would naively expect the times to be shorter in this regime due to the greater interaction between the phonon and its environment. For example, the damping rates of

(2.73)-(2.74) are proportional to the square of the coupling constant, but of course these rates were derived using mean-field theory. Experiments are planned to determine whether mean-field effects can be observed and, if so, what affect this has on the decoherence of phonons.

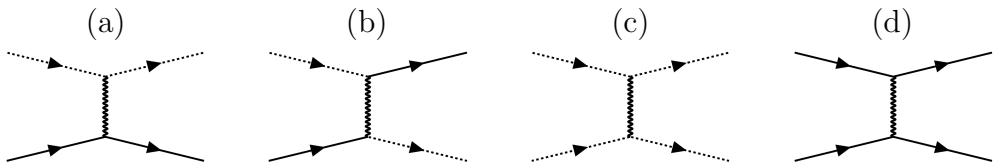

Figure 6.1: These vertex diagrams represent the interactions that make up the Hartree-Fock model, which are also the (i), (iv), (v) and (viii) vertex diagrams of Figure 1.1. The solid line represents a noncondensate particle, the dashed line a condensate particle, and the wavy line the s-wave scattering. Diagram (a) is the Hartree interaction between a condensate and noncondensate particle, and (b) is the Fock interaction where the the condensate and noncondensate particles are exchanged. Diagrams (c) and (d) represent interparticle interactions between only condensate and noncondensate particles respectively.

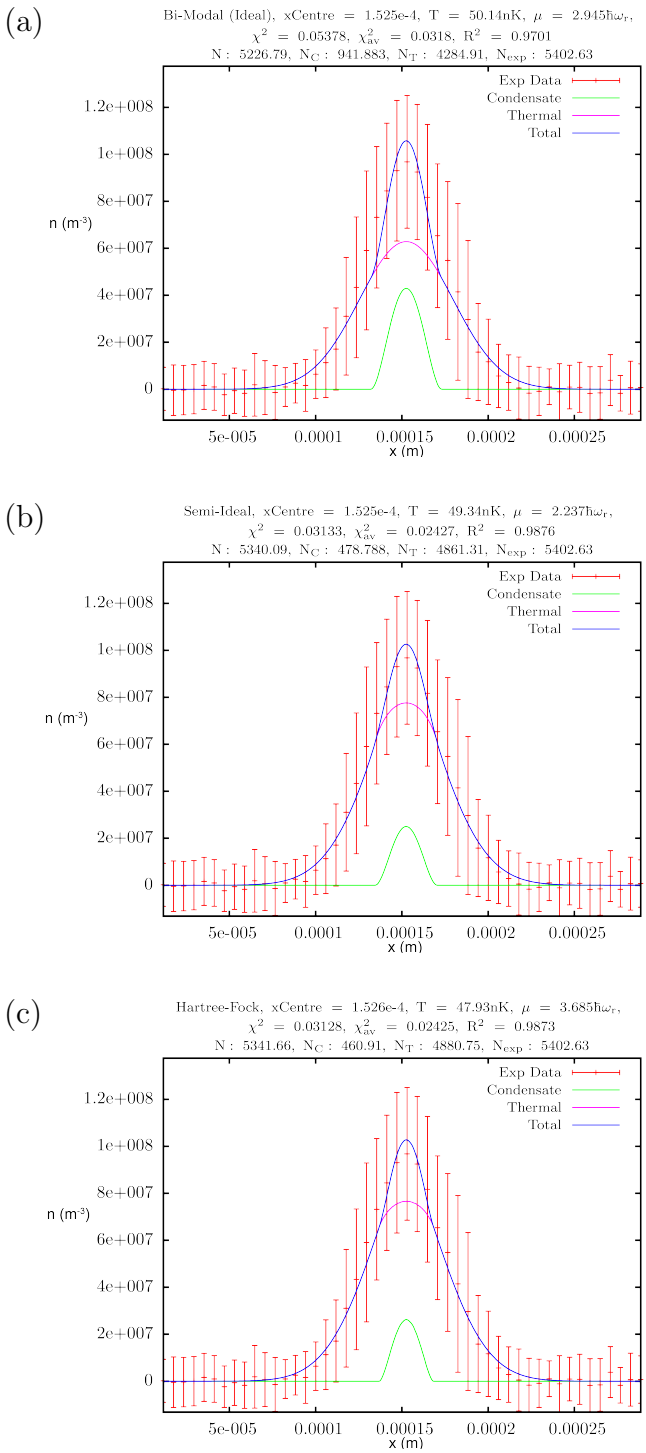

Figure 6.2: Fits to an absorption image of a ^{6}Li BEC in a harmonic trap using the (a) Bi-Modal model, (b) Semi-Ideal model and (c) Hartree-Fock model. The χ^2, $\chi^2_{av} := \chi^2/N_{dof}$ and R^2 values are provided within the header of each graph where N_{dof} is the number of degrees of freedom. Both the Semi-Ideal and Hartree-Fock model show improved fits over the Bi-Modal model. The absorption image was taken with an old camera and only represents preliminary results. The graphs were created using a C++ package developed by R. Howl.

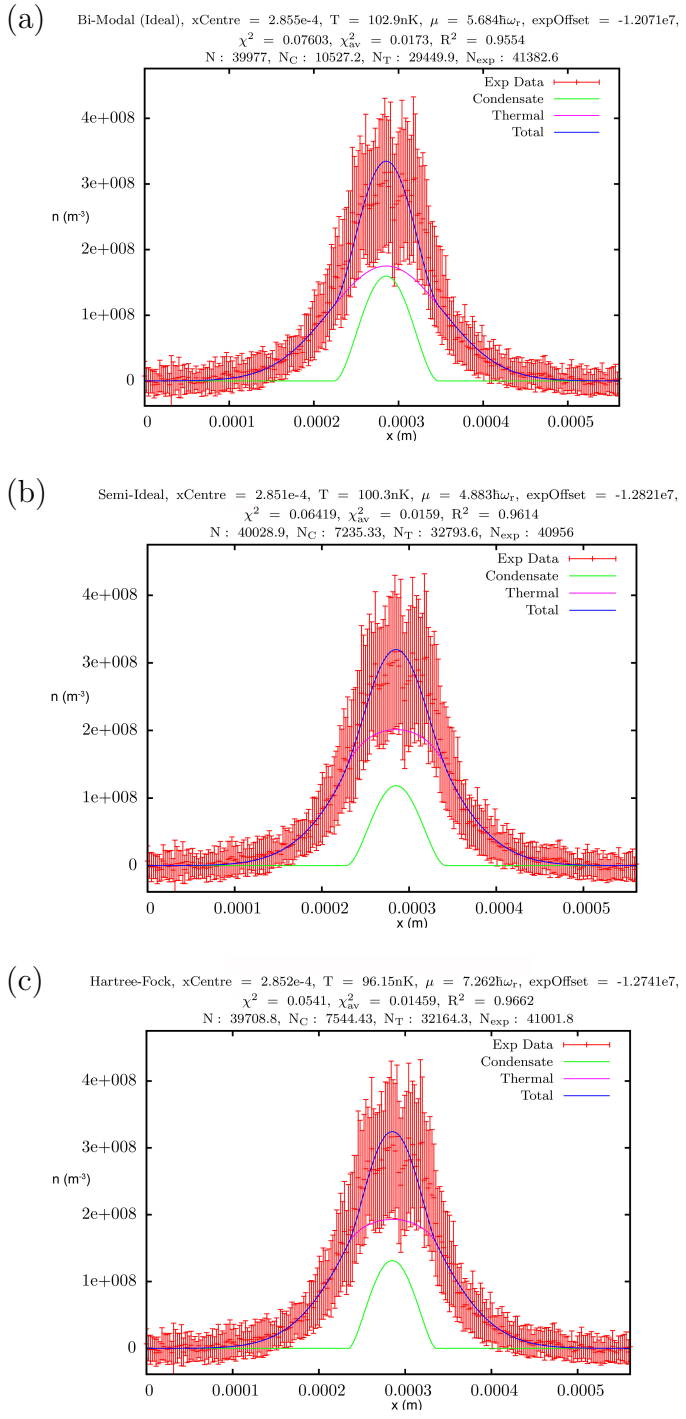

Figure 6.3: Fits to an absorption image of a ^{6}Li BEC in a harmonic trap using the (a) Bi-Modal model, (b) Semi-Ideal model and (c) Hartree-Fock model. The χ^2, $\chi^2_{av} := \chi^2/N_{dof}$ and R^2 values are provided within the header of each graph where N_{dof} is the number of degrees of freedom. Both the Semi-Ideal and Hartree-Fock model show improved fits over the Bi-Modal model. The absorption image only represents preliminary results and will, therefore, not be in the final publication. The graphs were created using a C++ package developed by R. Howl.

CHAPTER 7

Conclusions and Outlook

Overcoming or limiting quantum decoherence is vital to the practicality and potential of many quantum information tasks and their corresponding quantum technologies. For example, rapid decoherence can turn quantum computers into classical computers, invalidating the whole principle of their quantum algorithms. Recently new technologies have emerged from the application of relativity to quantum information [17, 18]. These have been shown to be, in principle, orders of magnitude more precise than their non-relativistic counterparts [17, 18]. However, decoherence has yet to be investigated in these devices, which could be integral to their physical realisation. The devices, an accelerometer and GW detector, utilize the phononic excitations of BECs by measuring how these excitations are disturbed by an acceleration or gravity in a process that is related to the dynamical Casimir effect [17, 187]. Their practicality is thus reliant on the decoherence time of the phononic excitations not being rapidly short.

Quantum decoherence of phononic excitations of BECs, the decay of the quantum coherences of phononic states due to interaction with their environment, has yet to be investigated in general, with studies instead concentrating on the process by which perturbed phonons relax back to equilibrium with the rest of the Bose gas. This latter process can set an upper limit for the decoherence time, the time in which quantum coherence is effectively lost, but often the actual decoherence time is significantly shorter [30–32]. Motivated by the recently proposed relativistic quantum technologies, the principle focus of this work has been to determine the

mechanism by which phonons decohere and to provide an estimate for their decoherence time.

As well as being vital to the practical realization of the proposed relativistic quantum devices, it is expected that estimations for the decoherence time of phononic excitations will also inform analogue gravity experiments that are based on BECs since these experiments are directly related to the proposed devices (see the Introduction). For example, although Hawking 'radiation' has recently been observed as propagating phonons in analogue gravity experiments based on BECs, at the time of writing, nonclassical properties such as entanglement have yet to be measured for this radiation.[1] Such a signature would be of major significance to the analogue gravity field and potentially to BH physics. However, the observation of nonclassical properties of Hawking radiation relies on this property existing for a non-negligible time in the BEC.[2] Similarly, although a classical analogue of the dynamical Casimir effect has been observed as the pair creation of phonons of a BEC, nonclassical properties such as entanglement have yet to be observed and this observation would also be reliant on these quantum properties not decaying too rapidly. Furthermore, understanding how the nonclassical properties of acoustic Hawking radiation or related processes degrade via decoherence processes could also inform studies on BH physics.

In this work the decoherence of phononic excitations of BECs has been investigated using a single-mode phonon system and treating it as an open quantum system in the Born-Markov approximation. For simplicity the state of the system was also assumed to be Gaussian, and an estimation of the decoherence time was extracted from the evolution of certain global entropic measures and nonclassical indicators of the Gaussian state such as purity and nonclassical depth [44]. The single-mode phonon state was found

[1]Subsequent to the submission of this thesis a measurement of the entanglement of acoustic Hawking radiation was reported in [39]. Entanglement was not observed at low frequencies but, given the results of this thesis and [33], this is unlikely to be due to decoherence effects since it is expected that this would only increase with frequency (although it is possible that, due to differences in experimental setup, this situation could change). This measurement opens the door to investigations into measuring the decoherence of phonons of BECs.

[2]In a related study, the robustness of entanglement generation in quasi-particles against temperature has also been theoretically analysed for these systems to inform experimental setups [36].

to primarily decohere due to the Landau and Beliaev interactions with all the other quasi-particle modes of the BEC, and the time in which this occurs is heavily dependent on the particular BEC setup such as the temperature of the gas and the frequency of the excited phonon mode. A decoherence time was estimated for several BEC setups including one inspired by the GW detector [18] where the decoherence time was found to be a few seconds.

An estimate for the relaxation time of phonons was also performed to provide a comparison for the decoherence time. In order to provide an appropriate comparison, the relaxation time was similarly calculated by treating the single-mode phonon system as a low-energy quasi-particle mode interacting via the Landau and Beliaev mechanisms with a continuum of quasi-particle modes in thermal equilibrium. The same Born-Markov master equation was then derived as for estimating the decoherence time, and the relaxation time is characterized by the decay rate obtained from this equation (see Section 4.1.6).

This approach to estimating the decay rate of the quasi-particles was also discussed in [27] and is very similar to that taken in [188] and [189] where a quantum Langevin approach is used. The estimated decay rate matches that of the Landau-Beliaev damping rate obtained using perturbation theory in a uniform system [70, 134, 190, 191].[3] This damping rate has been studied in great detail in Bose superfluids both theoretically [26] and experimentally [73]. Of the two processes, Landau damping has received the most attention. This damping process was first discussed for plasmas by Landau [193] and has since been explored by several authors within the context of dilute BECs. It was first investigated for a uniform Bose gas in [194] using Green's function techniques for low temperatures, and later for higher temperatures in [195]. After the first experimental measurements for the damping of collective oscillations[73, 123], the fact that Landau damping might be principally responsible was put forward in [196] and results obtained for the uniform gas were used to estimate the damping in a trapped gas [140] within the framework of an imaginary time path

[3]For a discussion on the relationship between the Markov approximation and the Fermi Golden Rule see e.g. [32, 192].

integral. Expressions for Landau damping in trapped systems were then shortly developed using perturbation theory in [190] that, when applied to the uniform case, reproduced the known results for both the low- and high-temperature asymptotic behaviour of the phonon damping and, as stated above, match those derived here. Other methods such as semi-classical approaches [79, 134, 197] and kinetic theories for superfluids [198] have also been performed. Furthermore, Landau damping has also been investigated in additional BEC contexts such as lower-dimensional BECs [199].

Beliaev damping, associated with the decay of an elementary excitation into a pair of excitations, was first studied by Beliaev in the case of uniform Bose superfluids [200]. It was investigated in trapped systems using a time-dependent mean-field approach based on the Popov approximation in [70], which also derived similar results to [190] for Landau damping and, as stated above, which also match the results derived here for both rates when applied to a uniform system. Beliaev damping has been explored experimentally [73] and also considered in other ultracold systems such as Fermi-Bose mixtures [201], colliding BECs and optical lattices [29]. The relaxation processes of Landau and Beliaev damping of quasi-particles have also been investigated when considering the de-phasing mechanism of the condensate [28].

Rather than simply using the inverse of the damping rate for the relaxation time [28, 32], this time was also considered from the point of view of state discrimination. The relaxation time is then taken to be the minimal time required for the initial state to freely reach the target state within a fixed fidelity (see e.g. [77]). Using an appropriate error parameter, the relaxation time was estimated to be of the order of 10s for the GW detector, which compares to a few seconds for the decoherence time. In fact, for all BEC setups, it was found that the decoherence time was shorter than the relaxation time and, in some cases, by several orders of magnitude. In contrast to the decoherence time, the relaxation time was determined for a generic initial state rather than just a Gaussian state since the relaxation time is independent of the initial state according to the Born-Markov master equation.

The short decoherence and relaxation times for the GW detector setup

suggest that these effects could be important in the realization of these devices. However, more work is required to determine exactly how the precision of the proposed GW detector and accelerometer are affected by the decoherence and relaxation channels for the phonons. For example, these devices respectively rely on a two-mode squeezed state and two single-mode squeezed states rather than just one single-mode squeezed state that was used in the analysis presented here. Furthermore, the sensitivity of the device is determined by the quantum Fisher information (QFI) since this is used to measure the distinguishability of states. Therefore, understanding how this is quantity is modified by the decoherence of phonons would properly identify how the device is affected by decoherence. Using the general techniques developed for Gaussian states in Chapter 3, it should be straightforward to determine how the QFI depends on the decoherence of the phonons once they are extended to two-mode states. In particular, this can be extracted from the time evolution of the covariance matrix of a two-mode state, which can then be used to determine the time evolution of the QFI.

Other future developments could include investigating the decoherence times of more realistic setups. In this work a uniform, dilute BEC in a three-dimensional box with Gaussian phonon states and an environment of quasi-particles in thermal equilibrium was assumed. However, in practice, BEC setups use traps and the phonon states will not be exactly Gaussian. Although it is expected that these approximations will lead to an analysis that is still applicable to general experimental setups [26, 70], more realistic results would be obtained, for instance, by analysing the decoherence of phonons of BECs in harmonic traps. Damping in such systems has already been analysed [139] and it should, therefore, be relatively straightforward to apply the results presented here to calculate the decoherence in such systems. An example of the changes that a trapped system can have on the damping mechanism compared to a homogeneous system is that Beliaev damping is not active for the lowest energy modes in the former systems due to the discretization of levels [70, 134]. Damping in lower-dimensional systems has also been analysed in [199] which could be useful for further

analysis of the decoherence of the proposed accelerometer and GW detector since the current theoretical analysis is based on a one-dimensional system.

Further improvements to the estimation of the decoherence time would be to investigate the changes that occur when the Born-Markov approximation is dropped and the initial state of the phonons and the environment is non-separable. Dropping thermal equilibrium of the environment and introducing a squeezed environment may also create interesting effects as discussed in Chapter 4. It was also highlighted in that chapter that, rather than using the time evolution of the purity and nonclassical depth to estimate the decoherence time, it could be more instructive to determine the evolution of proper coherent measures such as the relative entropy of coherence [118], although this would require the development of a coherent measure for Gaussian states. Another alternative to estimating the decoherence time would be to analyse the evolution of QFI [202] and, when two mode states are considered, the depletion of entanglement, which is currently being investigated [33].

As well as theoretically estimating the decoherence of the phonons, this work has also considered how the decoherence could be measured experimentally. In particular, an experiment that uses a molecular ^{6}Li BEC is currently being investigated for performing the measurement. This BEC is strongly-interacting and the effects introduced by such strong interactions in a Bose gas are not yet fully understood. This is important for the measurement of decoherence as the mutual interaction between the condensed and noncondensed components of a strongly-interacting Bose need to be understood in order to successfully extract information from an in-situ absorption image of the gas. In Chapter 6, three different models were investigated to determine their effectiveness in fitting density profiles from in-situ absorption images and extracting thermodynamic quantities. These models were the well-used bi-modal model, the semi-ideal model and a model based on the Hartree-Fock approximation. Currently in-situ absorption images are being generated for the ^{6}Li BEC at various interaction strengths and temperatures, and the models are then being fit to this data. Initial results suggest that, as expected, the Hartree-Fock fits the data most successfully

and that the bi-modal model can produce highly inaccurate results in certain sections of parameter space. However, it is currently too early in the experiment to draw any definite conclusions.

As well as being essential to the future measurement of decoherence of phonons, the investigation into the three models is also expected to further the current understanding of the effects of strongly-interacting Bose gases and how these effects can be observed in in-situ absorption images. The interactions strengths achievable should also be much higher than in similar past studies [53, 184, 185], and could potentially move the gas into a regime where beyond mean-field theory effects are observable (see Chapter 6). Once the in-situ absorption images of the ^{6}Li BEC are well understood and effectively modelled, a measurement of the decoherence time of phononic excitations should be possible. As discussed in Chapter 5, there are numerous ways this could be measured. However, a promising possibility would be to extract information on the purity of the state or, for two-mode states, the entanglement from density-density correlation functions extracted from in-situ imaging [157]. It is hoped that measurements of this kind will be able to appraise the legitimacy of the approximations used in the theoretical estimation of the decoherence time of the phononic excitations, as well as inform the theory of Bose-Einstein physics, particularly strongly-interacting BECs, and potentially other fields such as analogue gravity and black hole physics.

APPENDIX A

Derivation of the Beliaev and Landau Damping Rates

In this Appendix the expressions (2.73)-(2.74) damping rates for Beliaev and Landau damping are derived. From (2.72), these damping rates are defined as:

$$\gamma_B := \gamma_2^B - \gamma_1^B, \tag{A.1}$$

$$\gamma_L := \gamma_2^L - \gamma_1^L \tag{A.2}$$

where, from (2.36), each γ_i^X is defined in terms of environment correlation functions:

$$\Gamma_i^X := \frac{1}{2}\gamma_i^X + iS_i^X \tag{A.3}$$

where $X = L, B$; $i = 1, 2$; and each Γ_i^X is given by (2.65)-(2.68). These are:

$$\Gamma_1^B = \frac{1}{\hbar^2}\int_0^\infty dt' e^{i\omega_q t/\hbar}\langle \tilde{B}(t)\tilde{B}^\dagger(t-t')\rangle_E, \tag{A.4}$$

$$\Gamma_2^B = \frac{1}{\hbar^2}\int_0^\infty dt' e^{-i\omega_q t/\hbar}\langle \tilde{B}^\dagger(t)\tilde{B}(t-t')\rangle_E, \tag{A.5}$$

$$\Gamma_1^L = \frac{1}{\hbar^2}\int_0^\infty dt' e^{i\omega_q t/\hbar}\langle \tilde{L}(t)\tilde{L}^\dagger(t-t')\rangle_E, \tag{A.6}$$

$$\Gamma_2^L = \frac{1}{\hbar^2}\int_0^\infty dt' e^{-i\omega_q t/\hbar}\langle \tilde{L}^\dagger(t)\tilde{L}(t-t')\rangle_E \tag{A.7}$$

where $\tilde{L}$ and $\tilde{B}$ are the interaction picture environment operators for the Landau and Beliaev interactions. From Section 1.3, the corresponding Schrödinger picture operators are given by:

$$\hat{L}^\dagger = g\sqrt{\frac{n}{V}}\sum_{\boldsymbol{k},\boldsymbol{l}\neq\{\boldsymbol{0},\boldsymbol{q}\}} \mathcal{L}_{kl} b_{\boldsymbol{k}} b_{\boldsymbol{l}}^\dagger \delta_{\boldsymbol{q},\boldsymbol{l}-\boldsymbol{k}}, \tag{A.8}$$

$$\hat{B}^\dagger = g\sqrt{\frac{n}{V}}\sum_{\boldsymbol{k},\boldsymbol{l}\neq\{\boldsymbol{0},\boldsymbol{q}\}} \mathcal{B}_{kl} b_{\boldsymbol{k}}^\dagger b_{\boldsymbol{l}}^\dagger \delta_{\boldsymbol{q},\boldsymbol{k}+\boldsymbol{l}}. \tag{A.9}$$

Concentrating on just Landau damping, the interaction picture operator is given by:

$$\tilde{L}^\dagger = g\sqrt{\frac{n}{V}} e^{iH_E t/\hbar}\sum_{\boldsymbol{k},\boldsymbol{l}\neq\{\boldsymbol{0},\boldsymbol{q}\}} \mathcal{L}_{kl} b_{\boldsymbol{k}} b_{\boldsymbol{l}}^\dagger e^{-iH_E t/\hbar}\delta_{\boldsymbol{q},\boldsymbol{l}-\boldsymbol{k}}, \tag{A.10}$$

$$= g\sqrt{\frac{n}{V}}\sum_{\boldsymbol{k},\boldsymbol{l}\neq\{\boldsymbol{0},\boldsymbol{q}\}} \mathcal{L}_{kl}(e^{iH_E t/\hbar} b_{\boldsymbol{k}} e^{-iH_E t/\hbar})(e^{iH_E t/\hbar} b_{\boldsymbol{l}}^\dagger e^{-iH_E t/\hbar})\delta_{\boldsymbol{q},\boldsymbol{l}-\boldsymbol{k}}, \tag{A.11}$$

$$= g\sqrt{\frac{n}{V}}\sum_{\boldsymbol{k},\boldsymbol{l}\neq\{\boldsymbol{0},\boldsymbol{q}\}} \mathcal{L}_{kl} b_{\boldsymbol{k}} b_{\boldsymbol{l}}^\dagger e^{i(\omega_l-\omega_k)t/\hbar}\delta_{\boldsymbol{q},\boldsymbol{l}-\boldsymbol{k}}. \tag{A.12}$$

where H_E is given by (2.49) and hats on operators have been dropped for convenience. Similarly, the annihilation-like operator is given by:

$$\tilde{L} = g\sqrt{\frac{n}{V}}\sum_{\boldsymbol{k},\boldsymbol{l}\neq\{\boldsymbol{0},\boldsymbol{q}\}} \mathcal{L}_{lk} b_{\boldsymbol{k}}^\dagger b_{\boldsymbol{l}} e^{-i(\omega_l-\omega_k)t/\hbar}\delta_{\boldsymbol{q},\boldsymbol{l}-\boldsymbol{k}}. \tag{A.13}$$

Using the above expressions, the Landau correlation functions Γ_1^L and Γ_2^L are given by:

$$\Gamma_1^L = \frac{g^2 n}{V\hbar^2}\int_0^\infty dt' e^{i\omega_q t/\hbar}\delta_{\boldsymbol{q},\boldsymbol{l}-\boldsymbol{k}}\delta_{\boldsymbol{q},\boldsymbol{m}-\boldsymbol{n}}$$

$$\times \sum_{\boldsymbol{k},\boldsymbol{l},\boldsymbol{m},\boldsymbol{n}\neq\{\boldsymbol{0},\boldsymbol{q}\}} \mathcal{L}_{kl}\mathcal{L}_{mn} e^{i(\omega_k-\omega_l+\omega_n-\omega_m)t/\hbar} e^{i(\omega_m-\omega_n)t'/\hbar} \langle b^\dagger_{\boldsymbol{k}} b_{\boldsymbol{l}} b_{\boldsymbol{m}} b^\dagger_{\boldsymbol{n}}\rangle_E, \tag{A.14}$$

$$\Gamma^L_2 = \frac{g^2 n}{V\hbar^2}\int_0^\infty dt' e^{-i\omega_q t/\hbar}\delta_{\boldsymbol{q},\boldsymbol{l}-\boldsymbol{k}}\delta_{\boldsymbol{q},\boldsymbol{m}-\boldsymbol{n}}$$
$$\times \sum_{\boldsymbol{k},\boldsymbol{l},\boldsymbol{m},\boldsymbol{n}\neq\{\boldsymbol{0},\boldsymbol{q}\}} \mathcal{L}_{kl}\mathcal{L}_{mn} e^{-i(\omega_k-\omega_l+\omega_n-\omega_m)t/\hbar} e^{i(\omega_n-\omega_m)t'/\hbar} \langle b_{\boldsymbol{k}} b^\dagger_{\boldsymbol{l}} b^\dagger_{\boldsymbol{m}} b_{\boldsymbol{n}}\rangle_E. \tag{A.15}$$

Taking the environment to be in thermal equilibrium, the above expressions are only non-zero when $\boldsymbol{k}=\boldsymbol{m}$ and $\boldsymbol{l}=\boldsymbol{n}$ (with $\boldsymbol{k}\neq\boldsymbol{l}$). That is:

$$\delta_{\boldsymbol{q},\boldsymbol{l}-\boldsymbol{k}}\delta_{\boldsymbol{q},\boldsymbol{m}-\boldsymbol{n}}\langle b^\dagger_{\boldsymbol{k}} b_{\boldsymbol{l}} b_{\boldsymbol{m}} b^\dagger_{\boldsymbol{n}}\rangle_E = \delta_{\boldsymbol{q},\boldsymbol{l}-\boldsymbol{k}}\delta_{\boldsymbol{k},\boldsymbol{m}}\delta_{\boldsymbol{l},\boldsymbol{n}}(N_k N_l + N_k), \tag{A.16}$$

$$\delta_{\boldsymbol{q},\boldsymbol{l}-\boldsymbol{k}}\delta_{\boldsymbol{q},\boldsymbol{m}-\boldsymbol{n}}\langle b_{\boldsymbol{k}} b^\dagger_{\boldsymbol{l}} b^\dagger_{\boldsymbol{m}} b_{\boldsymbol{n}}\rangle_E = \delta_{\boldsymbol{q},\boldsymbol{l}-\boldsymbol{k}}\delta_{\boldsymbol{k},\boldsymbol{m}}\delta_{\boldsymbol{l},\boldsymbol{n}}(N_k N_l + N_l). \tag{A.17}$$

Plugging the above into (A.14)-(A.15) and then using (A.3) as well as taking a continuum of states i.e. introducing a density of states $p(\omega)$ such that $p(\omega)d\omega$ gives the number of oscillators with frequencies in the interval ω to $\omega+d\omega$, the rates γ^L_1 and γ^L_2 are given by:[1]

$$\gamma^L_1 = \frac{g^2 n}{V\hbar^2}\int_0^\infty \pi d\omega_k p(\omega_k)\mathcal{L}^2_{\omega_k,\omega_l}(N_k N_l + N_k)\delta(\omega_q+\omega_k-\omega_l), \tag{A.19}$$

$$\gamma^L_2 = \frac{g^2 n}{V\hbar^2}\int_0^\infty \pi d\omega_k p(\omega_k)\mathcal{L}^2_{\omega_k,\omega_l}(N_k N_l + N_l)\delta(\omega_q+\omega_k-\omega_l) \tag{A.20}$$

and the difference of these two rates is:

$$\gamma_L = \frac{g^2 n}{V\hbar^2}\int_0^\infty \pi d\omega_k p(\omega_k)\mathcal{L}^2_{\omega_k,\omega_l}(N_k - N_l)\delta(\omega_q+\omega_k-\omega_l), \tag{A.21}$$

which is the expression used in (2.74).

[1] Note that:

$$\int_0^\infty dt' e^{-i\epsilon t'} = \pi\delta(\epsilon) - i\frac{P}{\epsilon} \tag{A.18}$$

where P is the Cauchy principal value.

A similar derivation can also be performed for the Beliaev interactions. In this case γ_1^B and γ_2^B are given by:

$$\gamma_1^B = \frac{g^2 n}{V\hbar^2}\int_0^\infty \pi d\omega_k p(\omega_k)\mathcal{B}^2_{\omega_k,\omega_l}(N_k N_l)\delta(\omega_q-\omega_k-\omega_l), \tag{A.22}$$

$$\gamma_2^B = \frac{g^2 n}{V\hbar^2}\int_0^\infty \pi d\omega_k p(\omega_k)\mathcal{B}^2_{\omega_k,\omega_l}(N_k N_l + N_k + N_l + 1)\delta(\omega_q-\omega_k-\omega_l) \tag{A.23}$$

and so:

$$\gamma_B = \frac{g^2 n}{V\hbar^2}\int_0^\infty \pi d\omega_k p(\omega_k)\mathcal{B}^2_{\omega_k,\omega_l}(N_k + N_l + 1)\delta(\omega_q-\omega_k-\omega_l), \tag{A.24}$$

which is the expression used in (2.74).

The above expressions can also be used to verify that (2.71) holds for the single-mode phonon system (this equation holds for any Markov system when the environment is in thermal equilibrium [32]). First (2.71) is re-written in the form of (A.25):

$$\gamma_T := \gamma\coth(\frac{1}{2}\beta_q) = \gamma(1+2N_q^{th}) \tag{A.25}$$

where $\gamma_T := \gamma_{11}+\gamma_{22} = \gamma_1^B+\gamma_1^L+\gamma_2^B+\gamma_2^L$ and $\gamma := \gamma_{22}-\gamma_{11} = \gamma_B+\gamma_L$. We therefore need to verify that the following equality always holds:

$$\begin{aligned}
&\frac{g^2 n}{V\hbar^2}\int_0^\infty \pi d\omega_k p_{\omega_k}\Big(\mathcal{B}^2_{\omega_k,\omega_l}(2N_k N_l + N_k + N_l + 1)\delta(\omega_q-\omega_k-\omega_l)\\
&\qquad\qquad +\mathcal{L}^2_{\omega_k,\omega_l}(2N_k N_l + N_l + N_k)\delta(\omega_q+\omega_k-\omega_l)\Big)\\
&= (1+2N_q)\frac{g^2 n}{V\hbar^2}\int_0^\infty \pi d\omega_k p_{\omega_k}\Big(\mathcal{B}^2_{\omega_k,\omega_l}(N_k + N_l + 1)\delta(\omega_q-\omega_k-\omega_l)\\
&\qquad\qquad +\mathcal{L}^2_{\omega_k,\omega_l}(N_k - N_l)\delta(\omega_q+\omega_k-\omega_l)\Big).
\end{aligned} \tag{A.26}$$

By simple algebra, it is straightforward to show that this equality does

indeed always hold by simply verifying the following identities:

$$2N_kN_l + N_k + N_l = (1 + 2N_q)(N_k - N_l) \text{ when } \omega_q = \omega_l - \omega_l, \text{ and} \tag{A.27}$$

$$2N_kN_l + N_k + N_l + 1 = (1 + 2N_q)(N_k + N_l + 1) \text{ when } \omega_q = \omega_k + \omega_l \tag{A.28}$$

where N_q, N_k and N_l are given by the Bose-Einstein distribution (1.31).

APPENDIX B

Derivation of the Equations of Motion for the Displacement Vector and Covariance Matrix

In this Appendix the equations of motion for the displacement vector and covariance matrix given by (3.29)-(3.30) are derived. The Lindblad master equation (3.27) provides the equation of motion for the reduced density matrix and can be written as:

$$\frac{d\rho_S}{dt} = -\frac{i}{\hbar}[\hat{H}, \hat{\rho}_S] + (C^\dagger C)^*_{ij}\hat{x}_i\hat{\rho}_S\hat{x}_j - \frac{1}{2}(C^\dagger C)_{ij}\{\hat{x}_i\hat{x}_j, \rho_S\} \tag{B.1}$$

where $\hat{c} := C_{ij}\hat{x}_j$ as defined in Chapter 3.

Using the fact that, from Chapter 3, the Hamiltonian can be written as $\hat{H} = H_0 + \kappa\hat{\boldsymbol{x}}^T\boldsymbol{H}_1 + \kappa^2\hat{\boldsymbol{x}}^T\boldsymbol{H}_2\hat{\boldsymbol{x}}$ where H_0 is a constant; $\boldsymbol{H}_1$ is a $2M$-dimensional column vector; and $\boldsymbol{H}_2$ is a $2M \times 2M$ real, symmetric matrix; it is possible to show that the equation of motion of any operator $\hat{B}$ is:

$$\begin{aligned}\frac{d\langle B\rangle}{dt} = Tr\Big(\frac{d\rho_S}{dt}B\Big) =& \frac{i\kappa}{\hbar}H_{1i}Tr\Big(\rho_S[x_i, B]\Big) \\ &+i\Big(\frac{\kappa^2}{\hbar}H_{2ij} + \frac{1}{2}Im(C^\dagger C)_{ij}\Big)Tr\bigg(\rho_S\Big\{[x_i, B], x_j\Big\}\bigg) \\ &+\frac{1}{2}Re(C^\dagger C)_{ij}Tr\bigg(\rho_S\Big[[x_i, B], x_j\Big]\bigg)\end{aligned} \tag{B.2}$$

where $[AB, C] = A[B, C] + [A, C]B$ has been used as well as the cyclic

property of the trace, and $C^\dagger C$ has been separated into its real (symmetric) and imaginary (anti-symmetric) parts.

B.1 Displacement Vector

The displacement operator is defined as $d_k := \langle \hat{x}_k \rangle$ and so, to determine its equation of motion, $\hat{B} = \hat{x}_k$ should be substituted into (B.2)into the above equation. In this case $[x_i, B] = [x_i, x_k] = \frac{i}{2\kappa^2}\Omega_{ik}$ and thus $\Big[[x_i, B], x_j\Big]$ vanishes and $\Big\{[x_i, B], x_j\Big\} = \Big\{[x_i, x_k], x_j\Big\} = \frac{i}{2\kappa^2}\Omega_{ik}$, which just leaves:

$$\begin{aligned}
\frac{dd_k}{dt} &= -\frac{1}{2\kappa\hbar}H_{1i}\Omega_{ik}Tr(\rho_S) - \frac{1}{\hbar}\Omega_{ik}H_{0ij}Tr(\rho_S x_j) \\
&\qquad - \frac{1}{2\kappa^2}\Omega_{ik}Im(C^\dagger C)_{ij}Tr(\rho_S x_j) && \text{(B.3)} \\
&= \frac{1}{2\kappa\hbar}\Omega_{ki}H_{1i} + \frac{1}{\hbar}\Omega_{ki}H_{0ij}d_j + \frac{1}{2\kappa^2}\Omega_{ki}Im(C^\dagger C)_{ij}d_j && \text{(B.4)} \\
\implies \frac{d\boldsymbol{d}}{dt} &= \frac{1}{\hbar}\boldsymbol{\Omega H_1} + \boldsymbol{\Omega}\Big(\frac{1}{\hbar}\boldsymbol{H_0} + \frac{1}{2\kappa^2}Im(\boldsymbol{C^\dagger C})\Big)\boldsymbol{d} && \text{(B.5)} \\
&:= \boldsymbol{\mathcal{H}_1} + \boldsymbol{A}\boldsymbol{d} && \text{(B.6)}
\end{aligned}$$

B.2 Covariance Matrix

Taking $d_i = 0$, the covariance matrix can be written as $\sigma_{kl} = \frac{1}{2}\langle x_k, x_l \rangle$, so this case $B_{kl} = \frac{1}{2}\{x_k, x_l\}$ must be plugged into (B.2). Using $[A, BC] = B[A, C] = [A, B]C$, it is possible to show that:

$$\begin{aligned}
[x_i, B] &= \frac{1}{2}[x_i, \{x_k, x_l\}] && \text{(B.7)} \\
&= \frac{i}{2\kappa^2}(\Omega_{ik}x_l + \Omega_{il}x_k), && \text{(B.8)} \\
\Big[[x_i, B], x_j\Big] &= -\frac{1}{4\kappa^4}(\Omega_{ik}\Omega_{lj} + \Omega_{il}\Omega_{kj}), && \text{(B.9)} \\
\Big\{[x_i, B], x_j\Big\} &= \frac{i}{2\kappa^2}(\Omega_{ik}\{x_l, x_j\} + \Omega_{il}\{x_k, x_j\}) && \text{(B.10)}
\end{aligned}$$

and so the equation of motion for the covariance matrix is given by:

$$\begin{aligned}\implies \frac{d\sigma_{kl}}{dt} =& -\frac{1}{2\kappa\hbar}H_{1i}\Big(\Omega_{ik}Tr(\rho_S x_l)+\Omega_{il}Tr(\rho_S x_k)\Big)- \\ & \Big[\frac{1}{2\hbar}H_{0ij}+\frac{1}{4\kappa^2}Im(C^\dagger C)^*_{ij}\Big]Tr\Big[\rho_S\Big(\Omega_{ik}\{x_l,x_j\}+\Omega_{il}\{x_k,x_j\}\Big)\Big] \\ & -\frac{1}{8\kappa^4}Re(C^\dagger C)_{ij}\Big(\Omega_{ik}\Omega_{lj}+\Omega_{il}\Omega_{kj}\Big)Tr(\rho_S) \qquad \text{(B.11)} \\ =& \ \Omega_{ki}\Big(\frac{1}{\hbar}H_{0ij}+\frac{1}{2\kappa^2}Im(C^\dagger C)^*_{ij}\Big)\sigma_{jl}+ \\ & \sigma_{kj}\Big(\frac{1}{\hbar}H_{0ji}+\frac{1}{2\kappa^2}Im(C^\dagger C)^*_{ji}\Big)\Omega_{il}+\frac{1}{4\kappa^4}\Omega_{li}Re(C^\dagger C)_{ij}\Omega_{jk} \qquad \text{(B.12)}\end{aligned}$$

$$\implies \frac{d\boldsymbol{\sigma}}{dt} = \boldsymbol{A\sigma}+\boldsymbol{\sigma A}^T+\boldsymbol{D} \qquad \text{(B.13)}$$

where the fact that $\boldsymbol{\sigma}$ is symmetric by definition has been used as well as $Tr(\rho_S x_k)=d_k=0$, $Re(\boldsymbol{C^\dagger C})$ is symmetric, and $\boldsymbol{\Omega}$ is anti-symmetric.

APPENDIX C

Derivation of the Evolution of the Average Occupation of a Single-Mode Phonon State

In this Appendix the time evolution of the average occupation is derived (4.43). Similar to Appendix B, the master equation for the the single-mode phonon state (2.53) can be used to determine the time evolution of the average of any operator $\hat{B}$:

$$\frac{d}{dt}\hat{\rho}_S = -\frac{i}{\hbar}[\hat{H}_S, \hat{\rho}_S] + \gamma_{11}\Big(\hat{b}_{\boldsymbol{q}}\hat{\rho}_S\hat{b}^\dagger_{\boldsymbol{q}} - \frac{1}{2}\{\hat{b}^\dagger_{\boldsymbol{q}}\hat{b}_{\boldsymbol{q}}, \hat{\rho}_S\}\Big) + \gamma_{22}\Big(\hat{b}^\dagger_{\boldsymbol{q}}\hat{\rho}_S\hat{b}_{\boldsymbol{q}} - \frac{1}{2}\{\hat{b}_{\boldsymbol{q}}\hat{b}^\dagger_{\boldsymbol{q}}, \hat{\rho}_S\}\Big), \tag{C.1}$$

$$\implies \frac{d\langle\hat{B}\rangle}{dt} = Tr\Big(\frac{d\rho_S}{dt}\hat{B}\Big) \tag{C.2}$$

$$= i\omega Tr\Big(\rho_S[\hat{b}^\dagger_{\boldsymbol{q}}\hat{b}_{\boldsymbol{q}}, \hat{B}]\Big) \tag{C.3}$$

$$+ \frac{\gamma_{11}}{2}Tr\Big(\rho_S\Big([\hat{b}^\dagger_{\boldsymbol{q}}, \hat{B}]\hat{b}_{\boldsymbol{q}} - \hat{b}^\dagger_{\boldsymbol{q}}[\hat{b}_{\boldsymbol{q}}, \hat{B}]\Big)\Big) \tag{C.4}$$

$$+ \frac{\gamma_{22}}{2}Tr\Big(\rho_S\Big([\hat{b}_{\boldsymbol{q}}, \hat{B}]\hat{b}^\dagger_{\boldsymbol{q}} - \hat{b}_{\boldsymbol{q}}[\hat{b}^\dagger_{\boldsymbol{q}}, \hat{B}]\Big)\Big)\Big) \tag{C.5}$$

where $\hat{H}_S = \hbar\omega_{\boldsymbol{q}}\hat{b}^\dagger_{\boldsymbol{q}}\hat{b}_{\boldsymbol{q}}$, $[AB, C] = A[B, C] + [A, C]B$ has been used as well as the cyclic property of the trace. Substituting $\hat{B} = \hat{N}_i = \hat{b}^\dagger_{\boldsymbol{q}}\hat{b}_{\boldsymbol{q}}$, the average occupation at time t for a single-mode phonon state is then found to be:

$$N_q(t) = (N_q(0) - N_q^{th})e^{-\gamma t} + N_q^{th} \tag{C.6}$$

where:

$$N_q^{th} = \frac{1}{(\gamma_{11}/\gamma_{22}) - 1} \tag{C.7}$$

$$= \frac{1}{e^{\beta_q} - 1} \tag{C.8}$$

APPENDIX D

Density Waves

In this Appendix condensate density fluctuations are derived using the T=0 Gross-Pitaevskii (GP) equation. These are the classical counterparts of the elementary excitations described by the Bogoliubov theory and are shown to have an identical spectrum.

The T=0 Gross-Pitaevskii equation can be derived from the general quantum field Hamiltonian for a rarefied Bose gas, which is given by (1.8):

$$\hat{H} = \int d\boldsymbol{r}\hat{\psi}^{\dagger}(\boldsymbol{r})\Big[-\frac{\hbar^2}{2m}\nabla^2 + \mathcal{V}(\boldsymbol{r})\Big]\hat{\psi}(\boldsymbol{r}) + \frac{1}{2}\int d\boldsymbol{r}d\boldsymbol{r}'\hat{\psi}^{\dagger}(\boldsymbol{r})\hat{\psi}^{\dagger}(\boldsymbol{r}')\mathcal{U}(\boldsymbol{r}'-\boldsymbol{r})\hat{\psi}(\boldsymbol{r})\hat{\psi}(\boldsymbol{r}') \tag{D.1}$$

where $\mathcal{U}(\boldsymbol{r})$ is the two-body potential and $\mathcal{V}(\boldsymbol{r})$ is the external potential. The equation of motion for the Bose gas field operator $\hat{\psi}(\boldsymbol{r},t)$ in the Heisenberg picture is defined as:

$$i\hbar\frac{\partial}{\partial t}\hat{\psi}(\boldsymbol{r},t) = [\hat{\psi}(\boldsymbol{r},t),\hat{H}], \tag{D.2}$$

which, upon substitution in (1.8), results in:

$$i\hbar\frac{\partial}{\partial t}\hat{\psi}(\boldsymbol{r},t) = \Big[-\frac{\hbar^2}{2m}\nabla^2 + \mathcal{V}(\boldsymbol{r}) + \int d\boldsymbol{r}'\hat{\psi}^{\dagger}(\boldsymbol{r},t)\mathcal{U}(\boldsymbol{r}'-\boldsymbol{r})\hat{\psi}(\boldsymbol{r}',t)\Big]\hat{\psi}(\boldsymbol{r},t). \tag{D.3}$$

Analogous to (1.11), at temperatures below the critical temperature, the field operator can be split up into a condensate and noncondensate part:

$$\hat{\psi}(\boldsymbol{r}) = \hat{\psi}_0(\boldsymbol{r})\hat{a}_0 + \sum_{i\neq 0} \psi(\boldsymbol{r})\hat{a}_i \tag{D.4}$$

$$:= \hat{\Phi}(\boldsymbol{r}) + \delta\hat{\psi}(\boldsymbol{r}). \tag{D.5}$$

In the Bogoliubov approximation (see Section 1.2.1), $\Phi(\boldsymbol{r})$ is a classical field since $\hat{a}_0$ is taken to be a c-number. $\Phi(\boldsymbol{r})$ is then often referred to as the order parameter or wave function of the condensate. At very low temperatures $T \approx 0$, all the particles will be in the ground state to a very good approximation and so $\hat{\psi}(\boldsymbol{r},t) \approx \Phi(\boldsymbol{r},t)$. (D.3) then becomes an equation of motion for the classical field $\Phi(\boldsymbol{r},t)$. Further approximating the general potential $\boldsymbol{\mathcal{U}}(\boldsymbol{r}'-\boldsymbol{r})$ at low-energy by the contact potential $g\delta(\boldsymbol{r}'-\boldsymbol{r})$, (D.3) becomes:

$$i\hbar\frac{\partial}{\partial t}\Phi(\boldsymbol{r},t) = \Big[-\frac{\hbar^2}{2m}\nabla^2 + \mathcal{V}(\boldsymbol{r}) + g|\Phi(\boldsymbol{r},t)|^2\Big]\Phi(\boldsymbol{r},t). \tag{D.6}$$

This is the time-dependent T=0 GP equation [203], which is a non-linear Schrödinger equation and is the primary tool used to investigate non-uniform dilute Bose gases at low temperatures [48]. Analogous to the Madelung formulation of the Schrödinger equation [204], the classical field $\Phi(\boldsymbol{r},t)$ can be written in terms of the condensate density $n_c(\boldsymbol{r},t) = |\Phi(\boldsymbol{r},t)|^2$ and a phase $\theta(\boldsymbol{r},t)$:

$$\Phi(\boldsymbol{r},t) := \sqrt{n_c(\boldsymbol{r},t)}e^{i\theta(\boldsymbol{r},t)} \tag{D.7}$$

such that the GP equation splits up into an equation for the real and imaginary components:

$$\frac{\partial n_c}{\partial t} + \boldsymbol{\nabla}.(n_c\boldsymbol{v}_c) = 0, \tag{D.8}$$

$$m\frac{\partial \boldsymbol{v}_c}{\partial t} = -\boldsymbol{\nabla}\epsilon_c \tag{D.9}$$

where:

$$\boldsymbol{v}_c := \frac{\hbar}{m}\nabla\boldsymbol{\theta}(\boldsymbol{r},t), \tag{D.10}$$

$$\epsilon_c := \mu_c + \frac{1}{2}mv_c^2, \tag{D.11}$$

$$\mu_c := -\frac{\hbar^2\nabla^2\sqrt{n_c(\boldsymbol{r},t)}}{2m\sqrt{n_c(\boldsymbol{r},t)}} + \mathcal{V}(\boldsymbol{r}) + gn_c(\boldsymbol{r},t) \tag{D.12}$$

such that $\boldsymbol{v}_c$ is velocity of the condensate flow; $\mu_c(\boldsymbol{r},t)$ acts as a time and space-dependent chemical potential; ϵ_c plays the role of the local energy of a condensate particle having potential energy μ_c and kinetic energy $\frac{1}{2}mv_c^2$; and so (D.8) is a continuity equation, and $\boldsymbol{\nabla}\epsilon_c$ in (D.9) is a quantum force. The description offered by (D.8)-(D.9) is analogous to the Madelung formulation of quantum mechanics (which is similar to Bohmian mechanics) but for a non-linear Schrödinger equation, and is often referred to as the hydrodynamic theory.

Considering a departure of the gas from its equilibrium, n_c is written as $n_c^{eq}+\delta n_c$ where n_c^{eq} is the equilibrium density and δn_c is the departure of the density from its equilibrium value. Treating δn_c and $\boldsymbol{v}_c$ as small quantities, (D.8)-(D.9) can then be linearized:

$$\frac{\partial\delta n_c}{\partial t} = -\boldsymbol{\nabla}.(n_c^{eq}\boldsymbol{v}_c), \tag{D.13}$$

$$m\frac{\partial\boldsymbol{v}_c}{\partial t} = -\boldsymbol{\nabla}\delta\mu_c \tag{D.14}$$

where $\delta\mu_c$ is obtained by linearizing (D.12). These two equations can be combined into a single equation of motion by taking the time derivative of (D.13) and eliminating the velocity by means of (D.14) [176, 205]:

$$\frac{\partial^2\delta n_c}{\partial t^2} = \frac{g}{m}\boldsymbol{\nabla}.[n_c^{eq}\boldsymbol{\nabla}\delta\mu_c]. \tag{D.15}$$

For a uniform gas ($\mathcal{V} = const$) the equilibrium density is the same everywhere and so it may be taken outside the spatial derivatives. The solutions

of (D.15) will then be plane waves $\delta n_c(\boldsymbol{k}, t) \propto e^{i\boldsymbol{k}.\boldsymbol{r}-\omega t}$ and, from (D.12), the change in μ_c will be given by:

$$\delta\mu_c = \Big(g + \frac{\hbar^2 k^2}{4mn_c^{eq}}\Big)\delta n_c \tag{D.16}$$

so that (D.15) becomes:

$$m\omega^2\delta n_c = \Big(n_c^{eq} g k^2 + \frac{\hbar^2 k^4}{4m}\Big)\delta n_c. \tag{D.17}$$

The solution of (D.15) is $\omega = \pm\epsilon_{p_k}/\hbar$ where ϵ_{p_k} satisfies:

$$\epsilon_{p_k} = \sqrt{c_s^2 {p_k}^2 + \Big(\frac{{p_k}^2}{2m}\Big)^2} \tag{D.18}$$

with:

$$\boldsymbol{p}_k := \hbar\boldsymbol{k}, \tag{D.19}$$

$$c_s := \sqrt{\frac{gn}{m}}. \tag{D.20}$$

Note that (D.18) is equivalent to spectrum of Bogoliubov quasi-particles given by (1.29) and the low-energy condensate oscillations are sound waves $\omega = c_s k$.[1]. Therefore, the condensate density fluctuations have an identical spectrum to that of the Bogoliubov quasi-particles (excitations involving the noncondensate). This is in fact a characteristic signature of Bose-condensed fluids and persists at finite temperatures [50]. The properties of elementary excitations may, therefore, be investigated by considering small deviations of the state of the gas from the equilibrium and finding periodic solutions to the hydrodynamic equations [58].

[1]This would have been the only solution had the Thomas-Fermi approximation been applied where the quantum pressure term (the first term in (D.14)), which comes from the kinetic energy term, is neglected in comparison to the Hartree interaction term gn_c [50]

Bibliography

[1] H. D. Zeh, Foundations of Physics **1**, 69 (1970).

[2] E. Joos and H. Zeh, English, Zeitschrift für Physik B Condensed Matter **59**, 223 (1985); W. H. Zurek, Rev. Mod. Phys. **75**, 715 (2003); W. H. Zurek, eprint arXiv:quant-ph/0306072 (2003), eprint: quant-ph/0306072.

[3] M. Schlosshauer, Rev. Mod. Phys. **76**, 1267 (2005).

[4] M. Brune, E. Hagley, J. Dreyer, X. Maître, A. Maali, C. Wunderlich, J. M. Raimond, and S. Haroche, Phys. Rev. Lett. **77**, 4887 (1996).

[5] M. Horodecki and J. Oppenheim, Nature Communications **4**, 2059, 2059 (2013), arXiv:1111 . 3834 [quant-ph]; C. A. Rodríguez-Rosario, T. Frauenheim, and A. Aspuru-Guzik, ArXiv e-prints (2013), arXiv:1308 . 1245 [quant-ph]; P. Skrzypczyk, A. J. Short, and S. Popescu, Nature Communications **5**, 4185, 4185 (2014), arXiv:1307 . 1558 [quant-ph]; M. Lostaglio, K. Korzekwa, D. Jennings, and T. Rudolph, Phys. Rev. X **5**, 021001 (2015); M. Lostaglio, D. Jennings, and T. Rudolph, Nature Communications **6**, 6383, 6383 (2015), arXiv:1405 . 2188 [quant-ph]; V. Narasimhachar and G. Gour, ibid. **6**, 7689, 7689 (2015), arXiv:1409 . 7740 [quant-ph]; J. Åberg, Phys. Rev. Lett. **113**, 150402 (2014); P. Ćwikliński, M. Studziński, M. Horodecki, and J. Oppenheim, ArXiv e-prints (2014), arXiv:1405.5029 [quant-ph]; L. A. Correa, J. P. Palao, D. Alonso, and G. Adesso, Scientific Reports **4**, 3949, 3949 (2014), arXiv:1308.4174 [quant-ph]; J. Roßnagel, O. Abah, F. Schmidt-Kaler, K. Singer, and E. Lutz, Phys. Rev. Lett. **112**, 030602 (2014); F. Brandão, M. Horodecki, N. Ng, J. Oppenheim, and S. Wehner, Proceedings of the National Academy of Science **112**, 3275 (2015); J. Gemmer, M. Michel, and G. Mahler, eds., *Quantum Thermodynamics: Emergence of Thermodynamic Behavior Within Composite Quantum Systems*, Vol. 657, Lecture Notes in Physics, Berlin Springer Verlag (2004); S. Bhattacharya and S. Roy, ArXiv e-prints (2013), arXiv:1303.1905 [quant-ph].

[6] P. Rebentrost, M. Mohseni, and A. Aspuru-Guzik, The Journal of Physical Chemistry B **113**, PMID: 19603843, 9942 (2009), eprint: http://dx.doi.org/10.1021/jp901724d; S. Lloyd, Journal of Physics: Conference Series **302**, 012037 (2011); C.-M. Li, N. Lambert, Y.-N. Chen, G.-Y. Chen, and F. Nori, Scientific Reports **2**, 885, 885 (2012), arXiv:1212.0194 [quant-ph]; S. Huelga and M. Plenio, Contemporary Physics **54**, 181 (2013), eprint: http://dx.doi.org/10.1080/00405000.2013.829687; N. Lambert, Y.-N. Chen, Y.-C. Cheng, C.-M. Li, G.-Y. Chen, and F. Nori, Nature Physics **9**, 10 (2013); A. W. Chin, S. F. Huelga, and M. B. Plenio, Philosophical Transactions of the Royal Society of London A: Mathematical, Physical and Engineering Sciences **370**, 3638 (2012); S. Hagan, S. R. Hameroff, and J. A. Tuszy ński, Phys. Rev. E **65**, 061901 (2002).

[7] P. Shor, in Foundations of computer science, 1994 proceedings., 35th annual symposium on (1994), pp. 124–134.

[8] L. K. Grover, eprint arXiv:quant-ph/9605043 (1996), eprint: quant-ph/9605043.

[9] G. Moore, Proceedings of the IEEE **86**, 82 (1998); *Overall technology roadmap characteristics*, tech. rep. (International Technology Roadmap for Semiconductors, 2010).

[10] F. S. Cataliotti, S. Burger, C. Fort, P. Maddaloni, F. Minardi, A. Trombettoni, A. Smerzi, and M. Inguscio, Science **293**, 843 (2001), eprint: http://www.sciencemag.org/content/293/5531/843.full.pdf; Salgueiro, A. N., de Toledo Piza, A.F.R., Lemos, G. B., Drumond, R., Nemes, M. C., and Weidemüller, M., Eur. Phys. J. D **44**, 537 (2007).

[11] D. S. Hall, M. R. Matthews, J. R. Ensher, C. E. Wieman, and E. A. Cornell, Phys. Rev. Lett. **81**, 1539 (1998); ibid. **81**, 1543 (1998).

[12] C. Gross, T. Zibold, E. Nicklas, J. Estève, and M. K. Oberthaler, Nature **464**, 1165 (2010), arXiv:1009.2374 [cond-mat.quant-gas]; Y.-J. Wang, D. Z. Anderson, V. M. Bright, E. A. Cornell, Q. Diot, T. Kishimoto, M. Prentiss, R. A. Saravanan, S. R. Segal, and S. Wu, Phys. Rev. Lett. **94**, 090405 (2005); W. Hänsel, P. Hommelhoff, T. W. Hänsch, and J. Reichel, Nature **413**, 498 (2001); T. Berrada, S. van Frank, R. Bücker, T. Schumm, J.-F. Schaff, and J. Schmiedmayer, Nature Communications **4**, 2077, 2077 (2013), arXiv:1303.1030 [cond-mat.quant-gas]; M. Fattori, C. D'Errico, G. Roati, M. Zaccanti, M. Jona-Lasinio, M. Modugno, M. Inguscio, and G. Modugno, Phys. Rev. Lett. **100**, 080405 (2008); T. Schumm, P. Krüger, S. Hofferberth, I. Lesanovsky, S. Wildermuth, S. Groth, I. Bar-Joseph, L. Andersson, and J. Schmiedmayer, English, Quantum

Information Processing **5**, 537 (2006); R. Folman, P. Krüger, D. Cassettari, B. Hessmo, T. Maier, and J. Schmiedmayer, Physical Review Letters **84**, 4749 (2000), eprint: quant-ph/9912106.

[13] T. Byrnes, K. Wen, and Y. Yamamoto, Phys. Rev. A **85**, 040306 (2012); W. Hänsel, P. Hommelhoff, T. W. Hänsch, and J. Reichel, Nature **413**, 498 (2001); R. Folman, P. Krüger, D. Cassettari, B. Hessmo, T. Maier, and J. Schmiedmayer, Physical Review Letters **84**, 4749 (2000), eprint: quant-ph/9912106; A. Sørensen, L.-M. Duan, J. I. Cirac, and P. Zoller, Nature **409**, 63 (2001), eprint: quant-ph/0006111; I. Buluta and F. Nori, Science **326**, 108 (2009), eprint: http://www.sciencemag.org/content/326/5949/108.full.pdf; T. Byrnes, K. Wen, and Y. Yamamoto, Phys. Rev. A **85**, 040306 (2012).

[14] W. Hänsel, P. Hommelhoff, T. W. Hänsch, and J. Reichel, Nature **413**, 498 (2001); W. Hänsel, J. Reichel, P. Hommelhoff, and T. W. Hänsch, Phys. Rev. Lett. **86**, 608 (2001); S. Whitlock, R. Gerritsma, T. Fernholz, and R. J. C. Spreeuw, New Journal of Physics **11**, 023021, 023021 (2009), arXiv:0803.2151 [physics.atom-ph].

[15] M. Czachor, Phys. Rev. A **55**, 72 (1997); A. Peres, P. F. Scudo, and D. R. Terno, Phys. Rev. Lett. **88**, 230402 (2002); R. M. Gingrich and C. Adami, ibid. **89**, 270402 (2002); D. Ahn, H.-j. Lee, Y. H. Moon, and S. W. Hwang, Phys. Rev. A **67**, 012103 (2003); T. F. Jordan, A. Shaji, and E. C. G. Sudarshan, ibid. **75**, 022101 (2007); N. Friis, R. A. Bertlmann, M. Huber, and B. C. Hiesmayr, ibid. **81**, 042114 (2010); M. Huber, N. Friis, A. Gabriel, C. Spengler, and B. C. Hiesmayr, EPL (Europhysics Letters) **95**, 20002 (2011); A. Peres and D. R. Terno, Rev. Mod. Phys. **76**, 93 (2004); T. C. Ralph and T. G. Downes, Contemporary Physics **53**, 1 (2012), eprint: http://dx.doi.org/10.1080/00107514.2011.640146.

[16] I. Fuentes-Schuller and R. B. Mann, Phys. Rev. Lett. **95**, 120404 (2005); P. M. Alsing, I. Fuentes-Schuller, R. B. Mann, and T. E. Tessier, Phys. Rev. A **74**, 032326 (2006); G. Adesso, I. Fuentes-Schuller, and M. Ericsson, ibid. **76**, 062112 (2007); D. E. Bruschi, J. Louko, E. Martín-Martínez, A. Dragan, and I. Fuentes, ibid. **82**, 042332 (2010); E. Martín-Martínez and I. Fuentes, ibid. **83**, 052306 (2011); N. Friis, P. Köhler, E. Martín-Martínez, and R. A. Bertlmann, ibid. **84**, 062111 (2011); M. Montero, J. León, and E. Martín-Martínez, ibid. **84**, 042320 (2011); G. Adesso and I. Fuentes-Schuller, Quant. Inf. Comp. **9**, 0657–0665 (2009), eprint: quant-ph/0702001; E. Martín-Martínez, L. J. Garay, and J. León, Phys. Rev. D **82**, 064006 (2010); M. Montero and E. Martín-Martínez, English, Journal of High Energy Physics **2011**, 6 (2011) 10.1007/JHEP07(2011)006; T. G. Downes, I. Fuentes, and T. C. Ralph, Phys. Rev. Lett. **106**, 210502 (2011); D. E. Bruschi, I.

Fuentes, and J. Louko, Phys. Rev. D **85**, 061701 (2012); N. Friis, A. R. Lee, D. E. Bruschi, and J. Louko, ibid. **85**, 025012 (2012); J. L. Ball, I. Fuentes-Schuller, and F. P. Schuller, Physics Letters A **359**, 550 (2006); E. Martín-Martínez, L. J. Garay, and J. León, Phys. Rev. D **82**, 064028 (2010); N. Friis, D. E. Bruschi, J. Louko, and I. Fuentes, ibid. **85**, 081701 (2012); D. E. Bruschi, A. Dragan, A. R. Lee, I. Fuentes, and J. Louko, Phys. Rev. Lett. **111**, 090504 (2013); N. Friis and I. Fuentes, Journal of Modern Optics **60**, 22 (2013), eprint: http://dx.doi.org/10.1080/09500340.2012.712725; B. Regula, A. R. Lee, A. Dragan, and I. Fuentes, ArXiv e-prints (2015), arXiv:1509.05931 [quant-ph]; C. Sabín, I. Fuentes, and G. Johansson, Phys. Rev. A **92**, 012314 (2015); J. Lindkvist, C. Sabín, G. Johansson, and I. Fuentes, Scientific Reports **5**, 10070, 70 (2015), arXiv:1409.4235 [quant-ph]; M. Ahmadi, D. E. Bruschi, and I. Fuentes, Phys. Rev. D **89**, 065028 (2014); D. E. Bruschi, T. C. Ralph, I. Fuentes, T. Jennewein, and M. Razavi, ibid. **90**, 045041 (2014); P. M. Alsing and I. Fuentes, Classical and Quantum Gravity **29**, 224001 (2012); D. E. Bruschi, A. Dragan, I. Fuentes, and J. Louko, Phys. Rev. D **86**, 025026 (2012); D. Šafránek, M. Ahmadi, and I. Fuentes, New Journal of Physics **17**, 033012 (2015).

[17] M. Ahmadi, D. E. Bruschi, C. Sabín, G. Adesso, and I. Fuentes, Scientific Reports **4**, 4996, 4996 (2014), arXiv:1307.7082 [quant-ph].

[18] C. Sabín, D. E. Bruschi, M. Ahmadi, and I. Fuentes, New Journal of Physics **16**, 085003, 085003 (2014), arXiv:1402.7009 [quant-ph]; ArXiv e-prints (2015), arXiv:1505.01302 [quant-ph].

[19] R. Ursin, T. Jennewein, J. Kofler, J. M. Perdigues, L. Cacciapuoti, C. J. de Matos, M. Aspelmeyer, A. Valencia, T. Scheidl, A. Acin, C. Barbieri, G. Bianco, C. Brukner, J. Capmany, S. Cova, D. Giggenbach, W. Leeb, R. H. Hadfield, R. Laflamme, N. Lütkenhaus, G. Milburn, M. Peev, T. Ralph, J. Rarity, R. Renner, E. Samain, N. Solomos, W. Tittel, J. P. Torres, M. Toyoshima, A. Ortigosa-Blanch, V. Pruneri, P. Villoresi, I. Walmsley, G. Weihs, H. Weinfurter, M. Zukowski, and A. Zeilinger, Europhysics News **40**, 26 (2009), arXiv:0806.0945 [quant-ph].

[20] S. Schiller, A. Görlitz, A. Nevsky, S. Alighanbari, S. Vasilyev, C. Abou-Jaoudeh, G. Mura, T. Franzen, U. Sterr, S. Falke, C. Lisdat, E. Rasel, A. Kulosa, S. Bize, J. Lodewyck, G. M. Tino, N. Poli, M. Schioppo, K. Bongs, Y. Singh, P. Gill, G. Barwood, Y. Ovchinnikov, J. Stuhler, W. Kaenders, C. Braxmaier, R. Holzwarth, A. Donati, S. Lecomte, D. Calonico, and F. Levi, ArXiv e-prints (2012), arXiv:1206.3765 [quant-ph].

[21] M. Visser and C. Molina-París, New Journal of Physics **12**, 095014 (2010); S Fagnocchi, S Finazzi, S Liberati, M Kormos, and A Trombettoni, ibid. **12**, 095012 (2010).

[22] W. G. Unruh, Phys. Rev. Lett. **46**, 1351 (1981); L. J. Garay, J. R. Anglin, J. I. Cirac, and P. Zoller, ibid. **85**, 4643 (2000); O. Lahav, A. Itah, A. Blumkin, C. Gordon, S. Rinott, A. Zayats, and J. Steinhauer, Physical Review Letters **105**, 240401, 240401 (2010), arXiv:0906.1337 [cond-mat.quant-gas]; A. Recati, N. Pavloff, and I. Carusotto, Phys. Rev. A **80**, 043603 (2009); L. J. Garay, J. R. Anglin, J. I. Cirac, and P. Zoller, Physical Review Letters **85**, 4643 (2000), eprint: gr-qc/0002015; I Zapata, M Albert, R Parentani, and F Sols, New Journal of Physics **13**, 063048 (2011).

[23] L. J. Garay, J. R. Anglin, J. I. Cirac, and P. Zoller, Phys. Rev. Lett. **85**, 4643 (2000).

[24] J. Steinhauer, Nature Physics **10**, 864 (2014), arXiv:1409.6550 [cond-mat.quant-gas].

[25] R. Howl, C. Sabín, I. Fuentes, and L. Hackermüller, "Working Title: Decoherence of Phonons of Bose-Einstein Condensates", 2015.

[26] L. D. Landau, J. Phys.(USSR) **10**, [Zh. Eksp. Teor. Fiz.16,574(1946)], 25 (1946); S. T. Beliaev, Sov. Phys. JETP **34**, 323 (1958); S. Beliaev, ibid. **7**, 299 (1958); P. Hohenberg and P. Martin, Annals of Physics **34**, 291 (1965); E. Lifshitz and L. Pitaevskii, *Physical kinetics* (Pergamon Press, Oxford, 1981); I. Kondor and P. Szépfalusy, Physics Letters A **47**, 393 (1974); W. Liu and W. Shieve, cond-mat/9702122 (1997); L. Pitaevskii and S. Stringari, Physics Letters A **235**, 398 (1997); W. Vincent Liu, Phys. Rev. Lett. **79**, 4056 (1997); S. Giorgini, Phys. Rev. A **57**, 2949 (1998); P. O. Fedichev, G. V. Shlyapnikov, and J. T. M. Walraven, Phys. Rev. Lett. **80**, 2269 (1998); P. O. Fedichev and G. V. Shlyapnikov, Phys. Rev. A **58**, 3146 (1998); G. Bene and P. Szépfalusy, ibid. **58**, R3391 (1998); R. Graham, English, Journal of Statistical Physics **101**, 243 (2000); M. Rusch and K. Burnett, Phys. Rev. A **59**, 3851 (1999); B Jackson and E Zaremba, New Journal of Physics **5**, 88 (2003).

[27] A. Sinatra, Y. Castin, and E. Witkowska, Phys. Rev. A **75**, 033616 (2007).

[28] R. Graham, Phys. Rev. Lett. **81**, 5262 (1998); Phys. Rev. A **62**, 023609 (2000); Y. Castin and A. Sinatra, ArXiv e-prints (2012), arXiv:1203.4458 [cond-mat.quant-gas].

[29] N. Katz, R. Ozeri, E. Rowen, E. Gershnabel, and N. Davidson, Phys. Rev. A **70**, 033615 (2004); E. E. Rowen, "Coherence and decoherence of excitations in a trapped Bose-Einstein condensate", PhD thesis (The Weizmann Institute of Science (Israel, 2008); N.

Bar-Gill, E. E. Rowen, G. Kurizki, and N. Davidson, Phys. Rev. Lett. **102**, 110401 (2009).

[30] D. Walls and G. Milburn, *Quantum optics*, Second edition (Springer Berlin Heidelberg, 1995).

[31] C. J. Myatt, B. E. King, Q. A. Turchette, C. A. Sackett, D. Kielpinski, W. M. Itano, C. Monroe, and D. J. Wineland, Nature **403**, 269 (2000).

[32] H.-P. Breuer and F. Petruccione, *The theory of open qunatum systems*, Second edition (Oxford University Press, 2002).

[33] R. Howl, C. Sabín, I. Fuentes, and L. Hackermüller, "Working Title: De-Entanglement of Phonons of Bose-Einstein Condensation", 2015.

[34] X. Busch and R. Parentani, Phys. Rev. D **89**, 105024 (2014).

[35] S. Finazzi and I. Carusotto, Phys. Rev. A **90**, 033607 (2014).

[36] D. E. Bruschi, N Friis, I Fuentes, and S Weinfurtner, New Journal of Physics **15**, 113016 (2013).

[37] I. Carusotto, R. Balbinot, A. Fabbri, and A. Recati, English, The European Physical Journal D **56**, 391 (2010).

[38] J.-C. Jaskula, G. B. Partridge, M. Bonneau, R. Lopes, J. Ruaudel, D. Boiron, and C. I. Westbrook, Phys. Rev. Lett. **109**, 220401 (2012).

[39] J. Steinhauer, ArXiv e-prints (2015), arXiv:1510.00621 [gr-qc].

[40] M. Ahmadi, D. E. Bruschi, and I. Fuentes, Phys. Rev. D **89**, 065028 (2014).

[41] C. Weedbrook, S. Pirandola, R. García-Patrón, N. J. Cerf, T. C. Ralph, J. H. Shapiro, and S. Lloyd, Rev. Mod. Phys. **84**, 621 (2012); S. Olivares, English, The European Physical Journal Special Topics **203**, 3 (2012); A. Ferraro, S. Olivares, and M. Paris, *Gaussian states in continuous variable quantum information* (Napoli Series on Physics and Astrophysics (ed. Bibliopolis, Napoli, 2005), 2005).

[42] G. Adesso, "Entanglement of Gaussian states", PhD thesis (Università degli Studi di Salerno, 2007), arXiv:quant-ph/0702069.

[43] R Alicki and M Fannes, Journal of Physics A: Mathematical and General **37**, L55 (2004).

[44] A Serafini, M. G. A. Paris, F Illuminati, and S. D. Siena, Journal of Optics B: Quantum and Semiclassical Optics **7**, R19 (2005).

[45] R. Howl, L. Hackermüller, et al., "Working Title: Measurement of Decoherence of Phonons in a Strongly-Interacting BEC", 2016.

[46] S. Giorgini, L. P. Pitaevskii, and S. Stringari, Phys. Rev. A **54**, R4633 (1996); English, Journal of Low Temperature Physics **109**, 309 (1997).

[47] V. V. Goldman, I. F. Silvera, and A. J. Leggett, Phys. Rev. B **24**, 2870 (1981).

[48] L. Pitaevskii and S. Stringari, *Bose-einstein condensation* (Oxford University Press, 2003).

[49] L. H. Thomas, Mathematical Proceedings of the Cambridge Philosophical Society **23**, 542 (1927); E. Fermi, Rend. Accad. Naz. Lincei **6**, 602 (1927).

[50] A. Griffin, T. Nikuni, and E. Zaremba, *Bose-Condensed Gases at Finite Temperatures* (Feb. 2009).

[51] R. Howl, N. Welch, L. Hackermüller, et al., "Working Title: Imaging Strongly-Interacting BECs", 2015.

[52] M. Naraschewski and D. M. Stamper-Kurn, Phys. Rev. A **58**, 2423 (1998); A Minguzzi, S Conti, and M. P. Tosi, Journal of Physics: Condensed Matter **9**, L33 (1997).

[53] F. Gerbier, J. H. Thywissen, S. Richard, M. Hugbart, P. Bouyer, and A. Aspect, Phys. Rev. A **70**, 013607 (2004).

[54] A. Einstein, Phys. Math. K1 **22**, 261 (1924).

[55] N. N. Bogoliubov, J. Phys. (Moscow) **11**, 23 (1947).

[56] S. N. Bose, Z. Phys. **26**, 178 (1924).

[57] S. J. Blundell and K. M. Blundell, *Concepts in thermal physics*, Second edition (Oxford University Press, 2010).

[58] C. J. Pethick and H. Smith, *Bose-einstein condensation in dilute gases* (Cambridge University Press, 2002).

[59] F. London, Nature **141**, 643 (1938).

[60] L. D. Landau, J. Phys. (Moscow) **5**, 71 (1941).

[61] R. Feynman, in , Vol. 1, edited by C. Gorter, Progress in Low Temperature Physics (Elsevier, 1955), pp. 17 –53.

[62] H. F. Hess, Phys. Rev. B **34**, 3476 (1986); W. Ketterle and N. J. van Druten, *Adv. At Mol. Opt. Phys.* **37**, 181 (1996).

[63] M. H. Anderson, J. R. Ensher, M. R. Matthews, C. E. Wieman, and E. A. Cornell, Science **269**, 198 (1995), eprint: `http://www.sciencemag.org/content/269/5221/198.full.pdf`.

[64] K. B. Davis, M. O. Mewes, M. R. Andrews, N. J. van Druten, D. S. Durfee, D. M. Kurn, and W. Ketterle, Phys. Rev. Lett. **75**, 3969 (1995).

[65] C. C. Bradley, C. A. Sackett, J. J. Tollett, and R. G. Hulet, Phys. Rev. Lett. **75**, 1687 (1995); ibid. **78**, 985 (1997).

[66] H. Shi and A. Griffin, Physics Reports **304**, 1 (1998).

[67] L. D. Landau and E. M. Lifshitz, *Quantum mechanics*, Third edition (Pregamon, Oxford, 1987).

[68] T. D. Lee and C. N. Yang, Phys. Rev. **105**, 1119 (1957); T. D. Lee, K. Huang, and C. N. Yang, ibid. **106**, 1135 (1957).

[69] R. Ozeri, N. Katz, J. Steinhauer, and N. Davidson, Rev. Mod. Phys. **77**, 187 (2005).

[70] S. Giorgini, Phys. Rev. A **57**, 2949 (1998).

[71] G. Kónya, G. Szirmai, and P. Domokos, Phys. Rev. A **90**, 013623 (2014).

[72] D. C. Burnham and D. L. Weinberg, Phys. Rev. Lett. **25**, 84 (1970).

[73] N. Katz, J. Steinhauer, R. Ozeri, and N. Davidson, Phys. Rev. Lett. **89**, 220401 (2002); S. S. Natu and S. Das Sarma, Phys. Rev. A **88**, 031604 (2013); S. S. Natu and R. M. Wilson, ibid. **88**, 063638 (2013); D. H. Santamore, S. Gaudio, and E. Timmermans, Phys. Rev. Lett. **93**, 250402 (2004); S. K. Yip, Phys. Rev. A **64**, 023609 (2001); D. H. Santamore and E. Timmermans, ibid. **72**, 053601 (2005); X.-J. Liu and H. Hu, ibid. **68**, 033613 (2003); J. H. Pixley, X. Li, and S. Das Sarma, Phys. Rev. Lett. **114**, 225303 (2015); R. Ozeri, N. Katz, J. Steinhauer, E. Rowen, and N. Davidson, ibid. **90**, 170401 (2003); E. Hodby, O. M. Maragò, G. Hechenblaikner, and C. J. Foot, Physical Review Letters **86**, 2196 (2001), eprint: `cond-mat/0010157`; D. S. Jin, J. R. Ensher, M. R. Matthews, C. E. Wieman, and E. A. Cornell, Phys. Rev. Lett. **77**, 420 (1996); ibid. **78**, 764 (1997); M.-O. Mewes, M. R. Andrews, N. J. van Druten, D. M. Kurn, D. S. Durfee, C. G. Townsend, and W. Ketterle, ibid. **77**, 988 (1996); E. E. Rowen, N. Bar-Gill, R. Pugatch, and N. Davidson, Phys. Rev. A **77**, 033602 (2008).

[74] D. S. Jin, J. R. Ensher, M. R. Matthews, C. E. Wieman, and E. A. Cornell, Phys. Rev. Lett. **77**, 420 (1996).

[75] M.-O. Mewes, M. R. Andrews, N. J. van Druten, D. M. Kurn, D. S. Durfee, C. G. Townsend, and W. Ketterle, Phys. Rev. Lett. **77**, 988 (1996).

[76] H. J. Carmichael, *Statistical methods in quantum optics 1*, Second edition (Springer Berlin Heidelberg, 2002).

[77] A. Carlini, A. Mari, and V. Giovannetti, Phys. Rev. A **90**, 052324 (2014).

[78] J. Rogel-Salazar, G. H. C. New, S. Choi, and K. Burnett, Phys. Rev. A **65**, 023601 (2002).

[79] B Jackson and E Zaremba, New Journal of Physics **5**, 88 (2003).

[80] G. Adesso and F. Illuminati, Journal of Physics A: Mathematical and Theoretical **40**, 7821 (2007).

[81] G. Adesso, S. Ragy, and D. Girolami, Class. Quant. Grav. **29**, 224002 (2012), arXiv:1205.0222 [quant-ph].

[82] G. Kaiser, "Quantum physics, relativity and complex space-time: Towards a new synthesis", PhD thesis (Massachusetts U., Lowell, 1990), arXiv:0910.0352 [math-ph].

[83] J.-P. A. Syed Twareque Ali and J.-P. Gazeau, *Coherent states, wavelets, and their generalizations* (Springer New York, 2014).

[84] M. Edwards, P. A. Ruprecht, K. Burnett, R. J. Dodd, and C. W. Clark, Phys. Rev. Lett. **77**, 1671 (1996).

[85] R. Simon, N. Mukunda, and B. Dutta, Phys. Rev. A **49**, 1567 (1994).

[86] R. Simon, E. C. G. Sudarshan, and N. Mukunda, Phys. Rev. A **36**, 3868 (1987).

[87] S. M. Barnett and P. M. Radmore, *Methods in Theoretical Quantum Optics*, Oxford Series in Optical and Imaging Sciences (Oxford University Press, 1997).

[88] L.-A. Wu, H. J. Kimble, J. L. Hall, and H. Wu, Phys. Rev. Lett. **57**, 2520 (1986); A. Furusawa, J. L. Sorensen, S. L. Braunstein, C. A. Fuchs, H. J. Kimble, and E. S. Polzik, Science **282**, 706 (1998).

[89] L.-A. Wu, H. J. Kimble, J. L. Hall, and H. Wu, Phys. Rev. Lett. **57**, 2520 (1986).

[90] D. J. Wineland, J. J. Bollinger, W. M. Itano, and D. J. Heinzen, Phys. Rev. A **50**, 67 (1994); J. Estève, C. Gross, A. Weller, S. Giovanazzi, and M. K. Oberthaler, Nature **455**, 1216 (2008), arXiv:0810.0600.

[91] A. C. J. Wade, J. F. Sherson, and K. Mølmer, Phys. Rev. Lett. **115**, 060401 (2015).

[92] J. Williamson, Am. J. of Math. **58**, 141 (1936).

[93] J. Laurat, G. Keller, J. A. Oliveira-Huguenin, C. Fabre, T. Coudreau, A. Serafini, G. Adesso, and F. Illuminati, Journal of Optics B: Quantum and Semiclassical Optics **7**, S577 (2005).

[94] Arvind, B Dutta, N Mukunda, and R Simon, English, Pramana **45**, 471 (1995).

[95] A. Serafini, J. Eisert, and M. M. Wolf, Phys. Rev. A **71**, 012320 (2005).

[96] B. L. Schumaker, Physics Reports **135**, 317 (1986).

[97] W. S. A. Isar and A. Sandulescu, J. Math. Phys. **32**, 2128 (1991).

[98] A. Isar, A. Sandulescu, H. Scutaru, E. Stefanescu, and W. Sceid, International Journal of Modern Physics E **03**, 635 (1994).

[99] A Sandulescu and H Scutaru, Annals of Physics **173**, 277 (1987).

[100] M. G. Genoni, S. Mancini, and A. Serafini, Phys. Rev. A **87**, 042333 (2013).

[101] Z. Gajic and M. T. J. Qureshi, *Lyapunov matrix equation in system stability and control*, Mathematics in science and engineering (Elsevier, Burlington, MA, 1995).

[102] P. Axelsson and F. Gustafsson, Automatic Control, IEEE Transactions on **60**, 632 (2015).

[103] H. Rome, Automatic Control, IEEE Transactions on **14**, 592 (1969).

[104] P. V. B. Demoen and A. Verbeure, Lett. Math. Phys. **2**, 161 (1977); C. Caves and P. Drummond, Rev. Mod. Phys. **66**, 481 (1994); G. Lindblad, J. Phys. A **33**, 5059 (2000); J. Harrington and J. Preskill, Phys. Rev. A **64**, 062301 (2001); J. Eisert and M. Plenio, Phys. Rev. Lett. **89**, 097901 (2002); M. P. A. Serafini, F. Illuminati and S. D. Siena, Phys. Rev. A 69, 022318 (2004); M. S. A.S. Holevo and O. Hirota, Phys. Rev. A **59**, 1820 (1999); A. Holevo and R. Werner, ibid. **63**, 032312 (2001); L. M. V. Giovannetti, S. Lloyd and P. Shor, Phys. Rev. Lett. **91**, 047901 (2003); Phys. Rev. A **68**, 062323 (2003); A. Serafini, J. Eisert, and M. M. Wolf, ibid. **71**, 012320 (2005).

[105] J. P. P. B. L. Hu and Y. Zhang, Phys. Rev. D **45**, 2843 (1992); F. Intravaia, S. Maniscalco, and A. Messina, Phys. Rev. A **67**, 042108 (2003).

[106] J. Cirac, J Eisert, G Giedke, M Lewenstein, M. Plenio, R. Werner, and M. Wolf, *Gaussian quantum states and gaussian operations (in press)* (Springer, 2004).

[107] G. Torre, W. Roga, and F. Illuminati, Physical Review Letters **115**, 070401, 070401 (2015), arXiv:`1504.00671 [quant-ph]`.

[108] R. Bathia, *Matrix analysis* (Springer Verlag, Berlin, 1997).

[109] A. Renyi, *Probability Theory*, English (North-Holland Pub. Co Amsterdam, 1970); K. Życzkowski, English, Open Systems and Information Dynamics **10**, 297 (2003).

[110] M. J. Bastiaans, J. Opt. Soc. Am. A **1**, 711 (1984); C. Tsallis, English, Journal of Statistical Physics **52**, 479 (1988).

[111] U. Singh, M. N. Bera, H. S. Dhar, and A. K. Pati, Phys. Rev. A **91**, 052115 (2015).

[112] G. Adam, J. Mod. Opt. **1311**, 052115 (1995).

[113] M. G. A. Paris, F. Illuminati, A. Serafini, and S. De Siena, Phys. Rev. A **68**, 012314 (2003).

[114] A. Serafini, PhD thesis (Università degli Studi di Salerno, 2004).

[115] G. S. Agarwal, Phys. Rev. A **3**, 828 (1971).

[116] C. T. Lee, Phys. Rev. A **44**, R2775 (1991).

[117] C. T. Lee, in Squeezed states and uncertainty relations, edited by D. Han, Y. S. Kim, and W. W. Zachary (Feb. 1992), pp. 365–367.

[118] T. Baumgratz, M. Cramer, and M. B. Plenio, Phys. Rev. Lett. **113**, 140401 (2014).

[119] V. Vedral and M. B. Plenio, Phys. Rev. A **57**, 1619 (1998); F. G. S. L. Brandao and M. B. Plenio, Nature Physics **4**, 873 (2008), arXiv:0810.2319 [quant-ph]; F. Brandão and M. Plenio, English, Communications in Mathematical Physics **295**, 829 (2010).

[120] J. Eisert, C. Simon, and M. B. Plenio, Journal of Physics A: Mathematical and General **35**, 3911 (2002).

[121] J. Eisert and M. B. Plenio, International Journal of Quantum Information **01**, 479 (2003).

[122] A. Streltsov, U. Singh, H. S. Dhar, M. N. Bera, and G. Adesso, Phys. Rev. Lett. **115**, 020403 (2015).

[123] D. S. Jin, M. R. Matthews, J. R. Ensher, C. E. Wieman, and E. A. Cornell, Phys. Rev. Lett. **78**, 764 (1997).

[124] D. M. Stamper-Kurn, H.-J. Miesner, S. Inouye, M. R. Andrews, and W. Ketterle, Phys. Rev. Lett. **81**, 500 (1998).

[125] M. R. Andrews, D. M. Kurn, H.-J. Miesner, D. S. Durfee, C. G. Townsend, S. Inouye, and W. Ketterle, Phys. Rev. Lett. **79**, 553 (1997); ibid. **80**, 2967 (1998).

[126] S. E. Pollack, D. Dries, R. G. Hulet, K. M. F. Magalhães, E. A. L. Henn, E. R. F. Ramos, M. A. Caracanhas, and V. S. Bagnato, Phys. Rev. A **81**, 053627 (2010).

[127] D. M. Stamper-Kurn, A. P. Chikkatur, A. Görlitz, S. Inouye, S. Gupta, D. E. Pritchard, and W. Ketterle, Phys. Rev. Lett. **83**, 2876 (1999); J. M. Vogels, K. Xu, C. Raman, J. R. Abo-Shaeer, and W. Ketterle, ibid. **88**, 060402 (2002); J. Steinhauer, R. Ozeri, N. Katz, and N. Davidson, ibid. **88**, 120407 (2002).

[128] P. A. Ruprecht, M. Edwards, K. Burnett, and C. W. Clark, Phys. Rev. A **54**, 4178 (1996).

[129] J. R. Ensher, "The First Experiments with Bose-Einstein Condensation of Rb-87", PhD thesis (University of Colorado, 1998).

[130] C. Ciuti, G. Bastard, and I. Carusotto, Phys. Rev. B **72**, 115303 (2005).

[131] C. M. Wilson, G. Johansson, A. Pourkabirian, M. Simoen, J. R. Johansson, T. Duty, F. Nori, and P. Delsing, Nature **479**, 376 (2011); P. Lähteenmäki, G. S. Paraoanu, J. Hassel, and P. J. Hakonen, Proceedings of the National Academy of Sciences **110**, 4234 (2013).

[132] P. Engels, C. Atherton, and M. A. Hoefer, Phys. Rev. Lett. **98**, 095301 (2007); K. Staliunas, S. Longhi, and G. J. de Valcárcel, Phys. Rev. A **70**, 011601 (2004); Y. Kagan and L. A. Manakova, ibid. **76**, 023601 (2007); K. Staliunas, S. Longhi, and G. J. de Valcárcel, Phys. Rev. Lett. **89**, 210406 (2002).

[133] C. Tozzo and F. Dalfovo, Phys. Rev. A **69**, 053606 (2004).

[134] P. O. Fedichev, G. V. Shlyapnikov, and J. T. M. Walraven, Phys. Rev. Lett. **80**, 2269 (1998).

[135] N. Katz, J. Steinhauer, R. Ozeri, and N. Davidson, Phys. Rev. Lett. **89**, 220401 (2002).

[136] R. Ozeri, N. Katz, J. Steinhauer, E. Rowen, and N. Davidson, Phys. Rev. Lett. **90**, 170401 (2003).

[137] E. Hodby, O. M. Maragò, G. Hechenblaikner, and C. J. Foot, Physical Review Letters **86**, 2196 (2001), eprint: `cond-mat/0010157`.

[138] E. E. Rowen, N. Bar-Gill, R. Pugatch, and N. Davidson, Phys. Rev. A **77**, 033602 (2008).

[139] P. O. Fedichev, G. V. Shlyapnikov, and J. T. M. Walraven, Phys. Rev. Lett. **80**, 2269 (1998); P. O. Fedichev and G. V. Shlyapnikov, Phys. Rev. A **58**, 3146 (1998); G. Bene and P. Szépfalusy, ibid. **58**, R3391 (1998); M. Rusch and K. Burnett, ibid. **59**, 3851 (1999); B Jackson and E Zaremba, New Journal of Physics **5**, 88 (2003).

[140] W. Vincent Liu, Phys. Rev. Lett. **79**, 4056 (1997).

[141] R. Ozeri, J. Steinhauer, N. Katz, and N. Davidson, Phys. Rev. Lett. **88**, 220401 (2002).

[142] D. M. Stamper-Kurn, A. P. Chikkatur, A. Görlitz, S. Inouye, S. Gupta, D. E. Pritchard, and W. Ketterle, Phys. Rev. Lett. **83**, 2876 (1999).

[143] G. Mauro D'Ariano, M. G. A. Paris, and M. F. Sacchi, Phys. Rev. A **62**, 023815 (2000).

[144] M. G. A. P. G. M. D'Ariano and M. F. Sacchi, Advances in Imaging and Electron Physics **128**, 205 (2003).

[145] A. K. Ekert, C. M. Alves, D. K. L. Oi, M. Horodecki, P. Horodecki, and L. C. Kwek, Phys. Rev. Lett. **88**, 217901 (2002).

[146] R. Filip, Phys. Rev. A **65**, 062320 (2002).

[147] J. Fiurá šek and N. J. Cerf, Phys. Rev. Lett. **93**, 063601 (2004).

[148] L. J. Garay, J. R. Anglin, J. I. Cirac, and P. Zoller, Phys. Rev. A **63**, 023611 (2001).

[149] C. Barceló, S. Liberati, and M. Visser, Phys. Rev. A **68**, 053613 (2003).

[150] P. O. Fedichev and U. R. Fischer, Phys. Rev. Lett. **91**, 240407 (2003).

[151] M. Krämer, C. Tozzo, and F. Dalfovo, Phys. Rev. A **71**, 061602 (2005).

[152] P. Jain, S. Weinfurtner, M. Visser, and C. W. Gardiner, Phys. Rev. A **76**, 033616 (2007).

[153] A. Peres, Phys. Rev. Lett. **77**, 1413 (1996).

[154] P. Horodecki, Physics Letters A **232**, 333 (1997).

[155] L.-M. Duan, G. Giedke, J. I. Cirac, and P. Zoller, Phys. Rev. Lett. **84**, 2722 (2000).

[156] R. Simon, Phys. Rev. Lett. **84**, 2726 (2000).

[157] J. Steinhauer, Phys. Rev. D **92**, 024043 (2015).

[158] D. E. Bruschi, I. Fuentes, and J. Louko, Phys. Rev. D **85**, 061701 (2012).

[159] J. Estève, C. Gross, A. Weller, S. Giovanazzi, and M. K. Oberthaler, Nature **455**, 1216 (2008), arXiv:0810.0600.

[160] A. Sørensen, L.-M. Duan, J. I. Cirac, and P. Zoller, Nature **409**, 63 (2001), eprint: quant-ph/0006111; L.-M. Duan, J. I. Cirac, and P. Zoller, Phys. Rev. A **65**, 033619 (2002); A. Micheli, D. Jaksch, J. I. Cirac, and P. Zoller, ibid. **67**, 013607, 013607 (2003), eprint: cond-mat/0205369; T. Berrada, S. van Frank, R. Bücker, T. Schumm, J.-F. Schaff, and J. Schmiedmayer, Nature Communications **4**, 2077, 2077 (2013), arXiv:1303.1030 [cond-mat.quant-gas]; M. F. Riedel, P. Böhi, Y. Li, T. W. Hänsch, A. Sinatra, and P. Treutlein, Nature **464**, 1170 (2010), arXiv:1003.1651 [quant-ph]; C. Gross, H. Strobel, E. Nicklas, T. Zibold, N. Bar-Gill, G. Kurizki, and M. K. Oberthaler, ibid. **480**, 219 (2011), arXiv:1112.4594 [cond-mat.quant-gas]; C. D. Hamley, C. S. Gerving, T. M. Hoang, E. M. Bookjans, and M. S. Chapman, Nature Physics **8**, 305 (2012), arXiv:1111.1694 [cond-mat.quant-gas]; B. Lücke, M. Scherer, J. Kruse, L. Pezzé, F. Deuretzbacher, P. Hyllus, O. Topic, J. Peise, W. Ertmer, J. Arlt, L. Santos, A. Smerzi, and C. Klempt, Science **334**, 773 (2011), arXiv:1204.4102 [cond-mat.quant-gas]; C. Gross, T. Zibold, E. Nicklas, J. Estève, and M. K. Oberthaler, Nature **464**, 1165 (2010), arXiv:1009.2374 [cond-mat.quant-gas]; W. Muessel, H. Strobel, D. Linnemann, D. B. Hume, and M. K. Oberthaler, Physical Review Letters **113**, 103004, 103004 (2014), arXiv:1405.

6022 [quant-ph]; R. Bücker, J. Grond, S. Manz, T. Berrada, T. Betz, C. Koller, U. Hohenester, T. Schumm, A. Perrin, and J. Schmiedmayer, Nature Physics **7**, 608 (2011), arXiv:1012.2348 [cond-mat.quant-gas].

[161] J. M. Steele, *The Cauchy-Schwarz Master Class: An Introduction to the Art of Mathematical Inequalities* (Cambridge University Press, Cambridge, 2004).

[162] K. V. Kheruntsyan, J.-C. Jaskula, P. Deuar, M. Bonneau, G. B. Partridge, J. Ruaudel, R. Lopes, D. Boiron, and C. I. Westbrook, Phys. Rev. Lett. **108**, 260401 (2012).

[163] T. Wasak, P. Sza ńkowski, P. Zi ń, M. Trippenbach, and J. Chwede ńczuk, Phys. Rev. A **90**, 033616 (2014).

[164] W. D. Phillips and H. Metcalf, Phys. Rev. Lett. **48**, 596 (1982).

[165] A. Paris-Mandoki, M. D. Jones, J. Nute, J. Wu, S. Warriar, and L. Hackermüller, Review of Scientific Instruments **85**, 113103, – (2014).

[166] A. Paris-Mandoki, "A Single Apparatus for the Production of Ultracold Fermionic Lithium and Cold Bosonic Caesium Gases", PhD thesis (Univeristy of Nottingham, 2015).

[167] E. L. Raab, M. Prentiss, A. Cable, S. Chu, and D. E. Pritchard, Phys. Rev. Lett. **59**, 2631 (1987).

[168] G. A. Askar'yan, Sov. Phys.-JETP **15**, 1088 (1962); J. E. Bjorkholm, R. R. Freeman, A. Ashkin, and D. B. Pearson, Phys. Rev. Lett. **41**, 1361 (1978); S. Chu, J. E. Bjorkholm, A. Ashkin, and A. Cable, ibid. **57**, 314 (1986).

[169] G. A. Askar'yan, Sov. Phys.-JETP **15**, 1088 (1962).

[170] J. E. Bjorkholm, R. R. Freeman, A. Ashkin, and D. B. Pearson, Phys. Rev. Lett. **41**, 1361 (1978).

[171] S. Chu, J. E. Bjorkholm, A. Ashkin, and A. Cable, Phys. Rev. Lett. **57**, 314 (1986).

[172] R. Smith and Z. Hadzibabic, English, in *Physics of quantum fluids*, Vol. 177, edited by A. Bramati and M. Modugno, Springer Series in Solid-State Sciences (Springer Berlin Heidelberg, 2013), pp. 341–359; R. P. Smith, R. L. D. Campbell, N. Tammuz, and Z. Hadzibabic, Phys. Rev. Lett. **106**, 250403 (2011); M Zawada, R Abdoul, J Chwedeńczuk, R Gartman, J Szczepkowski, . Tracewski, M Witkowski, and W Gawlik, Journal of Physics B: Atomic, Molecular and Optical Physics **41**, 241001 (2008); F. Gerbier, J. H. Thywissen, S. Richard, M. Hugbart, P. Bouyer, and A. Aspect, Phys. Rev. A **70**, 013607 (2004); A Minguzzi, S Conti, and M. P. Tosi, Journal of Physics: Condensed Matter **9**, L33 (1997).

[173] D. A. Huse and E. D. Siggia, English, Journal of Low Temperature Physics **46**, 137 (1982).

[174] A. Griffin, Phys. Rev. B **53**, 9341 (1996).

[175] P. G. De Gennes, *Superconductivity of Metals and Alloys* (Benjamin, New York, 1996).

[176] F. Dalfovo, S. Giorgini, L. P. Pitaevskii, and S. Stringari, Rev. Mod. Phys. **71**, 463 (1999).

[177] M. A. Caracanhas, J. A. Seman, E. R. F. Ramos, E. A. L. Henn, K. M. F. Magalhães, K. Helmerson, and V. S. Bagnato, Journal of Physics B: Atomic, Molecular and Optical Physics **42**, 145304 (2009).

[178] N. Welch, "Non-Equilibrium Dynamics of Bose-Einstein Condensates", PhD thesis (Univeristy of Nottingham, 2015).

[179] F. Dalfovo, S. Giorgini, M. Guilleumas, L. Pitaevskii, and S. Stringari, Phys. Rev. A **56**, 3840 (1997).

[180] W. Krauth, Phys. Rev. Lett. **77**, 3695 (1996).

[181] Holzmann, M. and Castin, Y., Eur. Phys. J. D **7**, 425 (1999).

[182] R. J. Dodd, M. Edwards, C. W. Clark, and K. Burnett, Phys. Rev. A **57**, R32 (1998).

[183] B. P. Anderson and M. A. Kasevich, Phys. Rev. A **59**, R938 (1999).

[184] R. Smith and Z. Hadzibabic, English, in *Physics of quantum fluids*, Vol. 177, edited by A. Bramati and M. Modugno, Springer Series in Solid-State Sciences (Springer Berlin Heidelberg, 2013), pp. 341–359.

[185] R. P. Smith, R. L. D. Campbell, N. Tammuz, and Z. Hadzibabic, Phys. Rev. Lett. **106**, 250403 (2011).

[186] S. K. Adhikari and A Gammal, Physica A: Statistical Mechanics and its Applications **286**, 299 (2000).

[187] S. A. Fulling and P. C. W. Davies, Proceedings of the Royal Society of London A: Mathematical, Physical and Engineering Sciences **348**, 393 (1976).

[188] R. Graham, English, Journal of Statistical Physics **101**, 243 (2000).

[189] T Gasenzer, Journal of Physics B: Atomic, Molecular and Optical Physics **35**, 2337 (2002).

[190] L. Pitaevskii and S. Stringari, Physics Letters A **235**, 398 (1997).

[191] S. Giorgini, Phys. Rev. A **61**, 063615 (2000).

[192] R. Alicki, English, International Journal of Theoretical Physics **16**, 351 (1977).

[193] L. D. Landau, J. Phys.(USSR) **10**, [Zh. Eksp. Teor. Fiz.16,574(1946)], 25 (1946).

[194] P. Hohenberg and P. Martin, Annals of Physics **34**, 291 (1965).

[195] I. Kondor and P. Szépfalusy, Physics Letters A **47**, 393 (1974).

[196] W. Liu and W. Shieve, cond-mat/9702122 (1997).

[197] J. Reidl, A. Csordás, R. Graham, and P. Szépfalusy, Phys. Rev. A **61**, 043606 (2000).

[198] E. Lifshitz and L. Pitaevskii, *Physical kinetics* (Pergamon Press, Oxford, 1981).

[199] X.-D. Ma, Z.-J. Yang, J.-Z. Lu, and W. Wei, Chinese Physics B **20**, 070307, 070307 (2011); Z.-J. Yang, Z.-L. Chai, C.-X. Li, and X.-D. Ma, Communications in Theoretical Physics **57**, 789 (2012); C. Trallero-Giner, D. G. Santiago-Pérez, M.-C. Chung, G. E. Marques, and R. Cipolatti, ArXiv e-prints (2015), arXiv:1503.08884 [cond-mat.quant-gas]; S. Tan, M. Pustilnik, and L. I. Glazman, Phys. Rev. Lett. **105**, 090404 (2010); T. Kinoshita, T. Wenger, and D. S. Weiss, Nature **440**, 900 (2006); M.-C. Chung and A. B. Bhattacherjee, New Journal of Physics **11**, 123012, 123012 (2009), arXiv:0809.3632 [cond-mat.other]; Z. Ristivojevic and K. A. Matveev, Phys. Rev. B **89**, 180507 (2014); I. E. Mazets, Phys. Rev. A **83**, 043625 (2011).

[200] S. T. Beliaev, Sov. Phys. JETP **34**, 323 (1958); S. Beliaev, ibid. **7**, 299 (1958).

[201] W. Zheng and H. Zhai, Physical Review Letters **113**, 265304, 265304 (2014), arXiv:1408.6419 [cond-mat.quant-gas].

[202] S. Alipour, M. Mehboudi, and A. T. Rezakhani, Physical Review Letters **112**, 120405, 120405 (2014), arXiv:1302.1115 [quant-ph]; A. Shaji and C. M. Caves, Phys. Rev. A **76**, 032111 (2007); F. Nosraty, ArXiv e-prints (2015), arXiv:1506.06249 [quant-ph]; W. Zhong, Z. Sun, J. Ma, X. Wang, and F. Nori, Phys. Rev. A **87**, 022337 (2013); F. Ozaydin, ArXiv e-prints (2014), arXiv:1403.2376 [quant-ph].

[203] E. Gross, English, Il Nuovo Cimento (1955-1965) **20**, 454 (1961); L. P. Pitaevsk, Soviet Physics JETP-USSR **13** (1961).

[204] E. Madelung, German, Naturwissenschaften **14**, 1004 (1926).

[205] S. Stringari, Phys. Rev. Lett. **77**, 2360 (1996).